A novel passage from particle data to PDEs out of equilibrium

Thesis by

Peter Albrecht Embacher

in partial fulfilment of the requirements for the degree of
Doctor of Philosophy

29 June 2018

School of Mathematics
Cardiff University

Summary

Often in the natural and social sciences, a macroscopic perspective on a system's dynamics can simplify its description, while preserving the "essential" information. Nonetheless, the parameters in the macroscopic picture are typically abstract quantities and difficult to identify from direct observations. This text is about extracting these macroscopic parameters for a class of purely dissipative, microscopically stochastic systems out of equilibrium.

Particularly, we seek a macroscopic description of gradient flow type:

$$\partial_t \rho\,(t,x) = -\mathcal{K}\,(\rho)\,\mathcal{DS}\,(\rho)\,,$$

where ρ is the macroscopic state and $\mathcal{DS}$ is the variational derivative of the thermodynamic entropy $\mathcal{S}$. The so-called thermodynamic metric $\mathcal{K}$ reflects the local geometry of the state-space and is the main object of our consideration. This work focuses on dissipative, irreversible systems, for which $\mathcal{K}$ is a symmetric, positive semi-definite operator. The first part of this text is devoted to the (weighted) L^2-Wasserstein metric, thus related to optimal transport. In this case, the thermodynamic metric is characterised by the so-called mobility m and reads $\mathcal{K}\,(\rho)\,(.) = -\mathrm{div}\,(m\,(\rho)\,\nabla\,(.))$. We develop a method to extract this mobility from mesoscopic states, provided the system is in local equilibrium and exhibits suitable Gaussian fluctuations. This method is tested for several classical Markov processes, thus demonstrating good agreement with analytically known results.

This approach is then formally extended to other purely dissipative systems. To show its potential, this technique is applied to a system, that combines a transport with a reaction process as well as an Ising model with Glauber dynamics. Furthermore, it was used to forecast the macroscopic evolution of particle processes on-the-fly by a finite-element approach, again showing good agreement with a "classical" finite-element method for the analytic macroscopic evolution.

Acknowledgements

I would like to thank Nicolas Dirr for his patient and very helpful supervision of this research project, giving freedom as well as guidance and always being open and responsive to any question. I also want to thank Johannes Zimmer, my second supervisor, for his valuable feedback, mentoring and particularly for his efforts for pushing the project forward and keeping me motivated.

Special thanks go to Celia Reina, who was also a vital part of this research project and very helpful in many ways, particularly for the numerical implementation.

Further thanks go to my examination commitee for their time and insightful questions.

Additionally, I would like to thank the Cardiff University, notably its staff and research students at the Mathematics department, for providing research facilities and creating such a friendly and productive atmosphere to work in.

Eventually, I like to thank the Leverhulme Trust for funding this project.

Contents

I

Introduction

For many applications it is not necessary to know the precise atomistic behaviour of a system of interest, but it rather suffices to consider the system on a larger, "macroscopic", scale. This is familiar for instance in physics for rigid body mechanics or thermodynamics, where centre of mass or particle density would be examples for macroscopic quantities. But also in chemistry, biology or social sciences, such an approach is common - reaction-diffusion equations, predator-prey models (Lotka–Volterra equations; see for example [1]) or models for the dynamics of stock market prices (Black-Scholes-Merton model; see for example [2, Ch. 14]) could be mentioned among others.

Mathematically the transition from the microscopical description to the macroscopic model is typically carried out by a limit of a suitable transition parameter. This ratio of scales will be called ϵ from now on, where $\epsilon \searrow 0$ is the macroscopic limit. Such a macroscopic description is in general neither trivial to find nor is even the existence clear. There are two key ingredients necessary: One must be able to find a macroscopic "state", by which we mean, all information, that we are interested in, can be derived from it and it can be described by a closed equation, i.e. there exists an initial-value problem, which allows to predict all future states from the current state at the initial time (we are always interested in dynamical systems here). And as second ingredient one must be able to find this initial-value problem. Note that it is neither necessary for the macroscopic state to allow the extraction of the microscopic dynamics, nor to contain actually less information (in the sense of necessary independent measurements to characterise it): The knowledge of the position of each individual particle allows to compute the particle density but not (necessarily) vice versa. At the same time, the density is a function in an infinite-dimensional vector-space (therefore - in principle - requiring infinitely many measurements to identify it), whereas any finite number of particles (in classical mechanics) only has finitely many degrees of freedom. In such a case, the hope for the macroscopic description still to be simpler than its microscopic counterpart would be based on a Galerkin approach to conveniently approximate the macroscopic state in a finite-dimensional space.

As such, these macroscopic descriptions are abstract images of reality, obtained by mathematical limits and typically not having an actual realisation itself. Hence, notions of "higher order" estimates have been developed, to better capture the observed behaviour "close to" but not quite in the limit, i.e. on a mesoscopic level. It is the concurrence of quantities in the meso- and macroscopic scale, that is the key for us, to determine the parameters in the macroscopic behaviour. This is conceptually represented in fig. 0.1. This text is mostly concerned with characterising the above-mentioned initial-value problems, given a set of observed, mesoscopic states. For this, we focus on microscopically stochastic processes, that turn purely deterministic on the macroscopic scale, but we try to preserve as much information as possible about the stochasticity of large, finite systems in the quantities

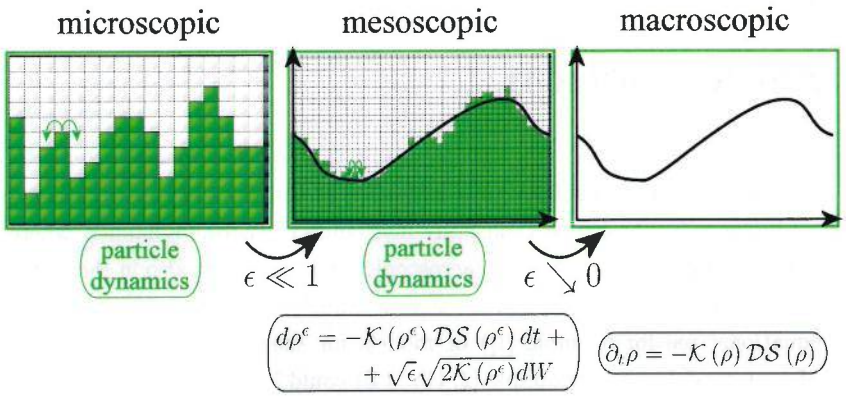

Figure 0.1: Schematic representation of the role of the micro-, meso- and macroscopic scaling: The actual, stochastic particle process happens on the microscopic level. On the macroscopic level, i.e. for the parameter $\epsilon \searrow 0$, theoretical descriptions exist, but are only abstract and the quantities characterising these models are often difficult to relate to the atomistic scenarios. The mesoscopic level links these two, as it allows for both, (sometimes costly) particle observations and (approximate) theoretical models.

constituting the macroscopic model. The microscopic (and mesoscopic) states are thus probability measures, typically themselves defined on measure spaces: For the examples we will study later on, for instance, the systems are microscopically atomistic and their dynamics is given on the particle level by respective stochastic processes on the particle positions X_i (with i denoting the individual particle). Thus, on the microscopic scaling, the setting is characterised by probability measures on the empirical measures $\epsilon \cdot \sum_i [\delta_{X=X_i}]$. In a suitable sense of the limit (and upon rescaling of time and space appropriately) the state in the macroscopic limit is described by a Lebesgue density, which can be identified with the solution of a PDE. More precisely we consider systems, that macroscopically can be described as gradient flows of the thermodynamic entropy $\mathcal{S}$ of the system

$$\partial_t \rho(t,x) = -\mathcal{K}(\rho)\,\mathcal{DS}(\rho)\,, \tag{1}$$

where ρ shall be the macroscopic state, $\mathcal{K}$ is a self-adjoint, positive semi-definite operator and will be called the "thermodynamic metric" and $\mathcal{DS}$ is the variational derivative of the entropy $\mathcal{S}$. The operator $\mathcal{K}$ here plays the same role, which the transpose operation plays for states in the simple Euclidean setting, i.e. it maps from the co-tangent space of the state space into its tangent space (just like the transpose maps the derivative to the gradient). In the rest of this text we will mostly consider so-called weighted Wasserstein settings, in which case these tangent and co-tangent spaces can be identified with weighted versions of the H^1 and H^{-1} spaces.

In principle, gradient flows – when considered as a type of differential equations – can arise in many different contexts, like for instance overdamped mechanical systems (where eq. (1) would need to be replaced formally by an ODE (or system of ODEs) for the particle positions with the mechanical energy playing the role of the entropy $\mathcal{S}$ in the equation above, the operator $\mathcal{K}$ simply being the transpose operation and the inertia term would be dropped from Newton's equation, due to being considered negligible compared to the first order drag term). Gradient flows occur somewhat more naturally however in the macroscopic description of dissipative, thermodynamic processes, such as the diffusion equation or its generalisations in form of the Fokker-Planck equation or the porous-medium equation. In fact it was the influential work by Jordan-Kinderlehrer-Otto [3] and Otto [4], that revived the interest in the more abstract setting of gradient flows by relating these long-established equations to gradient flows with respect to the so-called Wasserstein metric, which plays a major role in optimal transport problems. In the sequel, advances were made by expanding the set of evolution equations, that can be cast in gradient flow shape (see e.g. [5], [6], [7], [8]), establishing a rigorous framework, that introduces a generalised notion of gradient flow for a much wider class of metric spaces and allows to deduce existence and stability statements of solutions (see most notably [9]), and by linking the macroscopic quantities from the gradient flow formulation to statistical quantities from large deviations theory (see e.g. [10], [11]). While many of these examples show variations of the above-mentioned Wasserstein metric for $\mathcal{K}$, the concept is not limited to this, as work on geometric flows (e.g. mean curvature flow [12]) show. Note that further extensions of the gradient flow structure were studied as well, for instance Öttinger's GENERIC framework [13], which allows for applications beyond the purely dissipative setting considered in this text.

Our objective in part II will be, to make the gradient flow concept more accessible to applications, by presenting a new method for finding the thermodynamic metric $\mathcal{K}$ from experimental data, if the underlying dynamic is purely dissipative: We first focus on the case, where the underlying dynamics can be interpreted as a transport process. More precisely, we first consider metrics, that are of a Wasserstein type. To motivate this connection with optimal transport, some well-known theory on the Wasserstein metric is laid out in section 1. This is followed by an introduction to the computational method to find $\mathcal{K}$ in the slightly more general setup of weighted Wasserstein metrics in section 2. In section 3 the approach is further expanded to a more generalised setting of dissipative systems, allowing applications beyond transport processes. This is showcased for two species with independent random walk with inter-species reactions as well as a subcritical nearest neighbour Ising model with Glauber dynamics (non-conserved total magnetisation). How this approach can be used for on-the-fly forecasts of dynamical systems is demonstrated in subsection 3.1. In part III the results will be summarised and an outlook on possible future questions will be given.

II

Numerically extracting the thermodynamic metric from dissipative processes

This part is devoted to finding the metric $\mathcal{K}$ from a process, which at the macroscopic scale evolves according to eq. (1), given experimental data of the state at two points in time in quick succession. As our numerical examples are of this kind, we first introduce the so-called Wasserstein metric in section 1. Section 2 presents the main results of this work: A method is described and demonstrated by means of several numerical examples, that uses stochastic fluctuations around the macroscopic path $t \mapsto \rho(t,.)$ to find $\mathcal{K}$. Eventually, in section 3 this method is formally extended to dissipative systems beyond the Wasserstein case.

1 A quick introduction to the Wasserstein metric

We address a special case of eq. (1) first, before considering the generalised setting in sections 2 and 3: We assume the metric on the state space is a L^2-Wasserstein metric. This is a metric on the space of Borel probability measures with finite second moment $\mathscr{P}_2(\Omega)$, where for our purposes $\Omega \subset \mathbb{R}^d$ is a smooth domain in the d-dimensional real space, which shall be equipped with the standard Euclidean norm $|.|$. For a simpler notation, we will drop the "Borel" specification further on, but always assume that the underlying measure-space is $\mathbb{R}^d$ equipped with the Borel σ-algebra and all sets are Borel sets. Similarly, the σ-algebra on product spaces $\Omega \times \Omega$ shall be the respective product-σ-algebra. Apart from some heuristic considerations, this section closely follows [9, Ch. 5-8], [14, Ch. 1-4]. Also [15, Ch. 1,2] covers many aspects in a similar way. Note that we restrict ourselves to the simplest case of a finite-dimensional Euclidean space, while these references provide much more general results (a wider class of transport processes on Polish spaces).

1.1 Definition, Benamou-Brenier formula and basic intuition

Definition of the L^2-Wasserstein metric

Definition 1. (L^2-Wasserstein metric)
Let $\mu_0, \mu_1 \in \mathscr{P}_2(\Omega)$ be two probability measures with finite second moment, $\int_\Omega x^2 d\mu_t(x) < \infty$ for $t \in \{0,1\}$, $\Gamma(\mu_0,\mu_1)$ the set of all *admissible transport plans* (or couplings) between μ_0 and μ_1, i.e.

$$\Gamma(\mu_0,\mu_1) := \{\gamma \in \mathscr{P}_2(\Omega \times \Omega) | \, \pi_1(\gamma) = \mu_0, \pi_2(\gamma) = \mu_1\} \tag{1.1}$$

for π_1, π_2 the respective marginals $\pi_1(\gamma)\left(\tilde{\Omega}\right) = \gamma\left(\tilde{\Omega}, \Omega\right)$, $\pi_1(\gamma)\left(\tilde{\Omega}\right) = \gamma\left(\Omega, \tilde{\Omega}\right)$ $\forall \tilde{\Omega} \subset \Omega$. Then the *$L^2$-Wasserstein metric* is given by:

$$\begin{aligned} W_2(\mu_0, \mu_1) &= \inf_{\gamma \in \Gamma(\mu_0, \mu_1)} \left\{ \sqrt{\int_{\Omega \times \Omega} |x_2 - x_1|^2 \, d\gamma(x_1, x_2)} \right\} = \\ &= \inf_{\gamma \in \Gamma(\mu_0, \mu_1)} \left\{ \|x_2 - x_1\|_{L^2(\gamma; \Omega \times \Omega)} \right\}. \end{aligned} \tag{1.2}$$

See for instance [9, Ch. 7] for further information. In fact, the infimum in the definition above is always attained and therefore a minimum, as the cost-function $(x_1, x_2) \mapsto |x_2 - x_1|^2$ is continuous as well as bounded from below (see [14, Thm. 2.5] and specifically for this example: thm. 6 below). Moreover, the minimiser is even unique, if the "initial" measure μ_0 is absolutely continuous with respect to the Lebesgue-measure, thanks to its strict convexity (see [16, Thm. 1.2]). While this definition of the L^2-Wasserstein metric applies to probability measures, it can easily be extended to L^p-functions (normalised and with bounded second moment), by interpreting them as densities with respect to the Lebesgue measure.

Some basic intuitions This metric is related to optimal transport, in fact it is a special case of a Kantorovich problem, where the cost-function is quadratic. It can intuitively be thought of as a displacement metric: The Wasserstein metric gives the cost for a transition from μ_0 to μ_1 (or vice-versa due to symmetry), while keeping the total mass constant, i.e. by only rearranging the weight between different positions in Ω. In case of the L^2-Wasserstein metric, the cost for moving a unit-weight (i.e. a Dirac peak) from x_1 to x_2 in the domain is given by the Euclidean distance $|x_2 - x_1|$. Indeed, $\gamma\left(\tilde{\Omega}_1 \times \tilde{\Omega}_2\right)$ can be interpreted as the (probability) mass, that gets transported from $\tilde{\Omega}_1 \subset \Omega$ in the domain of the "initial state" μ_0 to $\tilde{\Omega}_2 \subset \Omega$ in the domain of the "target state" μ_1. While the above formulation does not a priori require the existence of an explicit transport map T, i.e. a Borel measurable function $T\colon \Omega \to \Omega$ with $\mu_0\left(T^{-1}(.)\right) = \mu_1(.)$, this case is included as a particularly graphical example: $\gamma(.,.) = \mu_0(.) \times \mu_0\left(T^{-1}(.)\right) \in \Gamma(\mu_0, \mu_1)$, thus $\int_{\Omega \times \Omega} (x_2 - x_1)^2 \, d\gamma(x_1, x_2) = \int_\Omega \left(T(x_1) - x_1\right)^2 d\mu_0(x_1)$. In fact, in our setting such a transport map can always be found ([14, Thm. 2.26] or, for a more general setting with respect to the cost-function [16]), if the initial state μ_0 is absolutely continuous; the formulation in def. 1 extends to more general settings in terms of the initial measure, the integrand in eq. (1.2) as well as the metric space and therefore appears more natural. Furthermore, it shall hereby be stressed that many of the following statements, particularly the ones involving interpolating measures $\{\mu_t | \, t \in [0,1]\}$, become more intricate for less simple setups. On the other hand, the existence and characterisation of such interpolating measures will be the foundation when considering gradient flows later on. For convenience of notation, let us introduce the push-forward operator:

Definition 2. (Push-forward)
Let $T\colon \Omega \to \Omega$ a Borel measurable function, $\mu \in \mathscr{P}(\Omega)$ a probability measure. Then the operator $T_{\#}\colon \mathscr{P}(\Omega) \to \mathscr{P}(\Omega), \forall \tilde{\Omega} \subset \Omega\colon T_{\#}\mu\left(\tilde{\Omega}\right) = \mu\left(T^{-1}\left(\tilde{\Omega}\right)\right)$ is called the *push-forward through* T.

In this context we will often use the identity map, which is denoted by the symbol $\mathbb{I}\colon \Omega \to \Omega, x \mapsto x$. Abusing notation, the same letter will be used for the identity on other spaces as well.

Contrary to the Wasserstein metric, the L^p-difference $\|\rho_1 - \rho_0\|_{L^p(\Omega)}$ between two probability measures $d\mu_{0,1}(x) = \rho_{0,1}(x)\,dx$ (for $\rho_{0,1} \in L^p(\Omega, \mathbb{R})$; note that the L^1-case coincides with the total variation distance between μ_0, μ_1), that are absolutely continuous with respect to the Lebesgue measure dx, allows to change the weight while transitioning between μ_0 and μ_1, which can be a lot cheaper, if the support of the weight is far apart. On the other hand, the Wasserstein cost does scale down, if initial and "target"-weights are located nearby. The following examples highlight this difference:

Example 3. (Displacement character of the Wasserstein metric)
Consider for $\Omega = \mathbb{R}$ and a fixed $\tau \in]0, 1]$ the density $\rho_\tau(x) = \begin{cases} \frac{1}{\tau} & \forall x \in \left[-\frac{\tau}{2}, \frac{\tau}{2}\right] \\ 0 & \text{otherwise} \end{cases}$, which is highly concentrated around zero (approximating a delta peak for $\tau \searrow 0$). The initial and final measures shall be $d\mu_0(x) = \rho_\tau(x)\,dx$ and $d\mu_1(x) = \rho_\tau(x-\tau)\,dx = (\mathbb{I}+\tau)_{\#}\mu_0(x)$ (note that the quantities μ_0 and μ_1 do depend on the parameter τ here as well, which is suppressed in this notation, to keep it more along the lines of def. 1; the parameter τ will only be needed in the last step), then

$$W_2^2(\mu_0, \mu_1) \leq \int_\Omega ((x_1 + \tau) - x_1)^2 \rho_t(x_1)\,dx_1 = \tau^2. \tag{1.3}$$

At the same time we get for the L^p-difference by Hölder's inequality:

$$1 = \|\rho_\tau\|_{L^1(\Omega)} \leq \|1\|_{L^{\frac{p}{p-1}}(\mathrm{supp}(\rho_\tau))} \cdot \|\rho_\tau\|_{L^p(\Omega)} = |\mathrm{supp}(\rho_\tau)|^{\frac{p-1}{p}} \cdot \|\rho_\tau\|_{L^p(\Omega)} = \tau^{\frac{p-1}{p}} \cdot \|\rho_\tau\|_{L^p(\Omega)}, \tag{1.4}$$

thus (due to non-overlapping support):

$$\|\rho_\tau(.) - \rho_\tau(. - \tau)\|_{L^p(\Omega)}^p = \|\rho_\tau(.)\|_{L^p(\Omega)}^p + \|\rho_\tau(. - \tau)\|_{L^p(\Omega)}^p \geq \frac{2}{\tau^{p-1}}. \tag{1.5}$$

Hence: $\lim_{\tau \searrow 0} \frac{W_2(\mu_0,\mu_1)}{\tau} \leq 1$ but $\lim_{\tau \searrow 0} \frac{\|\rho_\tau(.) - \rho_\tau(. - \tau)\|_{L^2(\Omega)}}{\tau} \to \infty$ (in fact, in case $p > 1$ it even holds: $\lim_{\tau \searrow 0}\left(\|\rho_\tau(.) - \rho_\tau(. - \tau)\|_{L^p(\Omega)}\right) \to \infty$).

Example 4. (Nucleation character of the L^p-distance)
With the same definitions of Ω as in the previous example and $\tau \in [0, 1]$, $\rho_\tau(x) = (1-\tau) \cdot \chi_{[0,1]}(x) + \tau \cdot \chi_{[2,3]}$, the initial and final measures shall be $d\mu_0(x) = \rho_0(x)\,dx$ and $d\mu_1(x) = \rho_\tau(x)\,dx = (1-\tau) \cdot$

$\mu_0(x) + \tau \cdot (\mathbb{I} + 2)_{\#} \mu_0(x)$, then

$$W_2^2(\mu_0, \mu_1) \geq \tau \cdot \operatorname{dist}(\operatorname{supp}([0,1]), \operatorname{supp}([2,3])) = \tau \tag{1.6}$$

(this lower bound comes from the fact that we have to move the total mass of τ from $[0,1]$ to $[2,3]$; we additionally might have to make rearrangements of the weights within these intervals, too, but these are non-negative terms and neglected in the inequality). At the same time we get for the L^p-difference:

$$\begin{aligned} \|\rho_0(.) - \rho_\tau(.)\|_{L^p(\Omega)}^p &= \|\rho_0(.) - ((1-\tau) \cdot \rho_0(.) + \tau \cdot \rho_0(. - 2))\|_{L^p(\Omega)}^p = \\ &= \tau^p \cdot \int_\Omega (\rho_0^p(x) + \rho_0^p(x-2))\, dx = 2 \cdot \tau^p. \end{aligned} \tag{1.7}$$

Hence: $\lim_{\tau \searrow 0} \frac{W_2(\mu_0,\mu_1)}{\tau} \to \infty$ but $\lim_{\tau \searrow 0} \frac{\|\rho_0(.) - \rho_\tau(.)\|_{L^p(\Omega)}}{\tau} = \sqrt[p]{2}$.

Note that the special case of $p = 1$ in these examples relates (up to a prefactor) to the total variation distance and can be identified with an optimal transport problem of the type of eq. (1.2) as well, however without the square root and with the integrand replaced with a cost $\delta_{x_1 \neq x_2} := \begin{cases} 1 & \text{for } x_1 \neq x_2 \\ 0 & \text{for } x_1 = x_2 \end{cases}$ (i.e. constant cost per mass, as soon as mass has to be moved, and zero cost otherwise; see [15, eq. (13)]).

The "locality" of the Wasserstein metric, that appears in these examples, can be found again in the natural isometry between the metric space $(\Omega, |.|)$ and the corresponding Wasserstein space $(\mathscr{P}_2(\Omega), W_2)$: $\Omega \to \mathscr{P}_2(\Omega), x \to \delta(. - x)$. Between two delta peaks there only exists one admissible transport plan $\Gamma(\delta(.), \delta(. - t)) = \{\delta(.) \times \delta(. - t)\}$. For an amount of K delta peaks at $\left(x_1^{(k)}\right)_{k \in \{1,\ldots,K\}}$ constituting μ_0 and likewise K delta peaks at $\left(x_2^{(k)}\right)_{k \in \{1,\ldots,K\}}$ constituting μ_1 there is not necessarily uniqueness anymore (see example 11), but the L^2-Wasserstein metric can be shown to be given by: $W_2(\mu_0, \mu_1) = \min_{\text{perm}} \left(\sum_{k=1}^K \left[\left|x_1^{(k)} - x_2^{(\text{perm}(k))}\right|\right]\right)$ where the minimum is taken over all permutations perm of $\{1, \ldots, K\}$ (see remark 8 below and references therein).

The characterisation by Benamou and Brenier The connection of the Wasserstein metric to optimal transport becomes apparent again, when considering its following characterisation by Benamou and Brenier (originally formulated for Lebesgue densities in [17]):

Theorem 5. *(Benamou-Brenier formula for the L^2-Wasserstein metric)*

$$W_2(\mu_0, \mu_1) = \inf_{\forall t: \mu_t \in \mathscr{P}_2(\Omega)} \left\{ \sqrt{\int_0^1 \|v_t\|_{L^2(\mu_t;\Omega)}^2 \, dt} \;\middle|\; \frac{d\mu_t}{dt} = -div(v_t \mu_t) \right\}, \tag{1.8}$$

where the so-called "flux" $(t,x) \mapsto v_t(x)$ *is a* $L^2(\mu_t; [0,1] \times \Omega)$*-function and the conditional equality is to be understood in the sense of distributions, i.e.:* $\forall f \in C_0^\infty(\Omega, \mathbb{R}) : \frac{d}{dt}\int_\Omega f(x)\, d\mu_t(x) = \int_\Omega (\nabla f(x)) \cdot v_t(x)\, d\mu_t(x)$.

The subscript zero in C_0^∞ shall denote compact support. Note that here the index notation was extended to represent the "time" $t \in [0,1]$, i.e. μ_0 is the initial and μ_1 is the final state. The condition

$$\frac{d\mu_t}{dt} = -\mathrm{div}(v_t \mu_t) \tag{1.9}$$

is the continuity equation, therefore ensuring conservation of total mass throughout the transport process: $\frac{d}{dt}\int_\Omega d\mu_t(x) = \int_{\partial\Omega} n_\perp(x) \cdot v_t(x)\, d\mu_t(x) = 0$ (for $n_\perp(x) \perp \partial\Omega(x)$ the standard normal vector on the boundary at $x \in \partial\Omega$).

While in thm. 5 no explicit regularity requirements are imposed on μ_t with respect to t, the continuity-equation itself guaranties absolute continuity, i.e.: $\exists f \in L^1([0,1]) : \forall 0 < t_0 < t_1 < 1 : W_2(\mu_{t_0}, \mu_{t_1}) \leq \int_{t_0}^{t_1} f(t)\, dt$. Furthermore, the metric derivative $|\dot{\mu}_t| := \lim_{h\to 0} \frac{W_2(\mu_{t+h}, \mu_t)}{|h|}$ is bounded from above by the flux: $|\dot{\mu}_t| \leq \|v_t\|_{L^2(\mu_t;\Omega)}$. See [9, Thm. 8.3.1] for an even more general version of both statements (as well as a somewhat converse statement).

The major difference from the original formulation of the Wasserstein metric to the Benamou-Brenier version is the introduction of a new parameter t, that transforms the initially static problem in eq. (1.2) into a dynamical one in eq. (1.8). This is possible, firstly, thanks to the existence and uniqueness of the transport map for the optimal plan γ in eq. (1.2). And second, because, by means of so-called constant-speed geodesics, it is possible to find interpolations, that preserve a sense of locality (if we forget the past sometime in between, we still get the same evolution). The rest of this section is devoted to defining these interpolations and characterising them, which will eventually lead to thm. 5 as well as gradient flows with respect to the Wasserstein metric. We start with the following version of Brenier's theorem:

1.2 Existence and uniqueness of optimal transport maps and duality

Theorem 6. *(Existence and uniqueness of optimal transport maps)*
Let $\mu_{0,1} \in \mathscr{P}_2(\Omega)$ *be absolutely continuous with respect to the Lebesgue measure. Then the minimisation problem eq. (1.2) has a unique solution* γ_0 *and this solution is induced by a transport map* T*, which is the gradient of a convex function.*

Proof. (Following [14, thm. 2.23] and [15, thm. 2.12])
Existence of a minimiser in eq. (1.2):
We want to show lower semi-continuity of the integral in eq. (1.2) as a function of the probability measure γ. As the set of admissible plans is non-empty (choose for instance $d\mu_0 \times d\mu_1$), let $(\gamma_k)_{k\in\mathbb{N}} \subset \Gamma(\mu_0, \mu_1)$ be a minimising sequence in this set, i.e. $\limsup_{k\to\infty} \int_{\Omega\times\Omega} |x_2 - x_1|^2\, d\gamma_k(x_1, x_2) = W_2^2(\mu_0, \mu_1)$.

Whenever the set of admissible measures $\Gamma(\mu_0,\mu_1)$ is compact with respect to narrow convergence (i.e. in duality to the bounded, continuous functions $C_b(\Omega\times\Omega)$: $(\gamma_k)_{k\in\mathbb{N}}$ converges narrowly to γ, iff $\forall f\in C_b(\Omega\times\Omega):\lim_{k\to\infty}\int_{\Omega^2} f(x_1,x_2)\,d\gamma_k(x_1,x_2)=\int_{\Omega^2} f(x_1,x_2)\,d\gamma(x_1,x_2)$; see [9, sec. 5.1] for further details) the sequence $(\gamma_k)_k$ admits a cluster point $\gamma_0\in\Gamma(\mu_0,\mu_1)$ and hence we achieve the desired lower semi-continuity by setting $f_{\tilde{k}}:\Omega\times\Omega\to\mathbb{R},(x_1,x_2)\mapsto\min\left\{\tilde{k},|x_2-x_1|^2\right\}$ (and thus $f_{\tilde{k}}$ bounded and continuous) and using monotone convergence for the equality in the first line of:

$$\begin{aligned}W_2^2(\mu_0,\mu_1)&\leq\int\limits_{\Omega\times\Omega}|x_2-x_1|^2\,d\gamma_0(x_1,x_2)=\lim_{\tilde{k}\to\infty}\int\limits_{\Omega\times\Omega}f_{\tilde{k}}(x_1,x_2)\,d\gamma_0(x_1,x_2)\leq\\&\leq\lim_{\tilde{k}\to\infty}\limsup_{k\to\infty}\int\limits_{\Omega\times\Omega}f_{\tilde{k}}(x_1,x_2)\,d\gamma_k(x_1,x_2)\leq\limsup_{k\to\infty}\int\limits_{\Omega\times\Omega}|x_2-x_1|^2\,d\gamma_k(x_1,x_2)=\\&=W_2^2(\mu_0,\mu_1).\end{aligned}\tag{1.10}$$

Relative compactness follows from applying Prokhorov's theorem twice: First to the sets $\{\mu_0\},\{\mu_1\}\subset\mathscr{P}_2(\Omega)$ (which are obviously compact each), it shows, they are tight (i.e. the weight outside a suitable compact subset of Ω is arbitrarily small, uniformly over all measures in the set). But then also each measure $\gamma\in\Gamma(\mu_0,\mu_1)$ must be tight, due to: $\forall$compact $K_0,K_1\subset\Omega$: $\gamma(\Omega\times\Omega\setminus K_0\times K_1)\leq\mu_0(\Omega\setminus K_0)+\mu_1(\Omega\setminus K_1)$. Making use of Prokhorov's theorem in the converse way, we get relative compactness for the set $\Gamma(\mu_0,\mu_1)$ (with respect to narrow convergence). Closedness and therefore compactness can be seen by testing against functions $f\in C_b(\Omega)$, that are independent of the other variable in $\Omega\times\Omega$: Let $(\gamma_k)_{k\in\mathbb{N}}\subset\Gamma(\mu_0,\mu_1)$ be a sequence narrowly converging to γ_0, then the limit is also admissible: $\int_\Omega f(x_1)\,d\mu_0(x_1)=\int_{\Omega\times\Omega}f(x_1)\,d\gamma_k(x_1,x_2)=\lim_{k\to\infty}\int_{\Omega\times\Omega}f(x_1)\,d\gamma_k(x_1,x_2)=\int_{\Omega\times\Omega}f(x_1)\,d\gamma_0(x_1,x_2)$ and likewise for the second marginal μ_1.

Induction of optimal plans by transport maps T and uniqueness:
Let us start with defining the following function: Suppose $(x_1,x_2)\in\operatorname{supp}(\gamma_0)\subset\Omega\times\Omega$, where γ_0 is an optimal transport plan, that we know to exist from the previous item. Set:

$$\varphi:\operatorname{supp}(\mu_0)\to\mathbb{R},x\mapsto\inf_{\left(x_1^{(k)},x_2^{(k)}\right)_{k\in\{1,\dots,K\}}}\left\{\sum_{k=1}^{K}\left[\left|x_1^{(k-1)}-x_2^{(k)}\right|^2-\left|x_1^{(k)}-x_2^{(k)}\right|^2\right]\right\},\tag{1.11}$$

where the infimum is taken over all sequences $\left\{\left(x_1^{(k)},x_2^{(k)}\right)_{k\in\{1,\dots,K\}}\right\}\subset\operatorname{supp}(\gamma_0)$ with $x_1^{(0)}=x$, $\left(x_1^{(K)},x_2^{(K)}\right)=(x_1,x_2)$ and $K\in\mathbb{N}$. The intuition here is that for any $x_1\mapsto x_2$ in the graph of a candidate transport map, φ gives the cost difference for instead using the mapping that maps $x\mapsto x_2$. The various differences occur, due to taking into account the conservation of mass, that is intrinsic to the Wasserstein metric (if now $x_1^{(k-1)}\mapsto x_2^{(k)}$, $x_1^{(k)}$ does not need to map to $x_2^{(k)}$ anymore to produce the respective weight; note that components $x_{1,2}^{(k)}$ can show up several times in the sequence). Also

note the overall offset, ignoring the "initial cost" we would have needed to pay for $x_1 \mapsto x_2$.
Choosing specifically $\left(x_1^{(1)}, x_2^{(1)}\right) = (x_1, x_2)$, but leaving the rest of the sequence still optimised by the infimum, gives a comparison:

$$\varphi(x) - |x - x_2|^2 \leq \varphi(x_1) - |x_1 - x_2|^2 . \tag{1.12}$$

This holds for all x in $\operatorname{supp}(\mu_0)$, therefore characterising x_1 as a maximum of the first component (fixing the second one as the corresponding x_2) of the function $\operatorname{supp}(\gamma_0) \to \mathbb{R}, (x, x_2) \mapsto \varphi(x) - |x - x_2|^2$. This function is $L^1(\mu_0; \operatorname{supp}(\mu_0))$, as can be seen by choosing $K = 1$ and making use of the bounded second moment of $\mu_0 \in \mathscr{P}_2(\Omega)$. So for a specified $x_2 \in \operatorname{supp}(\mu_1)$ we have found a way of finding the corresponding $x_1 \in \operatorname{supp}(\mu_0)$ by solving $\operatorname{argmin}_{x \in \operatorname{supp}(\mu_0)} \left(|x - x_2|^2 - \varphi(x)\right)$. While for every optimal transport plan γ_0 the corresponding x_1 is among this set by construction (i.e. particularly the minimum exists and the set is non-empty) there could be overlaps between two of such sets for different parameters x_2. As will be shown next, however, this minimum is unique, therefore demonstrating both, existence of the transport map T and uniqueness:
Define $\varphi^+(x_2) := \min_{x \in \operatorname{supp}(\mu_0)} \left(|x - x_2|^2 - \varphi(x)\right) = |x_1 - x_2|^2 - \varphi(x_1)$ on $\operatorname{supp}(\mu_1)$ and notice $\forall x \in \operatorname{supp}(\mu_0)$:

$$\varphi^+(x_2) + \varphi(x) \leq |x - x_2|^2 = |x|^2 + |x_2|^2 - 2x \cdot x_2, \tag{1.13}$$

for the dot " $\cdot$ " being the common Euclidean product on Ω, or equivalently (again, existence of the maximum is ensured by the fact that $(x_1, x_2) \in \operatorname{supp}(\gamma_0)$):

$$\frac{|x_2|^2 - \varphi^+(x_2)}{2} = \max_{x \in \operatorname{supp}(\mu_0)} \left(x \cdot x_2 - \frac{|x|^2 - \varphi(x)}{2} \right). \tag{1.14}$$

At the same time given $x_1 \in \operatorname{supp}(\mu_0)$: $\min_{x \in \operatorname{supp}(\mu_1)} \left(|x - x_1|^2 - \varphi^+(x)\right) = \varphi(x_1)$ by choosing $x = x_2$ (and equality in this case), which gives in the same way as above:

$$\frac{|x_1|^2 - \varphi(x_1)}{2} = \max_{x \in \operatorname{supp}(\mu_1)} \left(x_1 \cdot x - \frac{|x|^2 - \varphi^+(x)}{2} \right). \tag{1.15}$$

Thus, $x_2 \mapsto \frac{|x_2|^2 - \varphi^+(x_2)}{2}$ and $x_1 \mapsto \frac{|x_1|^2 - \varphi(x_1)}{2}$ are convex conjugates of each other and hence convex (see for instance [18, part 3] for an overview on convex conjugation). But then also $x \mapsto |x - x_2|^2 - \varphi(x)$ must be convex, which implies that the derivative exists almost everywhere in the Lebesgue sense [18, thm. 25.5](and due to absolute continuity also with respect to the marginals μ_0, μ_1). Hence we know that the minimiser of $x \mapsto |x - x_1|^2 - \varphi^+(x)$ is (almost everywhere) well-defined (i.e. unique). Furthermore, this transport map can be written as a gradient of a convex function (likewise for the

inverse):

$$\begin{aligned} \operatorname{supp}(\mu_0) \to \operatorname{supp}(\mu_1), x \mapsto T(x) &= x - \frac{1}{2}\nabla\varphi(x) = \nabla\left(\frac{|x|^2 - \varphi(x)}{2}\right) \quad (1.16) \\ \operatorname{supp}(\mu_1) \to \operatorname{supp}(\mu_0), x \mapsto T^{-1}(x) &= x - \frac{1}{2}\nabla\varphi^+(x) = \nabla\left(\frac{|x|^2 - \varphi^+(x)}{2}\right). \quad (1.17) \end{aligned}$$

The corresponding transport plan is given by: $\gamma_0 = (\mathbb{I} \times T)_{\#}\mu_0 = \left(T^{-1} \times \mathbb{I}\right)_{\#}\mu_1$. □

Some comments on the proof:

Remark 7. (Absolute continuity of the marginals, μ_0, μ_1)
The regularity assumption on the initial and final measures μ_0, μ_1 were only needed in the second part of the proof, about the existence of transport maps and uniqueness. For two counter-examples in case of singular measures, see below. If the regularity only holds for the initial measure μ_0 (or the final one, μ_1, respectively), then only the map T exists, but not its inverse (or only T^{-1} exists, but not T, respectively), i.e. T is not injective (just consider $\mu_1 = \delta$ as an example). On the other hand, the existence of an optimal transport plan γ_0 as such does not require this regularity.

Remark 8. (Optimality only depends on the support of the optimal transport plan γ_0)
First note that our intuition for eq. (1.11) is a pointwise intuition: The argument is about point-masses being redistributed within the support of the optimal transport plan. This intuition is valid, as we can always rather consider neighbourhoods $N_{x_1^{(k)}} \times N_{x_2^{(k)}} \subset \Omega \times \Omega$ of $\left(x_1^{(k)}, x_2^{(k)}\right)$ - due to continuity of the cost-function $|x_2 - x_1|^2$ in the integrand of the Wasserstein metric in eq. (1.2), the deviations from the pointwise view can be controlled by considering small enough neighbourhoods. Indeed, it turns out that a property called cyclical monotonicity of the set $\operatorname{supp}(\gamma_0)$ is sufficient (and necessary) for optimality of the transport plan γ_0. See [14, thm. 2.13] for more details. About, why the support of the transport plan is sufficient for deciding upon its optimality: While the integrand in eq. (1.2) is non-linear, the integral is linear with respect to the transport plan γ. Consequently, the minimum is achieved on the boundary, i.e. for each pair of measurable sets $N_{x_1^{(k)}} \times N_{x_2^{(k)}} \subset \operatorname{supp}(\gamma)$ either when all the mass $\mu_0\left(N_{x_1^{(k)}}\right)$ is moved to $N_{x_2^{(k)}}$ or if all the mass $\mu_1\left(N_{x_2^{(k)}}\right)$ is already fully supplied.

Remark 9. (Duality and Kantorovich potentials)
As indicated in the proof above, it is plausible to think of the function φ defined in eq. (1.11) as a cost for an optimal rearrangement of (point-) masses, if we impose that $(x, x_2) \in \operatorname{supp}(\gamma)$ for a given $x \in \operatorname{supp}(\mu_0)$, $x_2 \in \operatorname{supp}(\mu_1)$ (normalised to zero for the optimal plan). Given that its conjugate partner φ^+, which was introduced above in relation to φ^+: $\operatorname{supp}(\mu_1) \to \mathbb{R}, x \mapsto \varphi^+(x) := \min_{\tilde{x} \in \operatorname{supp}(\mu_0)}\left(|\tilde{x} - x|^2 - \varphi(\tilde{x})\right)$ can be characterised by:

$$\varphi^+(\tilde{x}) + \varphi(x) \leq |\tilde{x} - x|^2 \text{ with equality, iff } (x, \tilde{x}) \in \operatorname{supp}(\gamma_0) \quad (1.18)$$

for γ_0 an optimal plan. As φ is in $L^1(\mu_0; \mathrm{supp}(\mu_0))$ (see prove of thm. 6), $\varphi^+ \in L^1(\mu_1; \mathrm{supp}(\mu_1))$ and:

$$\int_{\Omega\times\Omega} |x_1 - x_2|^2 \, d\gamma_0(x_1, x_2) = \int_{\mathrm{supp}(\gamma_0)} |x_1 - x_2|^2 \, d\gamma_0(x_1, x_2) = \int_\Omega \varphi(x_1) \, d\mu_0(x_1) + \int_\Omega \varphi^+(x_2) \, d\mu_1(x_2), \tag{1.19}$$

where we made use of the equality-statement of the previous eq. (1.18) in the second equality. Likewise, if we only assume two functions $\varphi \in L^1(\mu_0; \mathrm{supp}(\mu_0))$, $\tilde{\varphi} \in L^1(\mu_1; \mathrm{supp}(\mu_1))$ are characterised by $\forall (x, \tilde{x}) \in \Omega \times \Omega$: $\tilde{\varphi}(\tilde{x}) + \varphi(x) \leq |\tilde{x} - x|^2$, then $\forall \gamma \in \Gamma(\mu_0, \mu_1)$:

$$\int_\Omega \varphi(x_1) \, d\mu_0(x_1) + \int_\Omega \tilde{\varphi}(x_2) \, d\mu_1(x_2) = \int_{\Omega\times\Omega} (\varphi(x_1) + \tilde{\varphi}(x_2)) \, d\gamma(x_1, x_2) \leq \int_{\Omega\times\Omega} |x_1 - x_2|^2 \, d\gamma(x_1, x_2). \tag{1.20}$$

Hence, due to uniqueness of the optimal transport plan γ_0, we can consider the problem:

$$\max_{\varphi, \tilde{\varphi}} \Bigg(\int_\Omega \varphi(x_1) \, d\mu_0(x_1) + \int_\Omega \tilde{\varphi}(x_2) \, d\mu_1(x_2) \Bigg| \\ \varphi \in L^1(\mu_0; \mathrm{supp}(\mu_0)), \tilde{\varphi} \in L^1(\mu_1; \mathrm{supp}(\mu_1)) : \forall (x, \tilde{x}) \in \Omega \times \Omega \colon \tilde{\varphi}(\tilde{x}) + \varphi(x) \leq |\tilde{x} - x|^2 \Bigg) \tag{1.21}$$

a dual problem to the minimisation of eq. (1.2) in the sense that:

$$W_2^2(\mu_0, \mu_1) = \text{eq. (1.21)}, \tag{1.22}$$

with equality being attained for φ, φ^+ as defined in the proof of thm. 6 above (particularly $\tilde{\varphi} = \varphi^+$ the conjugate partner of φ in the above sense is necessary).[1] Knowing the optimal transport plan γ_0 for the Wasserstein metric, gives the optimal functions φ, φ^+ (up to a constant), as it is only supported along the optimal transport map, which is given at the end of the proof of thm. 6. On the other hand, the optimal functions give the optimal transport map, which then gives the optimal transport plan. A pair of optimal functions (φ, φ^+) is known as *Kantorovich potentials*.

For some more heuristics about the role and where-from of these Kantorovich potentials, consider the following continuous analogy: Assume, there is a $s \in [0, 1]$, that allows for a smooth parametrisation along the support of the marginals μ_0, μ_1 (i.e. $\{(x_1(s), x_2(s)) | \, s \in [0, 1]\} = \mathrm{supp}(\mu_0) \times \mathrm{supp}(\mu_1)$ in a one-to-one fashion), such that $\forall s \in [0, 1]$ the pair is part of the optimal plan $(x_1(s), x_2(s)) \in \mathrm{supp}(\gamma_0)$.

[1] This is only unique up to a parameter $c \in \mathbb{R}$, as: (φ, φ^+) being optimal implies $(\varphi + c, \varphi^+ - c)$ also being optimal. Indeed, our definition in eq. (1.11) is somewhat asymmetric, as for $(x_1, x_2) \in \mathrm{supp}(\gamma_0)$: $\varphi(x_1) = 0 \neq |x_1 - x_2|^2 = \varphi^+(x_2)$.

Then

$$|x_2(s)-x_1(s)|^2 = |x_2(0)-x_1(0)|^2 + \int_0^s \frac{d}{d\tilde{s}} |x_2(\tilde{s})-x_1(\tilde{s})|^2 \, d\tilde{s} =$$

$$= \left(\int_0^s \partial_{x_1} |x_2(\tilde{s})-x_1(\tilde{s})|^2 \dot{x}_1(\tilde{s}) \, d\tilde{s} \right) +$$

$$+ \left(|x_2(0)-x_1(0)|^2 + \int_0^s \partial_{x_2} |x_2(\tilde{s})-x_1(\tilde{s})|^2 \dot{x}_2(\tilde{s}) \, d\tilde{s} \right), \tag{1.23}$$

which we could consider a continuous version of $|x_1 - x_2|^2 = \varphi(x_1) + \varphi^+(x_2)$. Then $\varphi(x) = \int_0^{s(x)} \partial_{x_1} |x_2(\tilde{s})-x_1(\tilde{s})|^2 \dot{x}_1(\tilde{s}) \, d\tilde{s}$ for $s(x) \in [0,1]$ the parameter, such that $x(s(x)) = x$ and:

$$x_1 - \frac{1}{2}\nabla\varphi(x_1) = x_1 - \frac{1}{2}\partial_{x_1}\left(|x_2-x_1|^2\right) \cdot \dot{x}_1 s'(x_1) = x_1 - \frac{2x_1-2x_2}{2} \cdot 1 = x_2 \tag{1.24}$$

in line with our result in the proof of thm. 6 for the optimal transport map $T(x) = x - \frac{1}{2}\nabla\varphi(x)$. The additional offset for $\varphi^+(x) = \left(|x_2(0)-x_1(0)|^2 + \int_0^{s(x)} \partial_{x_2} |x_2(\tilde{s})-x_1(\tilde{s})|^2 \dot{x}_2(\tilde{s}) \, d\tilde{s}\right)$ vanishes in the derivative, of course, giving a similar result for T^{-1}.

Example 10. (Non-existence of a transport map for singular measures)
Consider $\Omega = \mathbb{R}$ with $\mu_0(x) = \delta(x)$, $\mu_1(x) = \frac{1}{2}(\delta(x-1) + \delta(x+1))$, then both $(0,1)$ and $(0,-1)$ have to be in the support of any admissible transport plan γ, which makes the existence of a transport plan $\text{supp}(\mu_0) \to \text{supp}(\mu_1), x \mapsto T(x)$ impossible. On the other hand, a reverse map from μ_1 to μ_0 happens to exist (abusing notation): $\text{supp}(\mu_1) \to \text{supp}(\mu_0), x \mapsto T^{-1}(x) = 0$. The induced transport plan is indeed the only admissible plan and therefore optimal to both, the original and the reverse problem.

Example 11. (Non-uniqueness for singular measures)
Consider $\Omega = \mathbb{R}^2$ with

$$\mu_0(x) = \frac{1}{2}\left(\delta\left(x - \begin{pmatrix} 1 \\ 1 \end{pmatrix}\right) + \delta\left(x + \begin{pmatrix} 1 \\ 1 \end{pmatrix}\right)\right) \tag{1.25}$$

and

$$\mu_1(x) = \frac{1}{2}\left(\delta\left(x - \begin{pmatrix} 1 \\ -1 \end{pmatrix}\right) + \delta\left(x + \begin{pmatrix} 1 \\ -1 \end{pmatrix}\right)\right), \tag{1.26}$$

then, due to symmetry, there are two possible (and optimal) transport maps: Either clockwise or anticlockwise rotation around the origin by 90°. In fact, there are also transport plans, that are optimal but not induced by a map, like for instance $\gamma(x) = \mu_0(x) \times \mu_1(x)$, which distributes $1/4$

weight from each point in $\mathrm{supp}(\mu_0)$ to each point in $\mathrm{supp}(\mu_1)$.

1.3 Interpolations scheme and gradient flows

Constant-speed geodesics Knowing about the existence of a transport map from $\mathrm{supp}(\mu_0)$ to $\mathrm{supp}(\mu_1)$ we can define intermediate measures μ_t, $t \in [0,1]$, by interpolating between two points $x_1 \in \mathrm{supp}(\mu_0)$, $x_2 \in \mathrm{supp}(\mu_1)$ in their support. Constant-speed geodesics do this by moving equal parts of the total length $|x_2 - x_1|$ and of the total parameter interval $[0,1]$, i.e.:

Definition 12. (Constant-speed geodesics)
An interpolation $[0,1] \to \Omega, t \mapsto x(t)$, that connects $x(0) \in \Omega$ with $x(1) \in \Omega$, is called *constant-speed geodesic*, iff $\forall 0 \leq t_1 \leq t_2 \leq 1$:

$$|x(t_2) - x(t_1)| = (t_2 - t_1) \cdot |x(1) - x(0)|. \tag{1.27}$$

Note that this does not mean that, comparing the constant-speed geodesics of two different pairs of start- and end-points, the speed is the same - masses of μ_0, starting from different locations typically move with different speed, but constant in time. Also note that by the triangle inequality of $|.|$, it is sufficient in eq. (1.27) to only have an inequality " $\leq$ ": Let

$$\{t_k \in [0,1] | \, k \in \{0,1,\ldots,K\}, t_0 = 0, t_K = 1, t_{k-1} < t_k, K \in \mathbb{N}\} \tag{1.28}$$

be an arbitrary partition of the time interval $[0,1]$, then:

$$|x(1) - x(0)| \leq \sum_{k=1}^{K} [|x(t_k) - x(t_{k-1})|] \leq |x(1) - x(0)| \sum_{k=1}^{K} [t_k - t_{k-1}] = |x(1) - x(0)|. \tag{1.29}$$

Furthermore $\forall 0 \leq t_1 \leq t_2 \leq t_3 \leq 1$:

$$\begin{aligned} |x(t_3) - x(t_1)| = (t_3 - t_1)\,|x(1) - x(0)| = (t_3 - t_2 + t_2 - t_1)\,|x(1) - x(0)| = \\ = |x(t_3) - x(t_2)| + |x(t_2) - x(t_1)| \end{aligned} \tag{1.30}$$

and therefore $\forall t_2 \in [t_1, t_3] \subset [0,1]$ $x(t_2)$ is a minimiser of $\min_{x \in \Omega} (|x(t_3) - x| + |x - x(t_1)|)$. In this sense, a constant-speed geodesic is an optimal path between its two endpoints. While these properties are of more general nature, in the Euclidean context, it is easy to write down the constant-speed geodesic $x(t)$, that connects x_1 with x_2, explicitly: $[0,1] \to \Omega, t \mapsto x(t) = (1-t)\,x_1 + t x_2$.

Intermediate measures μ_t, that connect μ_0 with μ_1, can now be defined via push-forward:

$$[0,1] \to \mathscr{P}_2(\Omega), t \mapsto \mu_t = ((1-t)\,\mathbb{I} + tT)_{\#}\,\mu_0 = \left(\mathbb{I} - \frac{t}{2}\nabla\varphi\right)_{\#} \mu_0, \tag{1.31}$$

where φ is the Kantorovich potential of the "full" problem, i.e. of $W_2(\mu_0, \mu_1)$. This definition has the beneficial property that it itself is a constant-speed geodesic between μ_0 and μ_1 with respect to the Wasserstein metric. This can be seen as follows:

$$W_2^2(\mu_0, \mu_t) \leq \int_\Omega \left| x_1 - \left(x_1 - \frac{t}{2} \nabla\varphi(x_1) \right) \right|^2 d\mu_0(x_1) = t^2 \int_\Omega \left| \frac{1}{2} \nabla\varphi(x_1) \right|^2 d\mu_0(x_1) =$$
$$= t^2 W_2^2(\mu_0, \mu_1), \tag{1.32}$$

where the last step follows from $T(x) = x - \frac{1}{2}\nabla\varphi$ being an optimal map of $\Gamma(\mu_0, \mu_1)$. This means that there is actually even an equality in eq. (1.32) and consequently $x \mapsto T_t(x) = x - \frac{t}{2}\nabla\varphi(x)$ is already the optimal map between $\operatorname{supp}(\mu_0)$ and $\operatorname{supp}(\mu_t)$.

Furthermore, we can consider any partition in time without changing the intermediate measures, that we get based on eq. (1.31), i.e.: For any intermediate time $t_1 \in [0,1]$ we can consider the intermediate measure connecting μ_0 and μ_{t_1} and see that the graph is (up to linear rescaling of time) a subset of the graph between μ_0 and μ_1 (likewise between μ_{t_1} and μ_1):

$$\mu_t = \begin{cases} \left(\mathbb{I} - \frac{\tilde{t}}{2} \nabla\varphi_{0 \to t_1} \right)_\# \mu_0 = \left(\mathbb{I} - \frac{\tilde{t}t_1}{2} \nabla\varphi \right)_\# \mu_0 & \forall \tilde{t} \in [0,1] : \tilde{t}t_1 = t \\ \left(\left(\mathbb{I} - \frac{\tilde{t}}{2} \nabla\varphi_{t_1 \to 1} \right) \circ \left(\mathbb{I} - \frac{t_1}{2} \nabla\varphi \right) \right)_\# \mu_0 = \left(\mathbb{I} - \frac{t_1}{2} \nabla\varphi - \frac{(1-t_1)\tilde{t}}{2} \nabla\varphi \right)_\# \mu_0 & \\ & \forall \tilde{t} \in [0,1] : \tilde{t} + (1-\tilde{t}) t_1 = t, \end{cases} \tag{1.33}$$

where the intermediate Kantorovich potentials $\varphi_{s \to t}$ (i.e. the Kantorovich potentials for the transition between μ_s and μ_t, $0 \leq s < t \leq 1$) are characterised by:

$$\nabla\varphi_{s \to t} \left(\mathbb{I} - \frac{s}{2} \nabla\varphi \right) = (t-s) \nabla\varphi. \tag{1.34}$$

Note that, while this looks dependent on the absolute time, it only depends on the time difference $s - 0$ to the startpoint in time of the reference potential $\varphi = \varphi_{0 \to 1}$ as well as the timespan $t - s$. This way it is ensured that for any two points in time, $0 \leq s < t \leq 1$, the speed of the transition

$$t \mapsto x(t) = (1-t) x(0) + t T(x(0)) = x(0) - \frac{t}{2} \nabla\varphi(x(0)) \tag{1.35}$$

between $\operatorname{supp}(\mu_0)$ and $\operatorname{supp}(\mu_1)$ is given by:

$$\begin{aligned} \frac{x(t) - x(s)}{t - s} &= -\frac{1}{2} \nabla\varphi(x(0)) = -\frac{1}{2} \nabla\varphi_{s \to s+1}(x(s)) \\ &= -\frac{1}{2} \frac{\nabla\varphi_{s \to t}(x(s))}{t - s}. \end{aligned} \tag{1.36}$$

For the rest of this section, we will mostly need the quantity $\nabla\varphi_{s \to s+1}$, which by the previous equation

is characterised by as the slope of $t \mapsto x(t)$.

Derivation of the Benamou-Brenier formula This eq. (1.36) already hints at considering $\nabla\varphi$ the tangent vectors along the transport process μ_t — to make this more clear, we first take a closer look at the connection between $\nabla\varphi$ and the continuity equation and then complete the link to the Benamou-Brenier formula in thm. 5: We consider $\mu_t = (x(t))_{\#}\mu_0$ for $t \in [0,1]$ just as defined above and get $\forall f \in C_0^\infty(\Omega)$ (i.e. in the distributional sense):

$$\begin{aligned}
\frac{d}{dt}\int_\Omega f(x)\,d\mu_t(x) &= \frac{d}{dt}\int_\Omega f(x(t))\,d\mu_0(x) = \int_\Omega \nabla f(x(t))\cdot\dot{x}(t)\,d\mu_0(x) = \\
&= \int_\Omega \nabla f(x(t))\cdot\left(-\frac{1}{2}\nabla\varphi(x)\right)d\mu_0(x) = \\
&= \int_\Omega \nabla f(x)\cdot\left(-\frac{1}{2}\nabla\varphi(x_{-t}(x))\right)d\mu_t(x), \qquad (1.37)
\end{aligned}$$

where x_{-t} shall be the inverse of $x(t)$ understood as a function of the starting point $x(0)$ for a fixed time t, i.e. the inverse of: $\operatorname{supp}(\mu_0) \to \operatorname{supp}(\mu_1), x \mapsto (1-t)x + tT(x)$. If we now define the flux v_t to be equal to

$$v_t(x) = -\frac{1}{2}\nabla\varphi(x_{-t}) = -\frac{1}{2}\nabla\varphi_{t\to t+1}(x), \qquad (1.38)$$

we recover exactly the continuity equation (1.9) in the distributional sense: $\frac{d}{dt}\int f(x)\,d\mu_t(x) = \int \nabla f(x)\cdot v_t(x)\,d\mu_t(x)$ (for any smooth test function $f \in C_0^\infty(\Omega)$). Thus, for $t \mapsto \mu_t$ being a constant-speed geodesic on the Wasserstein space (i.e. $\mathscr{P}_2(\Omega)$ equipped with the Wasserstein metric W_2), the pair $\left(\mu_t, -\frac{1}{2}\nabla\varphi_{t\to t+1}\right)$ solves the continuity equation.

Note that we saw in eq. (1.32) in combination with eq. (1.33) that the transport map $\mathbb{I} - \frac{\delta t}{2}\nabla\varphi_{t\to t+1}$ is optimal in $\Gamma(\mu_t, \mu_{t+\delta t})$(for some $\delta t \in [0, 1-t]$). Hence, thanks to eq. (1.30), again in combination with eq. (1.33), we can piece together the total cost $W_2(\mu_0,\mu_1)$ by adding up all the individual costs of the time partition $\{0, \delta t, 2\delta t, \ldots, 1\}$ (for some small time increment $0 < \delta t \ll 1$, which is assumed to be a divisor of 1 here) along the geodesic $t \mapsto \mu_t$. This gives:

$$\begin{aligned}
W_2(\mu_0,\mu_1) &= \sum_{k=0}^{(1-\delta t)/\delta t}\left[W_2\left(\mu_{k\delta t}, \mu_{(k+1)\delta t}\right)\right] = \\
&= \sum_{k=0}^{(1-\delta t)/\delta t}\left[\delta t\sqrt{\int_\Omega \left|\frac{1}{2}\nabla\varphi_{k\delta t\to k\delta t+1}(x)\right|^2 d\mu_{k\delta t}(x)}\right] \xrightarrow{\delta t\searrow 0} \int_0^1 |\dot{\mu}_t|\,dt = \\
&= \int_0^1 \left\|\frac{1}{2}\nabla\varphi_{t\to t+1}\right\|_{L^2(\mu_t;\Omega)} dt = \int_0^1 \|v_t\|_{L^2(\mu_t;\Omega)}\,dt, \qquad (1.39)
\end{aligned}$$

where in the second line, we passed to the limit $\delta t \searrow 0$ and used the definition of the metric derivative $|\dot{\mu}_t| = \lim_{\delta t \to 0} \frac{W_2(\mu_{t+\delta t}, \mu_t)}{|\delta t|}$ (see [9, Thm. 1.1.2] for an introduction). Here the existence of the limit is clear from the fact that the right hand side of the equation does not depend on δt (as long as we stay on the geodesic, all partitions give the same result) and the substitution $k\delta t = t$ holds by definition. Note that for a general measure-flux-combination (μ_t, v_t), that solves the continuity equation (1.9), only $|\dot{\mu}_t| \leq \|v_t\|_{L^2(\mu_t;\Omega)}$ holds, but if $t \mapsto \mu_t$ is the constant-speed geodesic, then even equality is true. For any other pair $(\mu_t, v_t) \in \mathscr{P}_2(\Omega) \times L^2(\mu_t; \Omega)$ solving eq. (1.9), we get the inequality: $W_2(\mu_0, \mu_1) \leq \int_0^1 \|v_t\|_{L^2(\mu_t;\Omega)} dt$ (see [9, Thm. 8.3.1]), which gives one version of the Benamou-Brenier formula (see for instance [14, Prop. 3.30] or [15, Thm. 8.1]). By contrast, in Benamou and Brenier's original paper [17, Prop. 1.1] as well as in our version of thm. 5 we have also the L^2-norm with respect to time: As for the non-optimal cases, this is a consequence of Jensen's inequality ($-\sqrt{(.)}$ is convex and the Lebesgue measure is a probability measure on the unit-interval). As for the constant-speed geodesics, note that, if μ_t is a constant-speed geodesic with respect to the Wasserstein metric W_2, then it is also a constant-speed geodesic with respect to the "metric"[2]: $\frac{W_2^2(\mu_s,\mu_t)}{|t-s|}$ for $t \neq s$ and zero otherwise. This is a general property of constant-speed geodesics and becomes apparent as follows: $\forall 0 \leq s < t \leq 1:$

$$\frac{W_2^2(\mu_s, \mu_t)}{|t-s|} = (t-s) W_2^2(\mu_0, \mu_1) = (t-s) \frac{W_2^2(\mu_0, \mu_1)}{|1-0|} \tag{1.40}$$

and for $s = t$ the equality holds trivially. So analogue to eq. (1.39) we then get:

$$\begin{aligned} \frac{W_2^2(\mu_0, \mu_1)}{|1-0|} &= \sum_{k=0}^{(1-\delta t)/\delta t} \left[\frac{W_2^2\left(\mu_{k\delta t}, \mu_{(k+1)\delta t}\right)}{\delta t} \right] = \\ &= \sum_{k=0}^{(1-\delta t)/\delta t} \left[\delta t \int_\Omega \left| \frac{1}{2} \nabla \varphi_{k\delta t \to k\delta t+1}(x) \right|^2 d\mu_{k\delta t}(x) \right] \xrightarrow{\delta t \searrow 0} \\ &\xrightarrow{\delta t \searrow 0} \int_0^1 \left\| \frac{1}{2} \nabla \varphi_{t \to t+1} \right\|^2_{L^2(\mu_t;\Omega)} dt. \end{aligned} \tag{1.41}$$

Hence, we have verified thm. 5. In contrast to the def. 1 of the Wasserstein metric, the actual minimisation is only on a local scale in time t. Nonetheless, the macroscopical perspective is still present in the shape of the boundary conditions μ_0, μ_1 of the continuity condition, and particularly in the optimal flux $-\frac{1}{2}\nabla\varphi_{t\to t+1}$, where $\varphi_{t\to t+1}$ is a Kantorovich potential of the respective Wasserstein metric. In the examples, we will consider later on, this Kantorovich potential is indeed related to the thermodynamic entropy of the physical systems of interest. To conclude on the Benamou-Brenier formula, note that

[2] While symmetry and positive definiteness are clear, for the triangle inequality keep in mind that this quantity is only defined on the geodesics (with respect to W_2)(so the time parameter makes sense), so even equality holds $\forall 0 \leq t_1 < t_2 < t_3 \leq 1: \frac{W_2^2(\mu_{t_1},\mu_{t_2})}{|t_2-t_1|} + \frac{W_2^2(\mu_{t_2},\mu_{t_3})}{|t_3-t_2|} = ((t_2-t_1)+(t_3-t_2)) W_2^2(\mu_0,\mu_1) = \frac{W_2^2(\mu_{t_3},\mu_{t_1})}{|t_3-t_1|}$.

the expression (1.41) can be generalised to also be valid on different time intervals $[0,\tau]$ than just the unit interval $[0,1]$. Along the same arguments as above, we then get (see [17] for full details):

$$W_2^2(\mu_0,\mu_\tau) = \tau \cdot \int_0^\tau \left\| \frac{1}{2}\nabla\varphi_{t\to t+1} \right\|^2_{L^2(\mu_t;\Omega)} dt. \tag{1.42}$$

Tangent spaces on the space of square integrable probability measures Given a pair $(\mu_t, v_t) \in \mathscr{P}_2(\Omega) \times L^2(\mu_t;\Omega)$, which solves the continuity equation, there is a whole equivalence class of fluxes, that also solve the continuity equation with the same evolution $t \mapsto \mu_t$. This is, as, for a given evolution $t \mapsto \mu_t$, eq. (1.9) only defines v_t up to an additive term $w_t \in L^2(\mu_t;\Omega)$, for which it holds: $\forall t \in [0,1] : 0 = \operatorname{div}(\mu_t w_t)$ (in the distributional sense, i.e. $\forall f \in C_0^\infty(\Omega,\mathbb{R}) : 0 = \int_\Omega (\nabla f(x)) \cdot w_t(x)\, d\mu_t(x)$). Now fix a point in time $t \in [0,1]$. The functional $\|.\|^2_{L^2(\mu_t;\Omega)}$ is convex and thus allows to uniquely single out one solution v_t from the equivalence class of admissible fluxes, by considering its minimum. This minimum can be characterised as follows: Let $v_t \in L^2(\mu_t;\Omega)$ be the minimiser, then we want to show, it is the limit (in $L^2(\mu_t;\Omega)$ sense) of a sequence of gradients of $C_0^\infty(\Omega)$ functions, ∇f. We know $\|v_t + w_t\|_{L^2(\mu_t;\Omega)} \geq \|v_t\|_{L^2(\mu_t;\Omega)}$ holds $\forall w_t \in L^2(\mu_t;\Omega) : 0 = \operatorname{div}(\mu_t w_t)$. We can require equivalently

$$\left| \left\langle v_t, \frac{w_t}{\|w_t\|_{L^2(\mu_t;\Omega)}} \right\rangle_{L^2(\mu_t;\Omega)} \right| \leq \frac{1}{2}\|w_t\|_{L^2(\mu_t;\Omega)} \tag{1.43}$$

$\forall w_t \in L^2(\mu_t;\Omega) : 0 = \operatorname{div}(\mu_t w_t), w_t \not\equiv 0$ and thus equivalently again:

$$\langle v_t, w_t\rangle_{L^2(\mu_t;\Omega)} = 0 \qquad \forall w_t \in L^2(\mu_t;\Omega) : 0 = \operatorname{div}(\mu_t w_t). \tag{1.44}$$

If v_t is of the shape ∇f for $f \in C_0^\infty(\Omega)$ (or a limit of such gradients), then this eq. (1.44) clearly holds. Also the converse is true, as the following consideration shows: Assume (for contradiction), v_t is not approximable in $L^2(\mu_t;\Omega)$ by gradients of test functions $f \in C_0^\infty(\Omega)$, i.e.

$$\delta f_t := \inf\left\{ \|v_t - \nabla f\|_{L^2(\mu_t;\Omega)} \,\middle|\, f \in C_0^\infty(\Omega) \right\} > 0. \tag{1.45}$$

Let $(f_n)_n \subset C_0^\infty(\Omega)$ be a minimizing sequence in the sense of $\lim_{n\to\infty}\left(\|v_t - \nabla f_n\|_{L^2(\mu_t;\Omega)}\right) = \delta f_t$ and define the difference $v_{t,n} := v_t - \nabla f_n \in L^2(\mu_t;\Omega)$. But then: $\inf\left\{ \|v_{t,n} - \nabla f\|_{L^2(\mu_t;\Omega)} \,\middle|\, f \in C_0^\infty(\Omega) \right\} = \inf\left\{ \|v_t - \nabla(f_n + f)\|_{L^2(\mu_t;\Omega)} \,\middle|\, f \in C_0^\infty(\Omega) \right\} = \delta f_t$ and we can continue along the argument from eq. (1.43): $\lim_{n\to\infty}\left(\|v_{t,n} - \nabla f\|_{L^2(\mu_t;\Omega)} - \|v_{t,n}\|_{L^2(\mu_t;\Omega)}\right) \geq 0$ holds $\forall f \in C_0^\infty(\Omega)$ and thus implies: $\lim_{n\to\infty}\left(\langle v_{t,n}, \nabla f\rangle_{L^2(\mu_t;\Omega)}\right) = 0$, again for all smooth functions of bounded support. Hence: $\lim_{n\to\infty}(\operatorname{div}(\mu_t v_{t,n})) = 0$. Notice that for all $n \in \mathbb{N}$: $\|\nabla f_n\|_{L^2(\mu_t;\Omega)} \leq \delta f_t + \|v_t\|_{L^2(\mu_t;\Omega)} < \infty$

and thus $(\nabla f_n)_n$, weakly converges (upon possibly stripping it down to a subsequence without relabelling). This implies $v_{t,n}$ also converges weakly to some $v_{t,0} \in L^2(\Omega)$, for which also $\forall f \in C_0^\infty$: $\langle v_{t,0}, \nabla f\rangle_{L^2(\mu_t;\Omega)} \xleftarrow{n\to\infty} \langle v_{t,n}, \nabla f\rangle_{L^2(\mu_t;\Omega)} \xrightarrow{n\to\infty} 0$ and consequently $\operatorname{div}(\mu_t v_{t,0}) = 0$. This means, though, we can insert $v_{t,0}$ for w_t in eq. (1.44) above, giving:

$$\begin{aligned}\langle v_t, v_{t,0}\rangle_{L^2(\mu_t;\Omega)} &= \langle v_{t,n}, v_{t,0}\rangle_{L^2(\mu_t;\Omega)} + \langle \nabla f_n, v_{t,0}\rangle_{L^2(\mu_t;\Omega)} \xrightarrow{n\to\infty} \langle v_{t,0}, v_{t,0}\rangle_{L^2(\mu_t;\Omega)} = \\ &= \lim_{n\to\infty}\left(\|v_{t,n}\|^2_{L^2(\mu_t;\Omega)}\right) = (\delta f_t)^2 > 0 \end{aligned} \tag{1.46}$$

in contradiction to eq. (1.44).

Hence, we found the equivalence that allows us to characterise what we (formally) call the tangent space to the probability space $(\mathscr{P}_2(\Omega), W_2)$ at a point μ:

$$\begin{aligned}\operatorname{Tan}_\mu(\mathscr{P}_2(\Omega), W_2) &:= \overline{\{\nabla f |\, f \in C_0^\infty(\Omega)\}}^{L^2(\mu;\Omega)} = \\ &= \left\{ v \in L^2(\mu;\Omega) \middle|\, \forall w \in L^2(\mu;\Omega), \operatorname{div}(w\mu) = 0 : \langle v, w\rangle_{L^2(\mu;\Omega)} = 0 \right\}. \end{aligned} \tag{1.47}$$

Note that both definitions are totally independent of the evolution $t \mapsto \mu_t$, but can be applied pointwise for each $\mu \in \mathscr{P}_2(\Omega)$. Nonetheless, the minimiser of the norm $\left\| \|v_t\|_{L^2(\mu_t;\Omega)} \right\|_{L^2([0,1])}$, given (μ_t, v_t) validate the continuity equation (1.9), (therefore, according to the Benamou-Brenier formula (1.8), along the optimal transport between μ_0 and μ_1) is also part of the tangent space $\operatorname{Tan}_{\mu_t}(\mathscr{P}_2(\Omega), W_2)$ at each respective point μ_t. For the examples we consider in the next sections, we will later give a probabilistic motivation for using the minimal L^2-norm as well.

Gradient flows along constant-speed geodesics We eventually turn towards gradient flows with respect to the Wasserstein metric: We want to express the evolution $t \mapsto \mu_t$ along the constant-speed geodesic in the shape of a gradient flow like in eq. (1). We already know from the Benamou-Brenier formulation that μ_t satisfies: $\frac{d}{dt}\mu_t = -\operatorname{div}\left(\mu_t\left(-\frac{1}{2}\nabla\varphi_{t\to t+1}\right)\right)$. We will now show, how this heuristically relates to minimising movements along some (smooth, non-negative) energy potential $\mathcal{E} : \mathscr{P}_2(\Omega) \to \mathbb{R}_0^+$, i.e. the time-discrete dynamics recursively defined via (see [9, Ch. 2] for more details):

$$\mu_{t+\delta t} \in \operatorname{argmin}_\mu \left(\mathcal{E}(\mu) + \frac{W_2^2(\mu, \mu_t)}{2\delta t} \right) \tag{1.48}$$

in the limit of the timestep $\delta t \searrow 0$. First, for simplicity, we restrict ourselves to measures absolutely continuous with respect to the Lebesgue measure $d\mu_t = \rho_t dx$. Second, we focus on perturbations along the optimal path, i.e. along $\left(\mathbb{I} - \frac{\epsilon}{2}\nabla\varphi_{t\to t+\delta t}\right)_{\#}\mu_{t+\delta t} = \rho_{t+\delta t}\left(\mathbb{I} - \frac{\epsilon}{2}\nabla\varphi_{t\to t+\delta t}\right)dx$. In other words, we look for $\rho_{t+\delta t}$, which is optimal in the sense that, given the transition from ρ_t to $\rho_{t+\delta t}$ (and therefore determining the corresponding Kantorovich potential $\varphi_{t\to t+\delta t}$), a perturbation along

$\nabla\varphi_{t\to t+\delta t}$ is suboptimal. Such a perturbation changes the density by the increment $d\rho_t = \frac{d\rho_t}{dt}dt$, but the function $x \mapsto \nabla\varphi_{t\to t+\delta t}(x)$ stays the same, as long as we stay on the same constant-speed geodesic $t \mapsto x(t) = x(0) - \frac{t}{2}\nabla\varphi_{t\to t+\delta t}(x(0))$, which was exactly the path along which we perturbed the measure. Hence, on a purely formal level, we get as optimality condition of eq. (1.48) (for $\mathcal{E}(\mu_t) = \int_\Omega \tilde{\mathcal{E}}(\rho_t(x))\,dx$ and $\tilde{\mathcal{E}} : \mathbb{R}_0^+ \to \mathbb{R}_0^+$; note $\mathcal{E}$ as a functional has no explicit time dependence, but only depends on μ_t as a measure on Ω):

$$
\begin{aligned}
0 &= \left\langle \mathcal{DE}(\mu_t), \frac{d\rho_t}{dt} \right\rangle_{L^2(\Omega)} + \frac{\frac{d}{d(\delta t)} W_2^2(\mu_{t+\delta t}, \mu_t)}{2\delta t} = \\
&= \left\langle \mathcal{DE}(\mu_t), \frac{d\rho_t}{dt} \right\rangle_{L^2(\Omega)} + \frac{\int_t^{t+\delta t} \left\| \frac{1}{2}\nabla\varphi_{\tilde{t}\to\tilde{t}+1} \right\|^2_{L^2(\mu_{\tilde{t}};\Omega)} d\tilde{t} + \delta t \left\| \frac{1}{2}\nabla\varphi_{t\to t+1} \right\|^2_{L^2(\mu_t;\Omega)}}{2\delta t} = \\
&= \left\langle \mathcal{DE}(\mu_t), \frac{d\rho_t}{dt} \right\rangle_{L^2(\Omega)} + \frac{2\delta t \left\langle \frac{1}{2}\nabla\varphi_{t\to t+1}, \rho_t \frac{1}{2}\nabla\varphi_{t\to t+1} \right\rangle_{L^2(\Omega)} + o(\delta t)}{2\delta t} \xrightarrow{\delta t \searrow 0} \\
&\xrightarrow{\delta t \searrow 0} \left\langle \mathcal{DE}(\mu_t), \frac{d\rho_t}{dt} \right\rangle_{L^2(\Omega)} - 2 \cdot \frac{\left\langle \frac{1}{2}\varphi_{t\to t+1}, \frac{d\rho_t}{dt} \right\rangle_{L^2(\Omega)}}{2} = \left\langle \mathcal{DE}(\mu_t) - \frac{1}{2}\varphi_{t\to t+1}, \frac{d\rho_t}{dt} \right\rangle_{L^2(\Omega)},
\end{aligned}
\tag{1.49}
$$

where we used the Benamou-Brenier formulation of the Wasserstein metric from eq. (1.42) together with the continuity equation for ρ_t and the corresponding optimal flux $v_t = -\frac{1}{2}\nabla\varphi_{t\to t+1}$. Hence, as far as its projection on the optimal path is concerned, the variational derivative $\mathcal{DE}(\mu_t)$ can be identified with the Kantorovich potential $\frac{1}{2}\varphi_{t\to t+1}$ (up to a prefactor). Thus, the continuity equation then reads: $\frac{d}{dt}\rho_t = -\mathrm{div}(\rho_t(-\nabla\mathcal{DE}(\mu_t))) = -\mathcal{K}(\rho_t)\,\mathcal{DS}(\rho_t)$, in the notation of eq. (1), for $\mathcal{S}(\rho) = \mathcal{E}(\mu)$ being the entropy and $\mathcal{K}(\rho)(.) = -\mathrm{div}(\rho_t(\nabla(.)))$ being the thermodynamic metric of the Wasserstein space. Note that from a physical point of view, it is no problem to only know the potential $\mathcal{E}$ along the optimal path $t \mapsto \rho_t$, as this is the realised, observed path and we can not expect to gain information beyond this - except that the variational problem of eq. (1.48) admits its minimiser along this path. In fact, the restrictions to perturbations along the constant-speed geodesic amounts to the assumption that the potential $\mathcal{E}$ is "induced" by the Wasserstein metric W_2 in the sense that perturbations, that are (locally) suboptimal for the Wasserstein metric alone, are also suboptimal together with the potential $\mathcal{E}$. It therefore appears convenient to interpret $\mathcal{E}$ as a potential, that represents certain boundary conditions, that enforce a transport of the initial μ_0 to the final measure μ_1. Indeed, the physical perspective will typically rather be to give an initial state and the potential $\mathcal{E}$, that therefore allows to extrapolate the evolution into the future. In this spirit, it is the objective of the method proposed in the next sections to identify both, the metric $\mathcal{K}$ as well as the entropy $\mathcal{S}$, from experimental data.

A much more rigorous as well as more general framework can be established for gradient flows (see [14, Ch. 4] for a quick overview, [9] for a detailed and vast background and consider [9, Ch. 10], specifically [9, Lem. 10.4.1], for more rigorous versions of our statements above), for the purposes of

this text, it shall suffice to consider the above as an underlying motivation for studying thermodynamic metrics of the kind $\mathcal{K}(\rho)(.) = -\mathrm{div}(\rho \cdot \nabla(.))$.

2 Extracting the metric in the weighted Wasserstein case

Here we will take the "physical perspective" mentioned in the last paragraph of the previous section, namely that we want to use a (conveniently structured) set of measurements to predict the future evolution of a dynamical system. This amounts to finding a way for characterising the right hand side of the gradient flow equation (1). Particularly, for now, we want to focus on characterising the thermodynamic metric $\mathcal{K}$ for a certain type of transport processes, which extends the pure Wasserstein setting of the preceding section. This will be based on the method originally presented in [19] and uses the fluctuations on the mesoscopic scale in combination with Einstein's relation. Before we start with this, we first specify what type of processes can be treated by this approach, then describe and explain the method itself and close with presenting numerical evidence of its capabilities.

Note that we liberate ourselves from the notation (particularly concerning the indices) in the previous section. Also, for brevity, by the Wasserstein metric we always mean the L^2-Wasserstein metric.

2.1 Setting and motivation

This subsection introduces an overview over the setting and the main ideas and offers motivations for both. Setting and method will be explained in greater precision in the next subsection about the method.

Stochastic ODE version Before we introduce the setting for the main thm. 16, we first consider a simpler ODE version by considering a system, that does not depend on the space coordinate x (thus being an ODE version of the upcoming eq. (2.7)):

$$dX(t) = \mu \cdot dt + \sqrt{\sigma} \cdot dW, \tag{2.1}$$

where here dW is Gaussian time-white noise and μ, $\sqrt{\sigma}$ are scaling drift and standard deviation of the random variable X, respectively. We can think of $t \mapsto X(t)$ as a trajectory in $\mathbb{R}^d$ of a single particle, for instance, and the parameter σ can be extracted by computing the mean square displacement:

$$\sigma = \lim_{\delta t \searrow 0} \mathbb{E}\left[\frac{(X(t_0 + \delta t) - X(t_0))^2}{\delta t}\right] \cdot \frac{1}{d}. \tag{2.2}$$

Thm. 16 will follow along the same line by considering quadratic variations of, in its case, stochastic states ρ^ϵ. This greatly enhances the applicability, as we can work on a larger scale, considering particle densities rather than individual particles, and also allows for a wider class of stochastic processes to be evaluated. Moreover, just like X from eq. (2.1) being normally distributed, a large-deviations principle for its PDE counterpart is known on a formal level (and in several examples also rigorously)(see remark 13).

We will use eq. (2.2) in subsection 2.4 (then also referred to as particle tracking), in order to compare its performance to the outcomes of the new method based on thm. 16. Note, however, that this particle tracking is based on assumptions on the very particle level of the stochastic process and thus - a priori - only gives the particle diffusivity (i.e. σ for the Brownian motion of eq. (2.1)).

About the weighted Wasserstein metric Here we consider a slightly larger class of transport processes than the pure Wasserstein case, that generalises the setting of section 1 by allowing for an additional parameter, called mobility m. Such a setup was studied for example in [5] and [20] (in the context of zero-range processes; see subsection 2.3.2 later) and also comprises applications such as the porous medium equation ($\partial_t \rho = \Delta(\rho^n)$ for $n \in \mathbb{N}$) or thin-film-like equations ($\partial_t \rho = -\mathrm{div}(\rho^\alpha \nabla \Delta \rho)$ for $\alpha \in [0,1]$). The intuition behind this is that in contrast to the Benamou-Brenier formula, the dynamical cost for moving mass between two points in time is scaled non-linearly with respect to the local (in space and time) density $\rho(t,x)$ (see e.g. [20, eq. (13)]):

$$\tilde{W}_2(\rho(0,.),\rho(1,.)) = \inf_{\forall t:\, \rho(t,.)\in\mathscr{P}_2(\Omega)} \left\{ \sqrt{\int_0^1 \left\| \frac{\rho}{\sqrt{2m(\rho)}} v_t \right\|^2_{L^2(\Omega)} dt} \;\middle|\; \partial_t \rho = -\mathrm{div}(\rho v_t) \right\}. \tag{2.3}$$

Note that at positions and times, where the mobility $m(\rho(t,x))$ is large, the cost is low and vice versa. In fact, if we interpret v_t as a kind of velocity of a mass increment, then with $\sqrt{\frac{\rho}{2m(\rho)}}$ being the analogue of an inertial mass, the previous equation (2.3) could be understood as (minimising) the kinetic cost, when redistributing the mass, to get $\rho(1,.)$ from $\rho(0,.)$. For $2m(\rho) = \rho$ we recover the usual L^2-Wasserstein metric.

Assumptions We restrict ourselves to diffusive systems that exhibit a Gaussian stochasticity on the microscopic scale, but are deterministic on the macroscopic scale. To formulate this more precisely, let $\epsilon > 0$ be the parameter that translates between the microscopic level (finite ϵ) and the macroscopic level ($\epsilon = 0$). The microscopic state shall be called $\rho^\epsilon : \Omega \to R_0^+$, which we can consider non-negative $L^2(\Omega)$ functions for now, but will see later that measures on Ω can also be treated similarly. Let $\gamma \in C_0^\infty(\Omega, \mathbb{R})$ be a test function with compact support, then we assume:

- In a suitable sense of convergence $\rho^\epsilon \xrightarrow{\epsilon \searrow 0} \rho$ and ρ is a deterministic, macroscopic state that

evolves according to a gradient flow along the entropy $\mathcal{S}$ for a weighted Wasserstein metric, i.e.:

$$\partial_t \rho(t,x) = \operatorname{div}\left(m(\rho(t,x)) \nabla\left(\mathcal{DS}(\rho)(t,x)\right)\right) \tag{2.4}$$

for $m \in C^1\left(\mathbb{R}_0^+, \mathbb{R}_0^+\right)$ with $m(\rho) = 0 \iff \rho = 0$, being the so-called mobility. Thus, in the notation of eq. (1): $\mathcal{K}(\rho)(.) = -\operatorname{div}(m(\rho)\nabla(.))$. In the numerical considerations later on, we will only study finite-dimensional projections of this operator, but to establish (co-)domains of the full infinite-dimensional operator we can proceed along the lines this is done for the Laplace operator, i.e. we start with setting the domain to be the closure of the test function space $C_0^\infty(\Omega)$ with respect to the norm $\|.\|_{L^2(\Omega)} + \|\mathcal{K}(\rho)(.)\|_{L^2}$. As we will be interested in weak solutions only, we can make use of the Lax-Milgram theorem to extend the domain of $\mathcal{K}$ to functions in $H^1_{0;m} := W_0^{1,2}(m(\rho)\,dx;\Omega)$: The operator $\langle \nabla(.), m(\rho)\nabla(.)\rangle_{L^2(\Omega)}$ plays the role of the bilinear form (the analogon of the Dirichlet form in the Laplace case) in Lax-Milgram's theorem, which thus allows to characterise the weak version of the right hand side of eq. (2.4) via $\langle \nabla\gamma, m(\rho)\nabla\mathcal{DS}(\rho)\rangle_{L^2(\Omega)}$. The co-domain is given by the L^2-dual of $H^1_{0;m}$, i.e. $H^{-1}_{0;m}$.

- The stochastic fluctuations of the microscopic state, defined by

$$Y^\epsilon_\gamma(t) := \frac{1}{\sqrt{\epsilon}} \cdot \langle \gamma, \rho^\epsilon(t,.) - \rho(t,.)\rangle_{L^2(\Omega)}, \tag{2.5}$$

converge (in distribution) to macroscopic fluctuations Y, which satisfy the stochastic evolution equation:

$$dY_\gamma(t) = \langle \gamma, D(\rho)\, y(t,.)\, dt\rangle_{L^2(\Omega)} + \left\langle -\nabla\gamma, \sqrt{2m(\rho)}dW\right\rangle_{L^2(\Omega)}, \tag{2.6}$$

where dW is Gaussian space-time-white noise and D is a linear operator on the respective measure spaces (but possibly non-linear in the argument ρ) and $(t,x) \mapsto y(t,x)$ is the component of Y_γ with respect to γ (i.e. the weak limit of $y^\epsilon(t,x) := \frac{1}{\sqrt{\epsilon}} \cdot (\rho^\epsilon(t,x) - \rho(t,x))$). Note that eq. (2.6) describes an Ornstein-Uhlenbeck process, giving Gaussian fluctuations Y_γ for sufficiently smooth macroscopic states ρ.

Notice that the same quantity m shows up in both, the macroscopic eq. (2.4) as well as the stochastic part of eq. (2.6). This connection is at the heart of the so-called Einstein relation - see remark 15 for more details.

Remark 13. (Connection with large deviations)
If we neglect higher order terms in ϵ, fluctuation of the type of eq. (2.6) can be motivated by the following equation for ρ^ϵ:

$$d\rho^\epsilon(t,x) = \operatorname{div}\left(m(\rho^\epsilon)\nabla\left(\mathcal{DS}(\rho^\epsilon)\right)\right)dt + \sqrt{\epsilon}\cdot\operatorname{div}\left(\sqrt{2m(\rho^\epsilon)}dW\right), \tag{2.7}$$

where in our notation $\frac{1}{\sqrt{\epsilon}}\left(\operatorname{div}\left(m\left(\rho^{\epsilon}\right)\nabla\left(\mathcal{DS}\left(\rho^{\epsilon}\right)\right)\right)-\operatorname{div}\left(m\left(\rho\right)\nabla\left(\mathcal{DS}\left(\rho\right)\right)\right)\right)\xrightarrow{\epsilon\to 0}D\left(\rho\right)y$ is the first order term of the drift part of ρ^{ϵ}. Note that the existence of solutions of eq. (2.7) is not established, so this consideration is on a formal level only. Also note that such an eq. (2.7) does not necessarily have to be valid on the very microscopic level, but could also be an approximation on a mesoscopic scale, i.e. for small but finite $0<\epsilon\ll 1$. For this type of equations a large deviations principle is known (a variation of Schilder's theorem, see [21, Ch. 6]): In large deviations theory, the probability $\mathbb{P}\left[\rho^{\epsilon}\right]$ for a particular evolution $\rho^{\epsilon}\left(t,.\right)$ (with fixed initial and final state $\rho^{\epsilon}\left(0,.\right)$, $\rho^{\epsilon}\left(1,.\right)$) is characterised by an exponential function; roughly speaking it holds: $\mathbb{P}\left[\rho^{\epsilon}\right]\sim e^{-\frac{1}{\epsilon}I\left(\rho^{\epsilon}\right)}$, where the functional I in the exponent is referred to as rate functional. For a more precise formulation of the statement, see for instance [22]. For eq. (2.7) this rate functional reads:

$$I\left(\rho^{\epsilon}\right)=\frac{1}{2}\int_{0}^{1}\left\|\partial_{t}\rho^{\epsilon}\left(t,.\right)-\operatorname{div}\left(m\left(\rho^{\epsilon}\left(t,.\right)\right)\nabla\left(\mathcal{DS}\left(\rho^{\epsilon}\left(t,.\right)\right)\right)\right)\right\|_{wW\left(\rho^{\epsilon}\right)}^{2}dt, \tag{2.8}$$

where $\left\|.\right\|_{wW\left(\rho^{\epsilon}\right)}$ is a short-hand notation for a norm corresponding to our weighted Wasserstein case, namely:

$$\left\|\tilde{v}\right\|_{wW\left(\rho^{\epsilon}\right)}^{2}:=\inf_{\tilde{\tilde{v}}}\left\{\left\langle\tilde{\tilde{v}},\tilde{v}\right\rangle_{L^{2}(\Omega)}\middle|\quad\tilde{v}=-\operatorname{div}\left(2m\left(\rho^{\epsilon}\right)\nabla\left(\tilde{\tilde{v}}\right)\right)\right\}. \tag{2.9}$$

While the rate functional in eq. (2.8) was only formally derived above, rigorous results exist for several examples of classical particle processes like the ones we will study numerically later on (see subsection 2.3.2), namely independent Brownian particles (see [23]), zero-range processes (see [24]) and a symmetric simple-exclusion process (see [25]).

Note that due to the exponential structure of the way the probability $\mathbb{P}\left[\rho^{\epsilon}\right]$ is expressed, in the limit $\epsilon\to 0$ only those transitions ρ^{ϵ} have finite probability, for which $I\left(\rho^{\epsilon}\right)=0$, i.e. those, which satisfy: $\partial_{t}\rho^{\epsilon}\left(t,x\right)=\operatorname{div}\left(m\left(\rho^{\epsilon}\right)\nabla\left(\mathcal{DS}\left(\rho^{\epsilon}\right)\right)\right)$, which coincides with the deterministic gradient flow equation (2.4) or (1), respectively. To see this, note that in the notation of eq. (2.9) (i.e.: $\partial_{t}\rho^{\epsilon}\left(t,x\right)-\operatorname{div}\left(m\left(\rho^{\epsilon}\right)\nabla\left(\mathcal{DS}\left(\rho^{\epsilon}\right)\right)\right)=\tilde{v}=-\operatorname{div}\left(2m\left(\rho^{\epsilon}\right)\nabla\left(\tilde{\tilde{v}}\right)\right)$), given the condition for $\tilde{\tilde{v}}$, we have to minimise $\left\langle\tilde{\tilde{v}},\tilde{v}\right\rangle_{L^{2}(\Omega)}=\left\langle\sqrt{2m}\nabla\tilde{\tilde{v}},\sqrt{2m}\nabla\tilde{v}\right\rangle_{L^{2}(\Omega)}=\left\|\sqrt{2m}\nabla\tilde{\tilde{v}}\right\|_{L^{2}(\Omega)}^{2}\geq 0$, which is zero, if and only if $\sqrt{2m}\nabla\tilde{\tilde{v}}\equiv 0$ (up to a set of measure zero) in which case also $0=\tilde{v}=\partial_{t}\rho^{\epsilon}\left(t,x\right)-\operatorname{div}\left(m\left(\rho^{\epsilon}\right)\nabla\left(\mathcal{DS}\left(\rho^{\epsilon}\right)\right)\right)$. For an alternative way of seeing this, note the similarity of the rate functional I and eq. (2.3) for $\partial_{t}\rho^{\epsilon}=\tilde{v}$ and $\rho^{\epsilon}v_{t}=2m\nabla\tilde{\tilde{v}}$. In fact, if we only consider very short time intervals $0<\tau\ll 1$ instead of the interval $[0,1]$, then the weighted Benamou-Brenier formula eq. (2.3) gets an additional $\sqrt{\tau}$ coefficient just as in eq. (1.42). Hence, when we expand the rate functional in eq. (2.8), the term of the square of the

$\partial_t \rho$ can be expressed as:

$$\begin{aligned}
&\inf_{\rho^\epsilon}\left\{\frac{1}{2}\int_0^\tau \left\|\partial_t\rho^\epsilon(t,.)\right\|^2_{wW(\rho^\epsilon)}dt\,\middle|\quad \partial_t\rho^\epsilon(t,.)=-\mathrm{div}\left(\rho^\epsilon(t,.)\,v_t\right)\right\}=\\
&=\inf_{\rho^\epsilon}\left\{\frac{1}{2}\int_0^\tau \left\langle-\mathrm{div}\left(\rho^\epsilon(t,.)\,v_t\right),\tilde{v}\right\rangle_{L^2}dt\,\middle|\quad \partial_t\rho^\epsilon(t,.)=-\mathrm{div}\left(\rho^\epsilon(t,.)\,v_t\right)\right\}=\\
&=\frac{\tilde{W}_2^2\left(\rho(0,.),\rho(\tau,.)\right)}{2\tau},
\end{aligned}\tag{2.10}$$

which corresponds to the second term on the right hand side of the minimising movement scheme in eq. (1.48). Apart from ρ^ϵ being a heuristic quantity only, based on eq. (2.7), it might be questionable to only consider the infimum here: This is, as we are only interested in characterising an optimal path (i.e. minimising the rate functional in eq. (2.8)) for fixed initial and final states, $\rho^\epsilon(0,.)$ and $\rho^\epsilon(1,.)$, and it turns out a posteriori, that all other terms in the quadratic expansion are either constant or negligible: The mixed term in the expansion of eq. (2.8) gives $\frac{1}{2}\left(\mathcal{S}(\rho(\tau,.))-\mathcal{S}(\rho(0,.))\right)$, which represents the energy part $\mathcal{E}$ in eq. (1.48) (the $\frac{1}{2}$ cancels with the factor 2, that shows up in the definition of $\|.\|_{wW}$). Eventually, the term in the expansion that contains the square of the drift, can be argued to be of lower order with respect to τ (see for instance [20, sec. IV, A]).

To get a connection between the potential $\mathcal{S}$ in the gradient flow description (2.4) and a more physical notion of the entropy, we can consider this expansion of the rate functional in eq. (2.8) again: Comparing the probabilistic cost for the time-reversed path, $t\mapsto\rho^\epsilon_{rv}(t,.)=\rho^\epsilon(1-t,.)$, with the original one, ρ^ϵ, only the odd powers in t of $I(\rho^\epsilon)-I(\rho^\epsilon_{rv})$ survive, giving:

$$\begin{aligned}
I(\rho^\epsilon)-I(\rho^\epsilon_{rv}) &= \frac{1}{2}\int_0^1\left(\left\langle\partial_t\rho^\epsilon(t,.),\mathcal{DS}(\rho^\epsilon(t,.))\right\rangle_{L^2(\Omega)}-\left\langle\partial_t\rho^\epsilon_{rv}(t,.),\mathcal{DS}(\rho^\epsilon_{rv}(t,.))\right\rangle_{L^2(\Omega)}\right)dt=\\
&= \mathcal{S}(\rho^\epsilon(1,.))-\mathcal{S}(\rho^\epsilon(0,.)),
\end{aligned}\tag{2.11}$$

where we used the linearity and self-adjointness of the operator $-\mathrm{div}(m\nabla(.))$ in the first line. Hence, the asymmetry arises from the drift term in eq. (2.7) and only depends on the initial and final state, but not the time-scale, thanks to the particular shape of the drift. In fact, this way the ratio between the probability of ρ^ϵ and its time-reversed counterpart ρ^ϵ_{rv} coincides (up to a prefactor) with a fluctuation relation, known as Crook's relation ([26]; see also Jarzynski's earlier work [27]),

$$\frac{\mathbb{P}[\rho^\epsilon]}{\mathbb{P}[\rho^\epsilon_{rv}]}=e^{-(\mathcal{S}(\rho^\epsilon(1,.))-\mathcal{S}(\rho^\epsilon(0,.)))}\tag{2.12}$$

(note our use of the "mathematical" convention of the entropy, see the next remark).

Remark 14. (Comparison with physical conventions)
Note that in this text, we assume that the system evolves towards smaller values the potential $\mathcal{S}$, i.e. towards its (local) minimum. In contrast, the "physical" convention is usually the negative of this, with the system therefore tending towards larger values of this "entropy".

Also, unlike most applications, all quantities are considered to be dimensionless. Dimensions could be introduced in many ways depending on the physical interpretation of an application, but in typical situations time and space have their usual dimensions, labelled $[t]$ and $[x]$, and the states ρ, ρ^ϵ share the same dimension $[\rho]$, for instance the number of particles per volume $\frac{1}{[x]^d}$ or mass per volume $\frac{[\text{mass}]}{[x]^d}$. In physics the entropy $\mathcal{S}$ is typically associated with the dimension $[\mathcal{S}] = \frac{[\text{energy}]}{[\text{temperature}]}$. This gets balanced in the equations by respective dimensions for the mobility m in combination with an additional coefficient like the Boltzmann constant k_B (that has the same dimension as the entropy $\mathcal{S}$), which can be thought to correspond to the scaling parameter ϵ. Following [13, eq. (1.56)], for instance, eq. (2.7) would read:

$$d\rho^\epsilon(t,x) = \operatorname{div}\left(m\left(\rho^\epsilon\right)\nabla\left(\mathcal{DS}\left(\rho^\epsilon\right)\right)\right)dt + \sqrt{\epsilon}\cdot\operatorname{div}\left(\sqrt{2k_B\cdot m\left(\rho^\epsilon\right)}dW\right), \tag{2.13}$$

where now - although not explicitly relabelled - the quantities carry units ([13] is without the ϵ scaling, but k_B partly plays this role). In this case, the dimension of the variational derivative is $[\mathcal{DS}] = \frac{[\mathcal{S}]}{[x]^d\cdot[\rho]}$ and hence for the mobility $[m] = \frac{[x]^2}{[t]}\cdot\frac{[x]^d\cdot[\rho]^2}{[\mathcal{S}]} = \frac{[x]^{2-d}}{[t]}\cdot\frac{[\text{mass}]^2\cdot[\text{temperature}]}{[\text{energy}]}$ (for $[\rho] = \frac{[\text{mass}]}{[x]^d}$). For the large deviations rate functional we still get the dimensionless quantity:

$$I\left(\rho^\epsilon\right) = \frac{1}{2k_B}\int_0^1 \left\|\partial_t\rho^\epsilon(t,.) - \operatorname{div}\left(m\left(\rho^\epsilon(t,.)\right)\nabla\left(\mathcal{DS}\left(\rho^\epsilon(t,.)\right)\right)\right)\right\|^2_{wW\left(\rho^\epsilon\right)}dt, \tag{2.14}$$

as can be seen by thinking of the version from remark 13 as having the k_B absorbed in ϵ.

Remark 15. (Finding the diffusivity from mobility and entropy)
For applications it is sometimes more convenient to consider the so-called *diffusivity* $\tilde{D}(\rho)$, rather than the mobility $m(\rho)$, defined by:

$$\partial_t\rho = \operatorname{div}\left(\tilde{D}(\rho)\nabla\rho\right). \tag{2.15}$$

Given the variational derivative of the entropy, $\mathcal{DS}$, we can get this diffusivity from the mobility via:

$$\begin{aligned}\operatorname{div}\left(\tilde{D}(\rho)\nabla\rho\right) = \partial_t\rho &= \operatorname{div}\left(m(\rho)\nabla\left(\mathcal{DS}(\rho)\right)\right) = \\ &= \operatorname{div}\left(m(\rho)\cdot\mathcal{DDS}(\rho)\cdot\nabla\rho\right),\end{aligned} \tag{2.16}$$

where the $\mathcal{DDS}$ stands for the pointwise derivative of $\mathcal{DS}$ with respect to the $\rho(t,x)\in\mathbb{R}$. Up to terms

irrelevant for the evolution, we thus can identify:

$$\tilde{D}(\rho) = m(\rho) \cdot \mathcal{D}\mathcal{D}\mathcal{S}(\rho). \tag{2.17}$$

This relation is sometimes referred to as Einstein relation (see e.g. [28]) and establishes a relation between the macroscopic diffusivity and the thermodynamic quantities, entropy $\mathcal{S}$ and mobility m from the thermodynamic metric $\mathcal{K}$. We can think of $\tilde{D}$ as a local linearisation of the deterministic drift in the evolution of ρ^ϵ: Indeed for some processes (particularly the main examples, we will study numerically later) it has been shown that the linear drift operator D from eq. (2.6) can be identified with $D(\rho)(.) = \Delta\left(\tilde{D}(\rho)(.)\right)$ (see [29] for zero-range processes and [30] for the symmetric simple-exclusion process).

2.2 Method

This subsection describes a mathematical procedure to extract the mobility m from numerical or experimental data under the assumptions presented in the previous subsection 2.1. This mobility characterises the weighted Wasserstein metric in the gradient flow evolution in eq. (2.4). We particularly make use of the Gaussian fluctuations in eq. (2.6). The key element for doing this will be the quadratic variation of the microscopic state ρ^ϵ. We here focus on particle processes, i.e. the microscopic states are given by particle configurations. Namely we claim:

Theorem 16. *(Characterisation of the mobility via quadratic variation)*
Following subsection 2.1 we assume the following conditions:

- *Let the empirical measures $\rho^\epsilon(t,.) = \epsilon \cdot \sum_{x_i(t)} \left[\eta(x_i(t))\,\delta_{x_i(t)}\right]$ (with $x_i(t)$ being the positions, where particles are located, and η the number of particles at a given position) be the state of a stochastic process (with potentially rescaled time and space variables, which is omitted here for simplicity of notation) equipped with a weak L^2-topology and ν_ρ the translation invariant, ergodic equilibrium measure associated to the parameter $\rho \in \mathbb{R}^+$, i.e. $\mathbb{E}_{\nu_\rho}[\rho^\epsilon(t,.)] = \rho$, which is a product measure in space.*

- *The system is in* (weak) local equilibrium*: More precisely, the microscopic probability measures $(\mu^\epsilon)_\epsilon$ on the states $(\rho^\epsilon)_\epsilon$ are in (weak) local equilibrium of the (deterministic) profile ρ, i.e. for all function $f \in C(\Omega)$, bounded cylinder functions Ψ and parameters $\delta > 0$:*

$$\lim_{\epsilon \searrow 0} \mu^\epsilon \left[\left| \epsilon \sum_{x_i} \left[f(x_i)\, \Psi(\eta(x_i(t))) \right] - \int_\Omega f(x)\, \mathbb{E}_{\rho(t,x)}[\Psi]\, dx \right| > \delta \right] = 0, \tag{2.18}$$

where $\mathbb{E}_{\rho(t,x)}[\Psi] = \int \Psi(\eta)\, d\nu_{\rho(t,x)}(\eta)$ and $\nu_{\rho(t,x)}$ is the equilibrium measure associated to the constant density of the local profile value $\rho(t,x)$, i.e. marginals at any point x coincide with the

marginal of the equilibrium measure at that value of the density profile. For further reading on local equilibria and their shape in our examples see [36, sec. 3] as well as the respective paragraph of subsection 2.3.2 of this text. Furthermore, we require that the macroscopic profile ρ follows the evolution equation of a weighted Wasserstein gradient flow from eq. (2.4).

- *The fluctuations $\frac{1}{\sqrt{\epsilon}}\left(\rho^{\epsilon}(t,.)-\rho(t,.)\right)$ converge weakly and in distribution to $y(t,.)$, such that (for any test function $\gamma \in C_0^{\infty}(\Omega,\mathbb{R})$) $t \mapsto Y_{\gamma}(t) = \langle \gamma, y(t,.)\rangle_{L^2(\Omega)}$ is the Ornstein-Uhlenbeck process from eq. (2.6).*

Then the following identity holds:

$$\langle \nabla\gamma, m(\rho(t_0,.))\nabla\gamma\rangle_{L^2(\Omega)} = \lim_{\delta t \searrow 0} \mathbb{E}\left[\frac{\left(Y_{\gamma}(t_0+\delta t)-Y_{\gamma}(t_0)\right)^2}{2\delta t}\right], \tag{2.19}$$

where $t_0 \geq 0$, $\mathbb{E}$ is the expectation with respect to the probability measure that is induced by this limit process Y_{γ}, i.e. the weak limit of the probability measure induced by the process Y_{γ}^{ϵ} in local equilibrium.

Proof. We fix the point in time t_0 and start with eq. (2.6). We define $F:\mathbb{R}\to\mathbb{R}, x \mapsto (x-Y_{\gamma}(t_0))^2$, which is a C^{∞}-function. Considering the new random variable $F(Y_{\gamma}(t))$ with $t \geq t_0$ we get via Itô's formula (see for instance [**31**, Ch. 4]):

$$dF(Y_{\gamma}(t)) = F'(Y_{\gamma}(t))\,dY_{\gamma}(t) + \frac{1}{2}F''(Y_{\gamma}(t))\left\langle 1, \left(\sqrt{2m(\rho(t,.))}\nabla\gamma\right)^2\right\rangle_{L^2(\Omega)} dt, \tag{2.20}$$

where we used that dW is space-time-white noise and $(.)'$ stands for the pointwise derivative with respect to the argument. Thus, for our quadratic choice for F we get:

$$dF(Y_{\gamma}(t)) = 2\left(Y_{\gamma}(t)-Y_{\gamma}(t_0)\right)dY(t) + \langle \nabla\gamma, 2m(\rho(t,.))\nabla\gamma\rangle_{L^2(\Omega)}\,dt \tag{2.21}$$

and, having in mind the left hand side of eq. (2.19):

$$\begin{aligned}\mathbb{E}\left[\left(Y_{\gamma}(t_0+\delta t)-Y_{\gamma}(t_0)\right)^2\right] &= \mathbb{E}\left[F(Y_{\gamma}(t_0+\delta t))\right] = \mathbb{E}\left[\int_{t_0}^{t_0+\delta t} dF(Y_{\gamma}(t))\right] = \\ &= 2\mathbb{E}\left[\int_{t_0}^{t_0+\delta t}\left(Y_{\gamma}(t)-Y_{\gamma}(t_0)\right)dY_{\gamma}(t)\right] + \int_{t_0}^{t_0+\delta t}\langle\nabla\gamma, 2m(\rho(t,.))\nabla\gamma\rangle_{L^2(\Omega)}\,dt.\end{aligned} \tag{2.22}$$

Note that $\lim_{\delta t\searrow 0}\left(\frac{1}{\delta t}\int_{t_0}^{t_0+\delta t}\langle\nabla\gamma, 2m(\rho(t,.))\nabla\gamma\rangle_{L^2(\Omega)}\,dt\right) = \langle\nabla\gamma, 2m(\rho(t_0,.))\nabla\gamma\rangle_{L^2(\Omega)}$, due to continuity of the integrand. Therefore, the remaining task is, to show that in the limit $\delta t \searrow 0$, the first term on the right hand side of the last line in eq. (2.22) vanishes, when divided by δt. The noise term

in dY_γ gets neutralised thanks to the expectation, leaving us with:

$$\lim_{\delta t \searrow 0} \left(\mathbb{E}\left[\int_{t_0}^{t_0+\delta t} \left(Y_\gamma(t) - Y_\gamma(t_0)\right) dY_\gamma(t) \right] \right) =$$
$$= \lim_{\delta t \searrow 0} \left(\mathbb{E}\left[\int_{t_0}^{t_0+\delta t} \left(Y_\gamma(t) - Y_\gamma(t_0)\right) \left\langle \gamma, D(\rho)\, y(t,.) \right\rangle_{L^2(\Omega)} dt \right] \right). \tag{2.23}$$

Making consecutive use of Hölders inequality, Fubini's theorem and the binomial formula, this can be approximated as:

$$\mathbb{E}\left[\int_{t_0}^{t_0+\delta t} \left(Y_\gamma(t) - Y_\gamma(t_0)\right) \left\langle \gamma, D(\rho)\, y(t,.) \right\rangle_{L^2(\Omega)} dt \right] \leq$$
$$\leq \sqrt{\mathbb{E}\left[\int_{t_0}^{t_0+\delta t} \left(Y_\gamma(t) - Y_\gamma(t_0)\right)^2 dt \right] \cdot \mathbb{E}\left[\int_{t_0}^{t_0+\delta t} \left\langle \gamma, D(\rho)\, y(t,.) \right\rangle_{L^2(\Omega)}^2 dt \right]} =$$
$$= \sqrt{\int_{t_0}^{t_0+\delta t} \mathbb{E}\left[\left(Y_\gamma(t) - Y_\gamma(t_0)\right)^2 \right] dt \cdot \int_{t_0}^{t_0+\delta t} \mathbb{E}\left[\left\langle \gamma, D(\rho)\, y(t,.) \right\rangle_{L^2(\Omega)}^2 \right] dt} \leq \tag{2.24}$$
$$\leq \frac{1}{2} \int_{t_0}^{t_0+\delta t} \mathbb{E}\left[\left(Y_\gamma(t) - Y_\gamma(t_0)\right)^2 \right] dt + \frac{1}{2} \int_{t_0}^{t_0+\delta t} \mathbb{E}\left[\left\langle \gamma, D(\rho)\, y(t,.) \right\rangle_{L^2(\Omega)}^2 \right] dt. \tag{2.25}$$

Here, keeping eq. (2.22) in mind, we can apply Gronwall's lemma ([32, Lem. 4.1.2]) for $\dot{Z}(\delta t) \leq Z(\delta t) + R(\delta t)$ with:

$$Z(\delta t) := \int_{t_0}^{t_0+\delta t} \mathbb{E}\left[\left(Y_\gamma(t) - Y_\gamma(t_0)\right)^2 \right] dt \tag{2.26}$$

$$R(\delta t) := \int_{t_0}^{t_0+\delta t} \mathbb{E}\left[\left\langle \gamma, D(\rho)\, y(t,.) \right\rangle_{L^2(\Omega)}^2 \right] dt + \int_{t_0}^{t_0+\delta t} \left\langle \nabla\gamma, 2m(\rho(t,.))\, \nabla\gamma \right\rangle_{L^2(\Omega)} dt. \tag{2.27}$$

This gives an estimate for Z: $Z(\delta t) \leq e^{\delta t} \cdot \int_{t_0}^{t_0+\delta t} e^{t-t_0} R(t-t_0)\, dt$. Together with $R(\delta t) = \mathcal{O}(\delta t)$ (which can be seen by noting the (a.s.) continuity of the Ornstein-Uhlenbeck process y in time: In combination with the Weierstraß extreme value theorem on the compact interval $[t_0, t_0+\delta t]$ this gives boundedness of the integrand and thus even a Lipschitz estimate of R with respect to time) it follows

$Z(\delta t) = \mathcal{O}\left((\delta t)^2\right)$. Plugging this back into eq. (2.24), we arrive at:

$$\mathbb{E}\left[\int_{t_0}^{t_0+\delta t} \left(Y_\gamma(t) - Y_\gamma(t_0)\right) dY_\gamma(t)\right] \leq \sqrt{\mathcal{O}\left((\delta t)^2\right) \cdot \mathcal{O}(\delta t)} = \mathcal{O}\left((\delta t)^{3/2}\right), \tag{2.28}$$

which makes this term vanish for $\delta t \searrow 0$, leaving eq. (2.22) only with the desired terms in this limit. □

Remark 17. (Approximation of thm. 16 via observables)
While thm. 16 gives the main theoretical idea for finding the mobility m, in practice we can only approximate eq. (2.19): Estimating the expectation by the law of large numbers, i.e. the average over R many (essentially) independent samples, we have to choose a small enough δt such that for a large enough R we can choose a small enough ϵ to then approximate:

$$\frac{1}{R-1} \cdot \sum_r \left[\frac{\left(Y^\epsilon_{\gamma;r}(t_0+\delta t) - Y^\epsilon_{\gamma;r}(t_0)\right)^2}{2\delta t}\right] \approx \langle \nabla\gamma, m(\rho(t_0,.))\nabla\gamma\rangle_{L^2(\Omega)}, \tag{2.29}$$

where the index r identifies individual realisations of Y^ϵ_γ. A more precise meaning for the approximations abbreviated here by the "$\approx$" will be given in subsection 2.3.1 (note that, for simplicity of notation, we will not assign a new letter to the approximated mobility in the future, but only highlight the difference to the analytic value in the respective paragaphs).

Remark 18. (Regularity of the test functions γ)
While we originally required smooth test functions with compact support, $\gamma \in C_0^\infty(\Omega, \mathbb{R})$, the derivation of eq. (2.19) shows that it suffices to be in the Sobolev space $\gamma \in W_0^{1,2}(\Omega, \mathbb{R}) = \overline{C_0^\infty(\Omega, \mathbb{R})}^{W^{1,2}}$ (by $\overline{(.)}^{W^{1,2}}$ we mean the closure with respect to the Sobolev norm; see for instance [33, def. 5.14]), i.e. γ and its weak derivative $\nabla\gamma$ are square integrable and have compact support. Indeed, all functions, we will test this method with, have compact support, are continuous and have a bounded weak derivative, therefore being in $W_0^{1,2}(\Omega, \mathbb{R})$.

Remark 19. (Measures as mesoscopic states)
As the mesoscopic states ρ^ϵ only show up as L^2-projections on the test functions γ in both, the assumptions in subsection 2.1 and the proof of thm. 16, the theorem holds all the same, when $\rho^\epsilon(t,.)$ are actually not absolutely continuous with respect to the Lebesgue measure, but a (Borel-) measure themselves, for each time $t \geq 0$. In this case the fluctuations in eq. (2.5) are to be understood with respect to this measure instead, i.e.:

$$\langle \gamma, \rho^\epsilon(t,.) - \rho(t,.)\rangle_{L^2(\Omega)} = \int_\Omega \gamma(x)\, d\rho^\epsilon(t,x) - \int_\Omega \gamma(x)\,\rho(t,x)\, dx. \tag{2.30}$$

Note that the macroscopic state ρ is still a Lebesgue density, to ensure the meaning of eq. (2.4).

Remark 20. ("Continuous" method)
In terms of applicability, a drawback of the method described here is that we have to set up the same initial state $\rho(t_0,.)$ multiple times, to get a conveniently sized sample, to estimate the expectation $\mathbb{E}$ in eq. (2.19) via the law of large numbers. For experiments, it can hence be desirable to only prepare the system once and then observe it over a longer period of time, making snapshot-measurements every δt, to then get the mobility averaged over the whole observation time. An alternative method - henceforth called "continuous" method - is suggested here, that adapts the original method from thm. 16 to such an experimental situation: Instead of the fluctuations Y^ϵ, as defined in eq (2.5), we use the method with Y^ϵ_γ formally substituted by: $\tilde{Y}^\epsilon_\gamma(t) := \frac{1}{\sqrt{\epsilon}} \langle \gamma, \rho^\epsilon(t,.) \rangle_{L^2(\Omega)}$. In other words, we do not centre with the deterministic states ρ. Note, however, that this is expected to only amount to neglecting the differences $\langle \gamma, \rho(t_0+\delta t,.) - \rho(t_0,.) \rangle_{L^2(\Omega)}$ compared to their stochastic counterparts, as only the time differences occur in the final formula in eq. (2.19). This term is assumed of lower order with respect to δt, based on the deterministic state being differentiable in time. Nonetheless, this "continuous" approach is speculative, as it is not clear, how the limit $\delta t \searrow 0$ commutes with the hydrodynamic limit $\epsilon \searrow 0$, that is required to make sense of condition (2.6), i.e. we might not be able to pull the limit of the measurement times δt inside the hydrodynamic limit. For numerical results of this variation see fig. 2.9 and the end of subsection 2.4.

Hence, in this "continuous" approach, the expectation in eq. (2.19) is replaced by a time-average with respect to subsequent time-frames. While this might be viewed as an ergodicity principle, note that (for a fixed measurement time δt and ignoring the higher order terms in δt) each single measurement is an unbiased estimator for the mobility at that point in time, i.e. there are no systematic biases due to only considering a single sample. Particularly: In case we only consider equilibrium systems (where $m(\rho)$ is stationary and the deterministic terms $\rho(t_0+\delta t,.) - \rho(t_0,.) \equiv 0$ drop out analytically) we do not have to reset the system to the initial state $\rho(t_0,.)$ for repeated measurements as the state is stationary anyway and the "continuous" method coincides with the original one. While the law of large numbers thus applies all the same, error estimates are more difficult, as the individual measurements are not independent from each other anymore in the "continuous" setting (the final microscopic state of the previous measurement is identical to the initial state of the subsequent one). This could be potentially somewhat improved by leaving gaps between any two subsequent measurements to allow for mixing. But this would only be at the expense of overall accuracy, as fewer measurements are sampled in total. Similarly, in a non-equilibrium situation, the "continuous" method gives unbiased estimators for the time-average of $m(\rho(t,x))$ over the course of the whole observation time (if neglecting the deterministic states is valid, see above).

Another alternative "continuous" method to estimate the deterministic $\rho(t)$ on-the-fly, that was not tested here, would be to interpolate (for instance linearly) between the current state and a state, that was observed macroscopically far in the past, $\rho^\epsilon(t-\delta\tilde{t})$ for $\delta\tilde{t} \gg \delta t$, i.e. set $\rho(t+\delta t) = \frac{\delta t+\delta\tilde{t}}{\delta t} \cdot \rho^\epsilon(t) + \frac{\delta t}{\delta\tilde{t}} \cdot \rho^\epsilon(t-\delta\tilde{t})$.

2.3 Numerical implementation

In this subsection, it is explained, how thm. 16 was implemented in an algorithm (subsection 2.3.1) and how this algorithm was tested for specific examples of particle processes (subsection 2.3.2).

2.3.1 The algorithm for extracting the mobility from a given data set

We assume that we have a given data set, which originates from a stochastic process, that satisfies the conditions stated in subsection 2.1. We need the mesoscopic state ρ^ϵ (for "small" $0 < \epsilon \ll 1$) for two points in time, t_0 and $t_0 + \delta t$ (for "small" macroscopic time increments $0 < \delta t \ll 1$), and in R (for "large" $R \gg 1$) stochastically independent realisations (the latter will be used for estimating the expectations via the law of large numbers). To indicate the respective realisation, we write the states with an index $r \in \{1, \ldots, R\}$, i.e. ρ_r^ϵ. Note that, while $\epsilon > 0$ cannot be small enough, the time increment δt can be chosen too small for a fixed ϵ, as it is not clear a priori, how the hydrodynamic limit $\epsilon \searrow 0$ commutes with the limit $\delta t \searrow 0$ in eq. (2.19). Thus, in practice, it has to be tested specifically for each process, for what choice of parameters consistent results are obtained.

To implement eq. (2.19) we choose test functions of the type:

$$\Omega \subset \mathbb{R}^d \to \mathbb{R}, \gamma(x) = a_0 \cdot \prod_{j_d=1}^{d} \left[\max\left(0, 1 - \left(a_1 \cdot \left| x^{(j_d)} - x_0^{(j_d)} \right| \right)^{a_2} \right) \right]^{a_2}, \tag{2.31}$$

for $(.)^{(j_d)}$ being the j_d-th component of a $\mathbb{R}^d$ vector and the parameters: $x_0 \in \Omega$ will further on be called "concentration point" and is the point in the domain, where γ achieves its maximum. $a_0 > 0$ scales the overall height $\max_\Omega(\gamma)$ of the test function. $a_1 > 0$ scales the slope $\nabla\gamma$ (and is therefore inversely related to the support $|\mathrm{supp}(\gamma)| = \left(\frac{2}{a_1}\right)^d$), $a_2 \geq 1$ is parametrising the smoothness of the test function: For $a_2 = 1$ γ is piecewise linear along each of the d Cartesian axes, hence showing a tent-like graph, that is symmetric with respect to reflections at the concentration point x_0. For $a_2 = 2$ we get an overall similar but smoother shape, with the kinks of the $a_2 = 1$ case becoming quadratic and hence differentiable. For illustrations see fig. 2.1. Note that to ensure that the test function vanishes at the boundary, the concentration point x_0 must be at least $1/a_1$ away from the boundary.

Using eq. (2.19), we want to approximate the mobility m for a given ρ. We do this by choosing a large slope a_1 of the test function and thus right hand side (eq. (2.19)) $= \left\langle (\nabla\gamma)^2, m(\rho(t_0, .)) \right\rangle_{L^2(\Omega)}$ gets only evaluated in close proximity around the concentration point x_0 of the respective γ. Assuming continuity of $m(\rho(t_0, .))$ we can write:

$$m(\rho(t_0, x_0)) = \lim_{\delta t \searrow 0} \mathbb{E}\left[\frac{(Y_\gamma(t_0 + \delta t) - Y_\gamma(t_0))^2}{2 \cdot \delta t \cdot \|\nabla\gamma\|_{L^2(\Omega)}^2} \right] + o(1) \tag{2.32}$$

with respect to $a_1 \to \infty$. It is this formula, that we want to implement. To this end, the limit

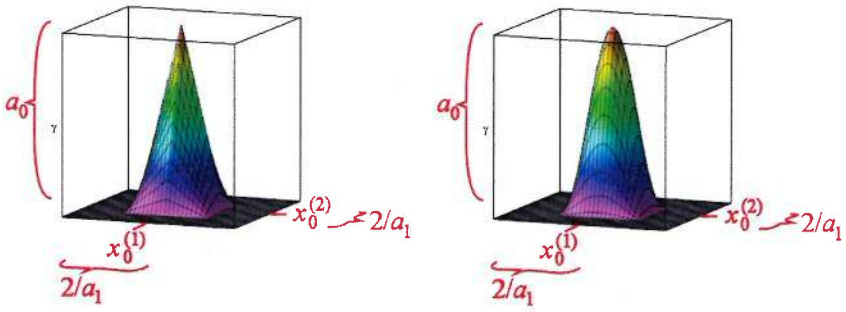

Figure 2.1: Example graphs of the test functions γ in eq. (2.31) for $a_2 = 1$ (left) and $a_2 = 2$ (right).

fluctuations Y_γ were approximated by Y_γ^ϵ for small $0 < \epsilon \ll 1$. Furthermore, to estimate the states ρ in the deterministic limit, that show up in the definition of the fluctuations, eq. (2.5), we use the statistical sample mean:

$$\rho = \frac{1}{R} \sum_{r=1}^{R} [\rho_r^\epsilon] + o(1), \tag{2.33}$$

with respect to $R \to \infty$. As we also want to replace the expectation $\mathbb{E}$ in eq. (2.32) by an unbiased estimator for it, we use the sample standard deviation (and thus stochastic independence of our R realisations of ρ_r^ϵ), i.e. formally substitute: $\mathbb{E}[.] \to \frac{1}{R-1} \sum_r [.]$ (see for instance [34, Ch. 2]). The factor $\frac{1}{R-1}$ (instead of $\frac{1}{R}$ in eq. (2.33)) accounts for the fact that the states ρ were determined via eq. (2.33) based on the same data set as the quantities Y^ϵ. Overall, this leads to the estimate:

$$\begin{aligned} & m(\rho(t_0, x_0)) \approx \\ & \approx \frac{1}{R-1} \sum_{r=1}^{R} \left[\frac{\frac{1}{\epsilon} \cdot \left\langle \gamma, \rho_r^\epsilon(t_0 + \delta t, .) - \rho_r^\epsilon(t_0, .) - \frac{1}{R} \sum_{\tilde{r}=1}^{R} [\rho_{\tilde{r}}^\epsilon(t_0 + \delta t, .) - \rho_{\tilde{r}}^\epsilon(t_0, .)] \right\rangle_{L^2(\Omega)}^2}{2 \cdot \delta t \cdot \|\nabla \gamma\|_{L^2(\Omega)}^2} \right] \end{aligned} \tag{2.34}$$

for small ϵ, δt and large R.

For testing this method of finding the mobility m, we will consider stochastic systems, that are atomistic on the microscopic scale, i.e. the state realisations are uniquely determined by the positions $X_{i,r}$ of the particles. Here the index $i \in \{1, \ldots, N\}$ identifies each of the overall N individual particles. In all the examples we will study in subsections 2.3.2, 2.4, the hydrodynamic limit will be achieved by adding more and more particles and simultaneously rescaling space and time in a diffusive way, more precisely: The microscopic space variable is $X = \frac{x}{\sqrt[d]{\epsilon}}$ and microscopic time variable is $T = \frac{t}{\sqrt[d]{\epsilon^2}}$, where the hydrodynamic parameter ϵ is scaling inversely with the number of particles, $\epsilon \propto \frac{1}{N}$. Note that this means that the particle density over the whole microscopic space stays constant. In the macroscopic

scaling, however, there are infinitely many particles on the fixed domain Ω in the hydrodynamic limit; to still get normalised quantities in a meaningful way, a weight is associated with each particle and gets rescaled with ϵ, giving the so-called empirical measure:

$$\rho_r^{\epsilon,N}(t,x) = \epsilon \sum_{i=1}^{N} \left[\delta_{x=\epsilon^{\frac{1}{d}} X_{i,r}\left(\frac{t}{\epsilon^{\frac{2}{d}}}\right)} \right], \tag{2.35}$$

where the argument of the particle position is the microscopic time of the configuration and $\delta_{x=\tilde{x}}$ is the Dirac measure, concentrated at point $\tilde{x} \in \Omega$. The mesoscopic state ρ_r^ϵ is identified with this empirical measure $\rho_r^{\epsilon,N}$ (note that, as mentioned above, the total number of particles N also depends on the ratio of scales ϵ; this relation will be fixed for our examples in a moment). In this case, following remark 19, the scalar products in the numerator of eq. (2.34) are to be understood with respect to the Dirac measure:

$$\langle f, \delta_{x=\tilde{x}} \rangle_{L^2} = f(\tilde{x}). \tag{2.36}$$

For the examples outlined in subsection 2.3.2, the microscopic dynamics $X(T)$ takes place on a periodic lattice space $\Lambda_L := \mathbb{Z}^d / (L\mathbb{Z})^d$, i.e. a d-dimensional torus with L elements at the integer positions in each direction. For these examples $\epsilon = \frac{1}{L^d}$ is the correct choice (to obtain the analytical results in the limit): If we keep the occupation numbers at each of the lattice sites proportional to a fixed profile on the macroscopic scale, the total particle number N is proportional to the site number L^d (up to rounding errors). Note that, while our examples are all living on such a lattice space, this is by no means necessary for the method. In general, it is a modelling task, that has to be done for each example specifically, to find a meaningful scaling ϵ, such that the assumptions of subsection 2.1 hold.

For a pseudo-code implementation of formula (2.34) with these microscopic settings, see alg. 1. While it is numerically advantageous to compute the expectation in the way described in the pseudo-code (or eq. (2.34)), it can be costly in time- and memory-consumption, as the states ρ_r^ϵ need to be read and processed twice. If this is indeed too costly, the expectation can be rewritten in the usual way, known from statistical variances:

$$\begin{aligned}
&\frac{1}{R-1} \sum_{r=1}^{R} \left[\left\langle \gamma, \rho_r^\epsilon(t_0+\delta t,.) - \rho_r^\epsilon(t_0,.) - \frac{1}{R} \sum_{\tilde{r}=1}^{R} \left[\rho_{\tilde{r}}^\epsilon(t_0+\delta t,.) - \rho_{\tilde{r}}^\epsilon(t_0,.) \right] \right\rangle_{L^2(\Omega)}^2 \right] = \\
&= \frac{1}{R-1} \sum_{r=1}^{R} \left[\langle \gamma, \rho_r^\epsilon(t_0+\delta t,.) - \rho_r^\epsilon(t_0,.) \rangle_{L^2(\Omega)}^2 \right] - \\
&\quad - \frac{R+1}{R-1} \left(\frac{1}{R} \sum_{\tilde{r}=1}^{R} \left[\langle \gamma, \rho_{\tilde{r}}^\epsilon(t_0+\delta t,.) - \rho_{\tilde{r}}^\epsilon(t_0,.) \rangle_{L^2(\Omega)} \right] \right)^2 .
\end{aligned} \tag{2.37}$$

This way, one only has to update the two quantities $\sum_{r=1}^{R} \left[\langle \gamma, \rho_r^\epsilon(t_0+\delta t,.) - \rho_r^\epsilon(t_0,.) \rangle_{L^2(\Omega)}^2 \right]$ and

Algorithm 1 Pseudo-code for the implementation of eq. (2.34) for a particle process, where the state realisations ρ_r^ϵ are given as empirical measures with a diffusive space-time scaling with $\epsilon = \frac{1}{L^d}$. $X_{i,r}$ are the (microscopical) positions of the i-th particle in the r-th realisation.

// Set scaling parameters:

$\epsilon = \frac{1}{L^d}$; *// parameter between micro- and macro-scale*

$\delta x = \frac{1}{L}$; *// lattice spacing in each direction*

// Define the test functions γ as a function:

function $\gamma(x)$:

return $\gamma(x) = a_0 \cdot \prod_{j_d=1}^{d} \left[\max\left(0, 1 - \left(a_1 \cdot \left|x^{(j_d)} - x_0^{(j_d)}\right|\right)^{a_2}\right)\right]^{a_2}$;

end function

// Compute denominator of eq. (2.34) in preliminary step:

for all lattice positions $X \in \Lambda_L$:

$G_X = \sum_{j_d=1}^{d} \left[\left(\frac{\gamma\left(\epsilon X + \delta x \cdot e^{(j_d)}\right) - \gamma\left(\epsilon X - \delta x \cdot e^{(j_d)}\right)}{2\delta x}\right)^2\right]$;

// can also be done on a finer scale, than the lattice spacing

end for

$G = \delta t \cdot (\delta x)^d \cdot \sum_{X \in \Lambda_L} [G_X]$; *// $\delta t \cdot \|\nabla\gamma\|^2_{L^2(\Omega)}$*

// Compute approximate deterministic states:

$M(t_0) = \frac{1}{R} \cdot \sum_{r=1}^{R} \left[\sum_{i=1}^{N} \left[\gamma\left(\epsilon^{\frac{1}{d}} X_{i,r}\left(\frac{t_0}{\epsilon^{\frac{2}{d}}}\right)\right)\right]\right]$; *// $\langle\gamma, \rho(t_0, .)\rangle_{L^2(\Omega)}$*

$M(t_0 + \delta t) = \frac{1}{R} \cdot \sum_{r=1}^{R} \left[\sum_{i=1}^{N} \left[\gamma\left(\epsilon^{\frac{1}{d}} X_{i,r}\left(\frac{t_0 + \delta t}{\epsilon^{\frac{2}{d}}}\right)\right)\right]\right]$; *// $\langle\gamma, \rho(t_0 + \delta t, .)\rangle_{L^2(\Omega)}$*

// Compute numerator of eq. (2.34):

for all R realisations r:

$Y_{\gamma,r}(t_0) = \sqrt{\epsilon} \cdot \left(\sum_{i=1}^{N} \left[\gamma\left(\epsilon^{\frac{1}{d}} X_{i,r}\left(\frac{t_0}{\epsilon^{\frac{2}{d}}}\right)\right)\right] - M(t_0)\right)$; *// $Y_\gamma(t_0)$*

$Y_{\gamma,r}(t_0 + \delta t) = \sqrt{\epsilon} \cdot \left(\sum_{i=1}^{N} \left[\gamma\left(\epsilon^{\frac{1}{d}} X_{i,r}\left(\frac{t_0 + \delta t}{\epsilon^{\frac{2}{d}}}\right)\right)\right] - M(t_0 + \delta t)\right)$; *// $Y_\gamma(t_0 + \delta t)$*

end for

$S = \frac{1}{R-1} \cdot \sum_{r=1}^{R} \left[\left(Y_{\gamma,r}(t_0 + \delta t) - Y_{\gamma,r}(t_0)\right)^2\right]$; *// $\mathbb{E}\left[\left(Y_\gamma(t_0 + \delta t) - Y_\gamma(t_0)\right)^2\right]$*

// Result:

$m = \frac{S}{G}$; *// mobility*

$\sum_{\tilde{r}=1}^{R}\left[\left\langle\gamma,\rho_{\tilde{r}}^{\epsilon}\left(t_0+\delta t,.\right)-\rho_{\tilde{r}}^{\epsilon}\left(t_0,.\right)\right\rangle_{L^2(\Omega)}\right]$ for each new realisation r, which can be done on-the-fly (without the memory consumption growing proportional to R). This comes with the numerical problem that both these sums grow with R and, if they exceed the machine accuracy of the computer, the lowest digits are forgotten, which might however be of importance, when the two sums are eventually subtracted from one another. To address this issue, for instance so-called Kahan summation can be used (see [35]), to store the lower digits in a separate floating point number, thus effectively doubling the machine accuracy (and required memory). This was done for the on-the-fly simulations mentioned in section 3.

2.3.2 The tested particle processes and the algorithm to simulate them

The method to determine the mobility m, described in the previous subsections, was tested for several numerical particle processes, for which analytical results are known. In particular, it is known that they satisfy the requirements from subsection 2.1 and what mobility they exhibit, therefore allowing a comparison with outcomes from the new approach. Namely, these processes are: A system of independent random walkers, a non-linear zero-range process and a symmetric simple-exclusion process. All of these are Markov processes with indistinguishable particles jumping symmetrically to nearest neighbours on a lattice Λ_L. For simplicity $d = 1$ space dimension with periodic boundary conditions was considered. Note that the independent random walkers are a particularly simple case of a zero-range process and will thus be presented in the same paragraph:

Zero-range processes Zero-range processes get their name from the fact that the jump rate of each particle does only depend on the occupation number at its very own, current site, not for instance the site it considers to jump to. We denote the jump rate per site by $g(k) \geq 0$, where $k \in \mathbb{N} \cup \{0\}$ is the occupation number at that site. This means, each site has its own alarm clock, that indicates when the next jump is going to happen (to some target site). The next alarm time is chosen from an exponential distribution with mean $\frac{1}{g(k)}$ (hence the number of jumps per time interval is Poisson distributed). As the particles are indistinguishable, all from that site jump with equal probability and the jump rate per particle at that site is $g(k)/k$ (for, why this is equivalent to considering individual exponential alarm clocks for each particle, see the paragraph about the Kinetic Monte-Carlo approach). Because we consider the nearest neighbour, symmetric case in one dimension, given a jump happens, the likelihood to jump to the right or the left is one half each. The infinitesimal generator of such a process is given by:

$$\left(\mathscr{L}^L f\right)(k) = \sum_{X,\tilde{X}}\left[\frac{1}{2}\cdot g\left(k\left(X\right)\right)\cdot\left(f\left(k^{X,\tilde{X}}\right)-f\left(k\right)\right)\right], \tag{2.38}$$

with the sum being over all $X \in \Lambda^L$ and $\tilde{X}$ nearest neighbours to X. $k^{X,\tilde{X}}$ denotes the identical configuration to k except some particle at X has jumped to $\tilde{X}$.

Zero-range processes are well-studied in the literature (see for instance [36, ch. 2,5]), in particular their equilibrium measures are known explicitly: For given scalar parameter $\varphi \geq 0$ (that is not too large, so it is inside the radius of convergence of the partition function, see below), called fugacity, the product measure with marginals:

$$\tilde{\nu}_{\varphi}\left(k : k\left(X\right) = k_0\right) = \frac{1}{Z\left(\varphi\right)} \cdot \frac{\varphi^{k_0}}{g!\left(k_0\right)} \tag{2.39}$$

is an invariant measure of the zero-range process with jump rate g per site. Here the notation $g!$ is a generalisation of the factorial: $g!\left(k_0\right) := \prod_{j=1}^{k_0}\left[g\left(j\right)\right]$. The normalisation constant Z is the so-called partition function $Z\left(\varphi\right) := \sum_{j \in \mathbb{N} \cup \{0\}}\left[\frac{\varphi^j}{g!(j)}\right]$. One can show that the expectation of the occupation number $k\left(0\right)$ with respect to this measure is a strictly increasing function (the position is of no importance here, due to translation invariance of process and measure), thus allowing to find a unique fugacity for a given expectation, i.e. $\varphi\left(\rho\right)$ is uniquely defined for a given $\rho \geq 0$ by being the solution to $\rho = \mathbb{E}_{\tilde{\nu}_{\varphi(\rho)}}\left[k\left(0\right)\right] = \frac{1}{Z(\varphi(\rho))} \cdot \sum_{j \in \mathbb{N} \cup \{0\}}\left[j \cdot \frac{(\varphi(\rho))^j}{g!(j)}\right]$. Thus the equilibrium measure can be parametrised by ρ via $\nu_\rho := \tilde{\nu}_{\varphi(\rho)}$. Furthermore, it is known that the empirical measures of these zero-range processes in local equilibrium have a hydrodynamic limit (in diffusive space-time scaling), that is deterministic and absolutely continuous with respect to the Lebesgue measure. Its density $(t, x) \mapsto \rho\left(t, x\right)$ evolves according to the evolution equation (see [36, thm. 5.1.1] with slightly different notation):

$$\partial_t \rho = \Delta \Phi\left(\rho\right), \tag{2.40}$$

where the Φ here coincides up to a prefactor with the fugacity $\varphi\left(\rho\right)$ mentioned above, with respect to which the occupation number has expectation ρ. Additionally, it has been shown in the past that the fluctuations are of the desired Gaussian type (see [29], [20]), thus fixing the shape of the thermodynamic metric $\mathcal{K}$ as of weighted Wasserstein type with Φ playing the role of m. Finally, [37] gives the entropy as: $\mathcal{S}\left(\rho\right) = \int\left(\rho \ln\left(\Phi\left(\rho\right)\right) - \ln\left(Z\left(\Phi\left(\rho\right)\right)\right)\right) dx$. A short computation, making use of the above-mentioned shape of the marginals of the equilibrium measure and definition of Z, shows that $\mathcal{DS} = -\frac{\Phi'(\rho)}{\Phi(\rho)}$. This makes the gradient flow eq. (1) coincide with the macroscopic evolution eq. (2.40) for exactly the weighted Wasserstein type of thermodynamic metric and $\Phi = m$.

Hence we expect zero-range processes to satisfy the requirements of our method, as detailed in subsection 2.1. More specifically, we consider the two cases:

- $g\left(k\right) = k$: This is a system of simple, independent random walkers (RW), as each particle has a constant jump rate of 1, independent of the other particles. In this case the analytic mobility m_{RW} is:

$$m_{RW}\left(\rho\right) = \frac{1}{2} \cdot \rho \tag{2.41}$$

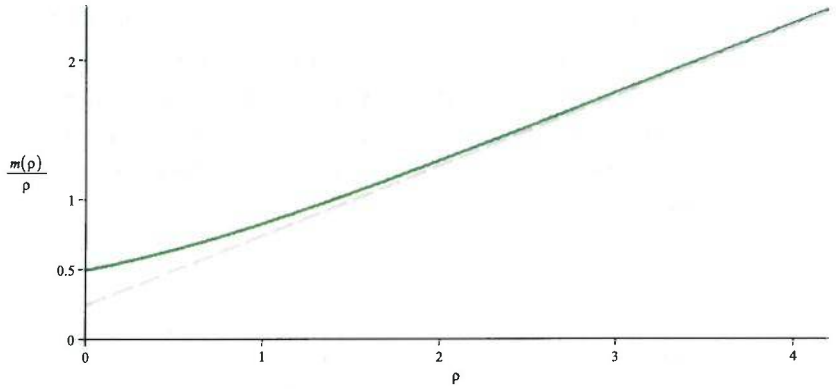

Figure 2.2: Numerical solution for the mobility m_{ZRP} of the non-linear zero-range process, see eq. (2.42). Depicted is $\rho \mapsto \frac{m_{ZRP}(\rho)}{\rho}$ in green, while the grey, dashed line shows the heuristic, asymptotic $\rho \mapsto \frac{1}{2}\left(\rho + \frac{1}{2}\right)$ for large densities ρ.

(while the coefficient $\frac{1}{2}$ here might appear artificial, it occurs along the same lines as for the standard normal distributions (with variance one) being the fundamental solution to the heat equation with the same coefficient $\partial_t \rho = \frac{1}{2}\Delta\rho$).

- $g(k) = k^2$: This is a non-linear version of the zero-range process (here denoted by ZRP), where the jump rate per particle is increasing, the more particles are at the same site. As can be found in [19] (note the factor 2 between the definition of m in that paper), the analytic mobility m_{ZRP} can be expressed implicitly as:

$$\rho(m_{ZRP}) = \sqrt{2m_{ZRP}} \cdot \frac{I_1\left(2\sqrt{2m_{ZRP}}\right)}{I_0\left(2\sqrt{2m_{ZRP}}\right)}, \tag{2.42}$$

where I_i are modified Bessel functions of the first kind. The function $m_{ZRP}(\rho)$ solving this equation, is almost of the shape of the quadratic function $\rho \mapsto \frac{1}{2} \cdot \rho \cdot \left(\rho + \frac{1}{2}\right)$ but slightly larger for small ρ. For a plot of the graph of $\frac{m_{ZRP}(\rho)}{\rho}$ see fig. 2.2.

Symmetric simple-exclusion process (SEP) This process is also a Poisson jump-process like the zero-range processes, however: The occupation number at any site is at most one, so $k \in \{0, 1\}$. Also, the particles attempt to jump with a rate of 1, but the jump is suppressed, if the destination site is already occupied by another particle (hard core interaction). Hence, in one dimension, the rate to jump to the neighbouring site to the right (or left) is one half, if there is a particle at the current site and no particle to the right (or left), otherwise it is zero: $g_{X \to \tilde{X}}(k) = \frac{1}{2} \cdot k(X) \cdot \left(1 - k\left(\tilde{X}\right)\right)$, where $X \mapsto k(X)$ is the current configuration of occupation numbers and X, $\tilde{X}$ are nearest neighbour sites.

The infinitesimal generator for such a process is given by:

$$\left(\mathscr{L}^L f\right)(k) = \sum_{X,\tilde{X}} \left[\frac{1}{2} \cdot k(X) \cdot \left(1 - k\left(\tilde{X}\right)\right) \cdot \left(f\left(k^{X,\tilde{X}}\right) - f(k)\right)\right], \tag{2.43}$$

with the sum being over all $X \in \Lambda^L$ and $\tilde{X}$ nearest neighbours to X. $k^{X,\tilde{X}}$ denotes the identical configuration to k except the particle at X has jumped to $\tilde{X}$.

Also this process is well-studied in the literature (see for instance [36, ch. 2,4]). In particular, Bernoulli product measures with translation invariant marginals are equilibrium measures:

$$\nu_\rho(k : k(X) = 1) = 1 - \nu_\rho(k : k(X) = 0) = \rho \in [0, 1]. \tag{2.44}$$

Again, the empirical measures in local equilibrium converge to a deterministic measure, that is absolutely continuous with respect to the Lebesgue measure with its density ρ evolving via (see [36, thm. 4.2.1]):

$$\partial_t \rho = \frac{1}{2}\Delta\rho. \tag{2.45}$$

Additionally, it has been shown (see [30]), that the fluctuations are of the desired weighted Wasserstein type, this time with mobility

$$m_{SEP}(\rho) = \frac{1}{2} \cdot \rho \cdot (1 - \rho). \tag{2.46}$$

Finally, [25] gives the entropy as: $\mathcal{S}(\rho) = \int (\rho \ln(\rho) + (1-\rho)\ln(1-\rho))\, dx$. A short computation shows again, that the macroscopic limit eq. (2.45) matches the gradient flow shape in eq. (1), if the thermodynamic metric $\mathcal{K}$ is a weighted Wasserstein metric with mobility equal to the m_{SEP} in the fluctuations.

Hence we also expect symmetric simple-exclusion processes to satisfy the requirements of our method, as detailed in subsection 2.1.

The Kinetic Monte-Carlo approach We now turn towards how the processes were implemented to produce a data set, that can be evaluated to find the mobility with the method described in previous subsections.

All the processes considered here are Poisson processes, i.e. the periods of time between two subsequent jumps are exponentially distributed. With this comes the property of "memorylessness" - by this it is meant that the time for the next jump can be redetermined at any time, without changing the expected waiting time. Or in other words: Having already waited some time for the next jump does not change the distribution for the remaining waiting time. This can be seen as follows: Let $\mathbb{P}[\delta T \leq T_0]$ be the probability that the random variable δT (which gives the waiting time until the next jump) is at most equal to some future point in time $T_0 \geq 0$. Similarly, assume we additionally know to already have waited a period $T_W > 0$ of time, then the probability for the same event

becomes: $\mathbb{P}[\delta T \leq T_0 + T_W | \delta T > T_W]$. But as the following computation shows, these are the same for exponentially distributed δT (here with jump rate one):

$$\mathbb{P}[\delta T \leq T_0 + T_W | \delta T > T_W] = \frac{\mathbb{P}[(\delta T \leq T_0 + T_W) \cap (\delta T > T_W)]}{\mathbb{P}[\delta T > T_W]} = \\ = \frac{\left(1 - e^{-(T_0+T_W)}\right) - \left(1 - e^{-T_W}\right)}{1 - (1 - e^{-T_W})} = 1 - e^{-T_0} = \mathbb{P}[\delta T \leq T_0]. \quad (2.47)$$

Note this still holds for other jump rates than one (just multiply each time with the rate). In fact, via the strong Markov property (see [38, thm. 2.4.2]), we can even restart the process at any stopping time without perturbing its dynamics. Hence the convenient situation arises that we can just reset each alarm clock at the moment some jump happens or in between jumps. This means, it suffices to have one global clock, that indicates the next jump, because in the moment the jump occurs, it is easy to distinguish, which particle actually exercised that jump: The probability for a particle to jump in that moment is simply proportional to the exponential distribution at time zero (we reset the alarm clocks of each random variable just the moment before the jump): $g_i \cdot e^{-g_i \cdot 0} = g_i$, where $g_i > 0$ is the jump rate of the i-th Poisson process.

It remains to find the stochastic process for the global clock (i.e. for the time of the next jump somewhere in the system) $\delta T_{gl} = \min_i (\delta T_i)$, for i labelling the individual exponential random variables: The accumulated probability distribution for the global clock is thus given by

$$\mathbb{P}[\delta T_{gl} \leq T_0] = 1 - \prod_i [\mathbb{P}[\delta T_i > T_0]] = \\ = 1 - \prod_i \left[1 - \left(1 - e^{-g_i T_0}\right)\right] = 1 - e^{-\sum_i [g_i] T_0}, \quad (2.48)$$

consequently being exponentially distributed as well, with jump rate equal to the sum of the jump rates of each sub-process δT_i: $g_{gl} = \sum_i [g_i]$.

Hence, if we want to determine, when the next jump happens somewhere in the entire system, we can consider the random variable $\mathbb{I}$, which is uniformly distributed in the interval $[0, 1]$, and identify $\delta T_{gl} = -\frac{\ln(\mathbb{I})}{g_{gl}}$. This gives the correct distributions, as we can use the symmetry of $\mathbb{I}$:

$$\mathbb{P}[\delta T_{gl} \leq T_0] = \mathbb{P}\left[\mathbb{I} \geq e^{-g_{gl} \cdot T_0}\right] = \mathbb{P}\left[1 - \mathbb{I} \geq e^{-g_{gl} \cdot T_0}\right] = \mathbb{P}\left[\mathbb{I} \leq 1 - e^{-g_{gl} \cdot T_0}\right] = \\ = 1 - e^{-g_{gl} \cdot T_0}. \quad (2.49)$$

This overall procedure is summarised in the pseudo-code in the top part of alg. 2 and is well-known as Kinetic Monte-Carlo approach (KMC)(see for instance [39, 40] for more information). It allows to drop the alarm clocks for each site (or particle) as part of the state description, but requires two (uniformly distributed) random numbers for each jump, rather than one: One for the time δT_{gl} and one

Algorithm 2 Pseudo-code for an implementation of a Poisson process with Kinetic Monte-Carlo approach. Although written for i referring to the particle index, i could stand for any Poisson process (like the jumps per site for the zero-range processes or the jump of a particle to a specific direction for the simple-exclusion process).

```
// evolution via Kinetic Monte-Carlo approach:
function evolution((X_i)_{i∈{1,...,N}}, (λ_i)_{i∈{1,...,N}}, t_0, δt):
  t = t_0;                                                    // initial time
  while 1                                                     // start evolution
    C_0 = 0;
    for all particles i ∈ {1,...,N}:
      C_i = C_{i-1} + λ_i;                                    // cumulated sum of jump rates
    end for
    r_1 = random_number_uniformly_distributed_in_[0,1];
    dt = -ln(r_1)/C_N;                                        // waiting time until next jump
    if (t + dt ≤ t_0 + δt):                                   // jump happens before end of evolution
      t = t + dt;
      r_2 = random_number_uniformly_distributed_in_[0,1];
      i_jump = binary_search_for(i ∈ {1,...,N} : C_{i-1} < r_2 · C_N ≤ C_i);
      carry_out_jump_of_particle_i_jump;
      update_jump-rates_λ_i_for_all_particles_i ∈ {1,...,N};
    else                                                      // jump would happen after end of evolution
      t = t_0 + δt;                                           // final time of evolution
      break;                                                  // stop evolution
    end if
  end while
  return (X_i)_{i∈{1,...,N}}, (λ_i)_{i∈{1,...,N}};
end function

// for preparing the data sets (X_{i,r}(t_0/ε^{2/d}))_{i,r}, (X_{i,r}((t_0+δt)/ε^{2/d}))_{i,r} evaluated in alg. 1:
prepare_pre-initial_states_(X_i((t_0 - t_fw)/ε^{2/d}))_i;
get_jump-rates_λ_i_for_all_particles_i ∈ {1,...,N};
for all R_fw realisations at time t_0 - t_fw:
  ((X_{i,r}(t_0 - t_sw)/ε^{2/d}))_i, (λ_{i,r})_i) =evolution(((X_i((t_0 - t_fw)/ε^{2/d}))_i, (λ_i)_i, t_0 - t_fw, t_fw - t_sw);
  for all R_sw realisations at time t_0 - t_sw:
    ((X_{i,r}(t_0/ε^{2/d}))_i, (λ_{i,r})_i) =evolution(((X_{i,r}(t_0 - t_sw)/ε^{2/d}))_i, (λ_{i,r})_i, t_0 - t_sw, t_sw);
    // preparation done, start evolution of actual measurement:
    ((X_{i,r}((t_0+δt)/ε^{2/d}))_i, (λ_{i,r})_i) =evolution(((X_{i,r}(t_0/ε^{2/d}))_i, (λ_{i,r})_i, t_0, δt);
  end for
end for
R = R_fw · R_sw;                                              // total number of realisations
```

for identifying the particle, that jumps at that time. Note, however, that we save a lot of initialisation effort when using KMC: We do not need to set up a clock for each individual particle (only, when a jump actually occurs, does it cost computational effort) and we do not need to order this list of alarm times (which is an $\mathcal{O}(N \ln(N))$ effort) to identify the next one. As we only run the particle processes for very short time intervals $0 < \delta t \ll 1$, the KMC is expected to be the better choice.

About local equilibrium Local equilibrium is a way to ensure that it makes sense to think of a macroscopic state ρ, like in eq. (2.4). In fact, it is the local equilibrium measure with respect to which the particle configurations (i.e. the microscopic states ρ^ϵ) converge (weakly) in probability to the Lebesgue measure $\rho(x)\,dx$. More specifically, in this context of particle processes where the microscopic state is given by the empirical measures (2.35) in diffusive space-time scaling the notion of weak local equilibrium measures $(\mu^\epsilon)_\epsilon$ from thm. 16 can be written as: For all functions $f \in C(\Omega)$, bounded cylinder functions Ψ and parameters $\delta > 0$:

$$\lim_{\epsilon \searrow 0} \mu^\epsilon \left[\left| \epsilon \sum_{X=\epsilon^{-\frac{1}{d}} x} \left[f(x)\, \Psi\left(k_{\epsilon^{-\frac{2}{d}} t}(X) \right) \right] - \int_\Omega f(x)\, \mathbb{E}_{\rho(t,x)}[\Psi]\, dx \right| > \delta \right] = 0, \tag{2.50}$$

where $k_T(X)$ is the occupation number at (microscopic) site X and (microscopic) time T and $\mathbb{E}_{\rho(t,x)}[\Psi] = \int \Psi(k)\, d\nu_{\rho(t,x)}(k)$ and $\nu_{\rho(t,x)}$ is the equilibrium product measure on the microscopic state space $\mathbb{N}_0^{\Lambda_L}$ associated to the constant density of the local profile value $\rho(t,x)$, i.e. each marginal at position $x = \epsilon^{\frac{1}{d}} X$ is parametrised by the local profile value $\rho(t,x)$. Note that such local equilibrium measures are (typically) not invariant under the generator of the stochastic process, but only vary slowly, as they are parametrised by the (smooth) macroscopic states ρ. For our test cases, the zero-range processes and the simple-exclusion process, the existence of these measures has been shown, leading rigorously to the desired setting of subsection 2.1 - for more details, see [36, Ch. 3, 4, 5].

In the simulations, we first pre-initialise a deterministic particle configuration $(X_i(t_0 - t_{fw}))_i$, but do not start the actual measurement immediately. Instead, we allow the the system to reach local equilibrium by waiting a relatively long time t_{fw}. Typically, this is much longer than the measurement time δt and tends to be the most time-consuming step in the simulation. To avoid having to do this for each of the R realisations, we only carry out individual simulations for each realisation during the waiting time evolution in the last period $t_{sw} < t_{fw}$ before the measurement is started, i.e. during $[t_0 - t_{sw}, t_0]$. Before that, only R_{fw} simulations are run during $[t_0 - t_{fw}, t_0 - t_{sw}]$ to save computation-time (for convenience R_{fw} is a divisor of R, such that: $R = R_{fw} \cdot R_{sw}$). The algorithmic implementation in a pseudo-code is given at the bottom of alg. 2 and a schematic visualisation can be seen in fig. 2.3. This pre-initial waiting serves as both, equilibration and mixing, i.e. for achieving that the sampling only depends on the macroscopic local equilibrium measure, but not (significantly) on the microscopic initialisation anymore. Hence, the appropriate length of these waiting times is expected to strongly

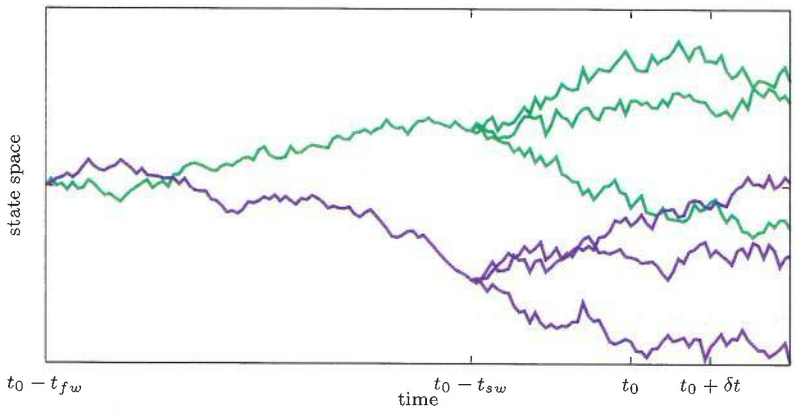

Figure 2.3: Schematic depiction of the initialisation procedure: R_{fw} many realisations are started from some initial configuration at time $t_0 - t_{fw}$. At time $t_0 - t_{sw}$ each of these branches into another R_{sw} many realisations, such that at the times of the measurements, t_0 and $t_0 + \delta t$, a total of $R = R_{fw} \cdot R_{sw}$ realisations can be considered (in the picture $R = R_{fw} \cdot R_{sw} = 2 \cdot 3$).

depend on the microscopic dynamics of the system and its prediction thus beyond the scope of the framework of this text, which only makes assumptions on the meso- and macroscopic level. Nonetheless, a plausibility test can be carried out (see fig. 2.7) by checking for instance, how the error bars scale with the number of repeated measurements, which should be $\propto \frac{1}{\sqrt{R_{fw}}} \cdot \frac{1}{\sqrt{R_{sw}}}$ for independent samples.

Default settings Unless stated otherwise, the following default settings were used for all measurements: The one-dimensional domain contained $L = \frac{1}{\epsilon} = 5000$ sites. The pre-initial particle configuration was for the zero-range processes $k\left(\frac{x}{\epsilon}\right) = 25 \cdot \sin(\pi x)$ and for the simple-exclusion process $k\left(\frac{x}{\epsilon}\right) = 0.95 \cdot \sin(\pi x)$ (note, after rescaling of Λ_L, the macroscopic domain becomes $\Omega = [0, 1]$). The waiting and measurement times are $t_{fw} = 4 \cdot 10^{-6}$, $t_{sw} = 4 \cdot 10^{-9}$, $\delta t = 4 \cdot 10^{-11}$. The number of realisations are $R_{fw} = 50$, $R_{sw} = 2000$ giving a total of $R = 100000$. Thus note that, while these measurement times appear rather short, the total number of jumps within one measurement is still about $3125 \cdot g(k) \cdot k \approx 80000$ for the RW at $\rho = 5$. The parameters in the test function γ (see eq. (2.31)) are $a_0 = 1$, $a_1 = 160$, $a_2 = 2$ and $x_0 \in \{0.025, 0.05, \ldots, 0.975\}$.

The relative errors are computed in comparison with analytic mobilities m_{analytic} via: $\frac{m - m_{\text{analytic}}}{m_{\text{analytic}}}$. Error-bars represent the statistical standard error over the R realisations, assuming stochastic independence: $\sqrt{\frac{1}{R \cdot (R-1)} \sum_{r=1}^{R} \left[\left(m_r - \frac{1}{R} \sum_{\tilde{r}=1}^{R} [m_{\tilde{r}}] \right)^2 \right]}$.

As the values for ρ on both sides of the sin-profile are equal, the results for measurements at symmetric positions are merged to one data point by averaging (and assuming stochastic independ-

ence). If only average errors over the entire domain are given, the results are averaged over the points $x_0 \in \{0.1, 0.2, \ldots, 0.9\}$, which are again treated as if stochastically independent.

2.4 Numerical results

This subsection presents numerical results for the systems described in subsection 2.3.2, using the method for finding the mobility m described in subsections 2.2, 2.3.1. The following parameters were studied:

Dependence of the mobility m on the density ρ Results are depicted in fig. 2.4. The numeric results show good agreement with the analytic expectations. The slight deviations of the ZRP for small ρ are likely because of the large slope of the profile at these positions, see item of slope dependence below.

Dependence on the measurement time δt Results are depicted in fig. 2.5. One can see that, depending on the process, there is a plateau for which the method gives consistent results, whereas for too small values of δt larger errors can occur. This is expectable, as the hydrodynamic limit $\epsilon \searrow 0$ does typically not commute with the limit $\delta t \searrow 0$. For large measurement times δt deviations from the analytic mobility occur again, due to higher order terms in δt perturbing the results (see proof of thm. 16).

Dependence on the number of sites L (i.e. $\frac{1}{\epsilon}$) Results are depicted in fig. 2.6. One can anticipate the expected convergence for the hydrodynamic limit $\epsilon = \frac{1}{L^a} = \frac{1}{L} \searrow 0$.

Dependence on the number of samples R Results are depicted in fig. 2.7. One can see that the relative error roughly scales with the power law $\propto \frac{1}{\sqrt{R}}$, as is expected for independent measurements.

Dependence on the slope of the test functions a_1 Results are depicted in fig. 2.8. For this measurement the pre-initial profiles were set to $k\left(\frac{x}{\epsilon}\right) = 5 \cdot \left(1 + \sin\left(\frac{2\pi}{a}\left(x - \frac{1}{2}\right)\right)\right)$ for the ZRP and $k\left(\frac{x}{\epsilon}\right) = \frac{1}{2} \cdot \left(1 + \sin\left(\frac{2\pi}{a}\left(x - \frac{1}{2}\right)\right)\right)$ for the SEP, where $a > 0$ squeezes the profile in the horizontal direction. Measurements were only evaluated at $x_0 = 0.5$. One can see that for larger slopes $\nabla\rho$ of the profile, i.e. as we deviate further from the equilibrium, the results show larger errors. This issue can be addressed, however, by choosing a more narrowly supported test function γ, i.e. a larger parameter a_1. Note that choosing a too narrow test function, on the other hand, can increase the error again, if we only estimate $\|\nabla\gamma\|^2_{L^2(\Omega)}$ in eq. (2.34) by approximating the integral by a Riemann sum on the lattice of the underlying particle process (with spacing $\frac{1}{L}$). In the data presented here, this is overcome by calculating this term analytically beforehand.

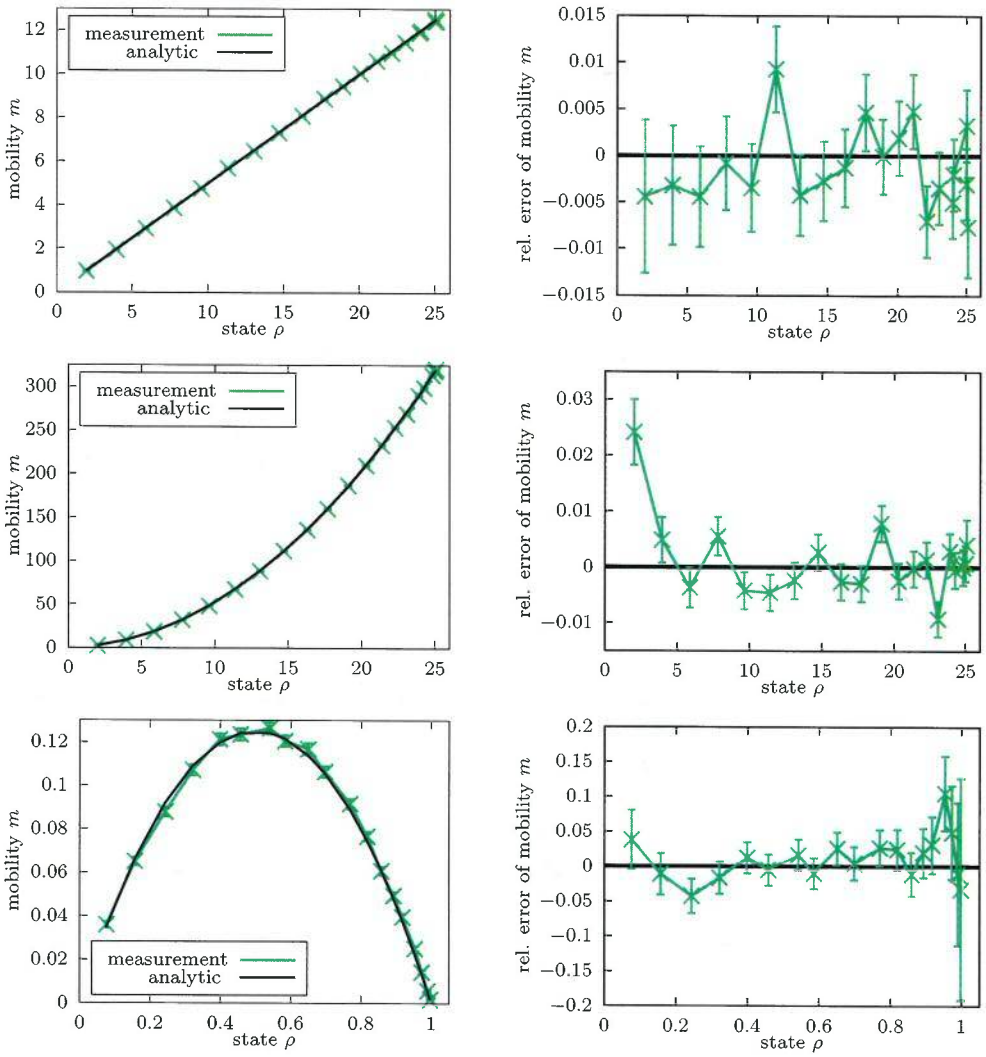

Figure 2.4: Comparison of numeric and analytic results for $\rho \mapsto m(\rho)$. To the left are the plots of the actual mobility, to the right are their relative errors compared to the respective analytic expectations. Top to bottom are the RW, ZRP and SEP.

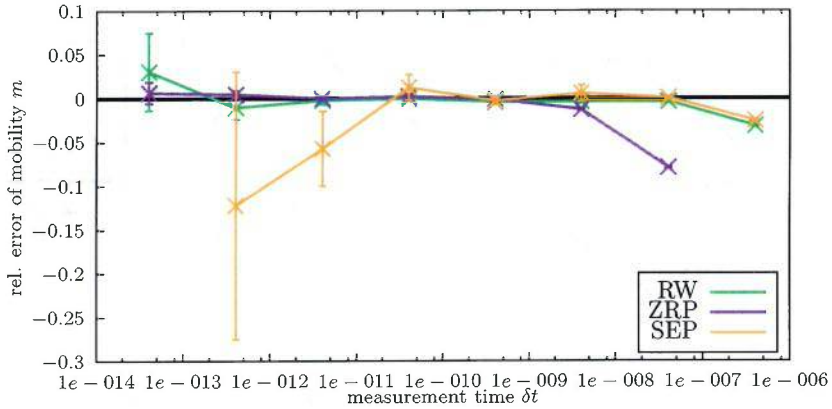

Figure 2.5: Dependence on the measurement time δt. Depicted are the averages over the whole domain of the relative errors of the measured mobilities m vs the respective analytic results for the three processes.

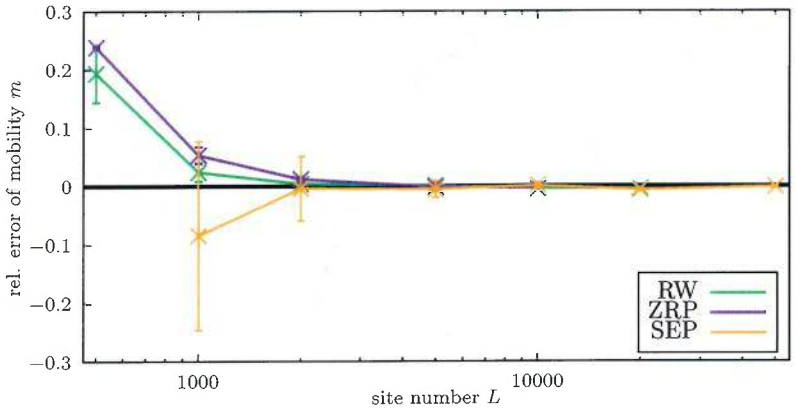

Figure 2.6: Dependence on the site number L. Depicted are the averages over the whole domain of the relative errors of the measured mobilities m vs the respective analytic results for the three processes.

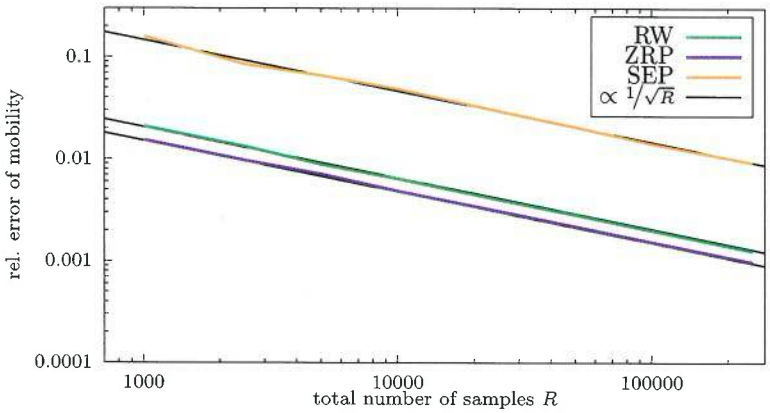

Figure 2.7: Dependence on the number of samples $R = R_{fw} \cdot R_{sw}$. Depicted are the standard errors of the averages of the measured mobilities m over the whole domain for the three processes, respectively. The black lines represent the expectation of a curve with slope $\propto R^{-1/2}$. For the graphs shown here, only R_{sw} is varied, while $R_{fw} = 50$ all the time, but a vice-versa procedure gave similar results.

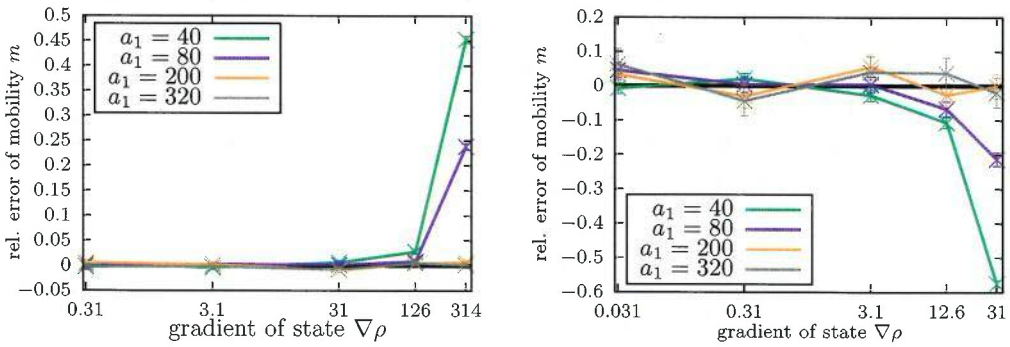

Figure 2.8: Dependence on the support of the test function. Depicted are relative errors of the measured mobilities m at the centre of the domain, $x_0 = 0.5$, vs the respective analytic results. To the left is the ZRP, to the right is the SEP. For the RW no significant dependence was observed.

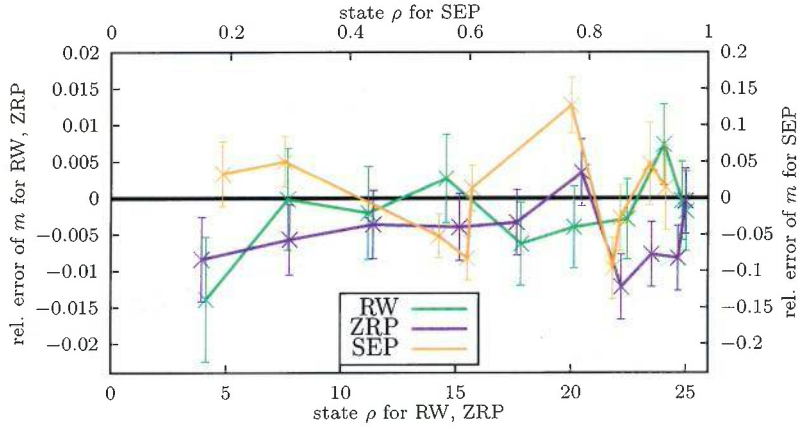

Figure 2.9: Relative errors of the measured mobility vs the analytic mobility, when the "continuous" method is used (see remark 20).

"Continuous" method Results are depicted in fig. 2.9. For this measurement only one pre-initial equilibration t_{fw} was simulated, to then make a total of 100000 snapshot measurements of the following evolution, using the "continuous" method described in remark 20. The numeric results show good agreement, when compared to the analytic mobility averaged over the measurement period.

Comparison with mean square displacement (MSD) in performance and applicability An alternative approach for finding the mobility of a particle process works along the introductory paragraph of subsection 2.1: Each particle gets tagged individually to track its motion and thus finds its mobility via eq. (2.2). The underlying assumption here is (approximate) Brownian dynamics on the particle level, see eq. (2.1). If there is no drift μ - like in our examples for a flat profile (constant in space) - we can even drop the $\lim_{\delta t \searrow 0}$. Such an approach is known to work for the zero-range processes, with the resulting σ (sometimes also known as self diffusion coefficient; see for instance [36, sec. 4.3]) being related to the mobility m via ([20, part II, B]):

$$m(\rho) = \sigma(\rho) \cdot \rho. \tag{2.51}$$

For our simple-exclusion process (in one space dimension and nearest neighbour jumps only), however, it does not work. Instead, the quadratic variations of the particle positions scale with $\sqrt{t}$ in that case (i.e. the particles themselves do not follow a Brownian motion; see [41]). Hence, while the new method could have been blindly applied to these processes, MSD is somewhat less modest, as it asks for Brownian behaviour on the very particle level.

Nonetheless, it is possible to draw a connection between the mobility from the new method and

particle tracking if certain circumstances are met, as the following considerations show:

Proposition 21. *(Connection with mean square displacement)*
We consider particle systems with a total of N particles on the macroscopic domain $\Omega = [0,1]^d$, with the i-th particle at macroscopic time t being located at the macroscopic positions $x_i(t)$. Using the notation $\delta x_i = x_i(t+\delta t) - x_i(t)$ we specifically assume the following conditions on the dynamics of the system:

1. *The macroscopical state ρ, which shall be the Lebesgue density of the limit of the empirical measure $\rho^\epsilon(t) = \epsilon \cdot \sum \left[\delta_{x=x_i(t)}\right]$ for $\epsilon = \frac{1}{N}$, is in global equilibrium (i.e. $\partial_t \rho(t,x) \equiv 0$ everywhere). We also assume translation invariance of the process, i.e. there is no explicit dependence of the dynamics of the particles on the space coordinate x (this implies $\rho(t,x) \equiv \rho_0$ is uniformly distributed). The hydrodynamic limit is achieved by adding more particles, i.e. $\frac{1}{\epsilon} = N \to \infty$ and rescaling time and space accordingly. All quantities, x_i, δx_i, t, δt are to be understood in the macroscopic scaling and are uniformly bounded.*

2. *The particles jump uncorrelated distances from each other, i.e. $\mathbb{E}\left[(e_1 \cdot \delta x_i) \cdot (e_2 \cdot \delta x_j)\right] = 0$ for $i \neq j$ (where "$\cdot$" denotes the standard Euclidean scalar product) and any choice of unit vectors $e_1, e_2 \in \mathbb{R}^d$.*

3. *For each particle i, fixing the jump distance $|\delta x_i|$, the jump directions are isotropically distributed, i.e. $\mathbb{E}\left[(e_1 \cdot \delta x)^2\right] = \mathbb{E}\left[(e_2 \cdot \delta x_i)^2\right]$ for any choice of unit vectors $e_1, e_2 \in \mathbb{R}^d$.*

4. *In the hydrodynamic limit the underlying particle process is almost-surely Hölder-continuous in time, with a Hölder-constant larger than $1/3$, i.e. $\lim_{N\to\infty}\left(\frac{|\delta x_i|^3}{\delta t}\right) \xrightarrow[a.s.]{\delta t \searrow 0} 0$ for each particle i (this property is known to hold for instance for Brownian motion, see e.g. [42, corr. 1.20]).*

5. *The right hand side of eq. (2.19) can be rewritten as (see remark 20 on "continuous" method):*

$$\lim_{\delta t \searrow 0} \lim_{N\to\infty} \mathbb{E}\left[\frac{N \left\langle \gamma, \rho^\epsilon(t+\delta t,.) - \rho^\epsilon(t,.)\right\rangle^2_{L^2(\Omega)}}{2\delta t}\right]. \tag{2.52}$$

Additionally we confine ourselves[3] to test functions γ, which are of the shape of

$$\gamma(x) = \max\left(0, 1 - a_1 \cdot |x - x_0|_1\right), \tag{2.53}$$

where $|.|_1$ is the 1-norm on $\mathbb{R}^d$, $x_0 \in \mathbb{R}^d$ is the location of the peak of the pyramid and $a_1 > 0$ is its slope (this is not a C_0^∞ but has compact support and $\nabla\gamma \in L^\infty(\Omega)$, which suffices, see remark 18). We claim:

[3] This is for simplifying the arguments here, but most likely not necessary.

$$\lim_{\delta t \searrow 0} \lim_{N \to \infty} \mathbb{E}\left[\frac{N \left\langle \gamma, \rho^{\epsilon}\left(t+\delta t, .\right) - \rho^{\epsilon}\left(t, .\right)\right\rangle_{L^2(\Omega)}^2}{2\delta t \left\|\nabla \gamma\right\|_{L^2(\Omega)}^2}\right] = \lim_{\delta t \searrow 0} \lim_{N \to \infty} \mathbb{E}\left[\frac{1}{N} \sum_i \left[\frac{\chi_{\nabla \gamma_i}}{|supp\left(\gamma\right)|} \frac{\left|\delta x_i\right|^2}{d \cdot \delta t}\right]\right], \quad (2.54)$$

where $\chi_{\nabla \gamma_i} \in \{0,1\}$ indicates so-called "good" particles and will be given more specifically later, but selects essentially all particles within the support of γ (considering it the characteristic function of $\nabla \gamma$ would be a slight abuse of notation, though). Here the right hand side can be interpreted as a collective particle tracking on infinitesimal time-intervals.

Proof. To see this, we use the definition of the empirical measure ρ^N to reformulate the left hand side of this equation:

$$N \left\langle \gamma, \rho^{\epsilon}\left(t+\delta t, .\right) - \rho^{\epsilon}\left(t, .\right)\right\rangle_{L^2(\Omega)}^2 = \frac{1}{N}\left(\sum_i \left[\gamma\left(x_i\left(t+\delta t\right)\right) - \gamma\left(x_i\left(t\right)\right)\right]\right)^2. \quad (2.55)$$

Now we notice:

$$\gamma\left(x_i\left(t+\delta t\right)\right) - \gamma\left(x_i\left(t\right)\right) = \nabla \gamma_i \cdot \delta x_i \quad (2.56)$$

for $\nabla \gamma_i = \nabla \gamma\left(x_i\left(t\right)\right)$ for all particles, that do not cross any kinks of the pyramid-shaped γ (i.e. are inside the support of the same of its faces at both times t and $t+\delta t$) - we call these the "good" particles further on. For all others, we identify the "$\nabla \gamma_i$" (abusing notation), such that eqns. (2.55), (2.56) hold and, knowing that a_1 is the Lipschitz constant of the test function, we get $|\nabla \gamma_i| = c_i \cdot a_1$ with the additional prefactor $c_i \in [0,1[$.

The mixed first terms in eq. (2.55) drop out, because of condition 2 with $e_1 = \nabla \gamma_i$, $e_2 = \nabla \gamma_j$ and the translation invariance of the process from condition 1:

$$\mathbb{E}\left[\frac{1}{N}\left(\sum_{i \neq j} \left[\left(\nabla \gamma_i \cdot \delta x_i\right)\left(\nabla \gamma_j \cdot \delta x_j\right)\right]\right)\right] = 0. \quad (2.57)$$

For the quadratic parts of the good particles, we get thanks to the isotropy:

$$\begin{aligned} \mathbb{E}\left[\left(\nabla \gamma_i \cdot \delta x_i\right)^2\right] &= \left|\nabla \gamma_i\right|^2 \mathbb{E}\left[\left(e_1 \cdot \delta x_i\right)^2\right] = \left|\nabla \gamma_i\right|^2 \mathbb{E}\left[\frac{1}{d} \sum_{j=1}^{d} \left(e_j \cdot \delta x_i\right)^2\right] = \\ &= a_1^2 \mathbb{E}\left[\frac{1}{d}\left|\delta x_i\right|^2\right], \end{aligned} \quad (2.58)$$

where here the $(e_j)_j$ are the Cartesian set of orthonormal basis vectors. Together with $\langle \nabla \gamma, \nabla \gamma \rangle_{L^2(\Omega)} = a_1^2 \cdot |\text{supp}\left(\gamma\right)|$ and $\chi_{\nabla \gamma_i}$ being one, iff $|\nabla \gamma_i| = a_1$ (i.e. for good particles) and zero otherwise, this gives the desired result (2.54), if the effect of the particles, that are not good, vanishes. To see this, notice

that only those particles can be not good, that are $|\delta x_i|$ away from one of the kinks of γ. But the Lebesgue measure of the set of these points scales with $|\delta x_i|$ as well and by condition 1 we can estimate the amount of such particles . Hence, the term gets dominated by the good particles (for constant $c > 0$):

$$\lim_{N\to\infty} \mathbb{E}\left[\frac{1}{N}\sum_{i\notin \text{good}}\left[c_i\frac{|\delta x_i|^2}{\delta t}\right]\right] \leq c\cdot \lim_{N\to\infty}\mathbb{E}\left[\frac{1}{N}\sum_i\left[\frac{|\delta x_i|^3}{\delta t}\right]\right] \xrightarrow{\delta t\searrow 0} 0, \tag{2.59}$$

as $\lim_{N\to\infty}\left(\frac{|\delta x_i|^3}{\delta t}\right) \xrightarrow[a.s.]{\delta t\searrow 0} 0$ for all particles by condition 4. □

Note that, in case the system lives on a lattice domain with L sites in each of the d directions and $\rho = \frac{N}{L^d}$ being the average occupation number per site, we could have defined the empirical measure as $\rho^N(t) = \frac{1}{L^d}\cdot\sum_i\left[\delta_{x=x_i(t)}\right]$ instead. The additional factor ρ carries through to give exactly, what we expect for the ZRP (see eq. (2.51)). Furthermore, given that in the particle tagging method, i.e. using the right hand side of eq. (2.54), we use the analytical statement that the mixed terms vanish, we would expect a smaller statistical error compared to using the left hand side of eq. (2.54), where these terms only drop out statistically. In other words, being able to distinguish the particles does give an advantage.

Note on the other hand that the fact that the MSD gives different results for the simple-exclusion process is also in line with the statement of this proposition, where the simple-exclusion process violates the uncorrelatedness condition 2, while for the zero-range processes only the jump rate depends on the other particles as well, which is not affected by the assumptions of the proposition. Also note that tagging a particle is a more specific information, than just the mesoscopic states ρ^ϵ (that do not distinguish particles), that might not be available for all applications. Furthermore, tracking particles has computational complexity proportional to δt, whereas the new method only requires the states at two points in time, t_0 and $t_0+\delta t$. Also note that MSD is (typically) only possible in equilibrium states, whereas the new method from thm. 16 allows to measure the mobility $m(\rho)$ at a whole range of values ρ at once by considering an appropriate profile $x\mapsto\rho(x)$ like it was showcased in fig. 2.4. This can be particularly convenient for on-the-fly computations like those we will carry out in subsection 3.1.

To get an idea of the relative performance of the new method, compared to MSD, in terms of computation time per statistical error, we consider the two zero-range processes for a flat profile $\rho\equiv 5$ in equilibrium. For the MSD, we take the average of $\sigma\cdot\rho$ over all particles in the system. For the new method, we evaluate the mobility for $x_0\in\{0.02, 0.04, \ldots, 0.98\}$ and set $R_{fw} = 1$, thus generating individual realisations only during the period $[t_0 - t_{sf}, t_0]$. Statistical errors are estimated by running the same measurement multiple times. The equilibration time t_{fw} is subtracted from the computation time for both methods. We compare the methods based on the assumption that equivalent measurements can be repeated arbitrarily often, leading to a scaling of the standard error proportional to $\frac{1}{\sqrt{\text{comp. time}}}$. This leads to 17 times or 2 times larger error of the new method for the

RW or ZRP, respectively. To a large extend, these larger errors are caused by the repetition of t_{sw} for each measurement and the efforts for storing the states in an external text file, so they can be processed twice (see last paragraph in subsection 2.3.1), as, if $t_{sw} = 0$ is set instead of the default $t_{sw} = 4 \cdot 10^{-9}$, the factors reduce to 12 or 0.7, respectively, and for choosing the "continuous" version of the new method (see remark 20), even to 3 or 0.2, respectively. Thus, while the RW is still slightly slower for the new method relative to the MSD approach, the ZRP even is faster. The difference between both processes is likely, because of the increased tracking effort, due to the five times higher jump rate of the nonlinear zero-range process compared to the independent random walkers.

Sometimes another possibility to find mobilities m can be, to just determine the expected frequency with which particles jump in an equilibrium system by counting the total number of jumps in a given time interval. This is known to give the desired mobility (up to a prefactor) for instance for the zero-range processes (see eq. (6) in [20]). Note, however, that the mobility gives a relation between time and space (see for instance remark 14 on the units) and thus cannot be expected to be determined by the jump frequency alone, when more complex systems are considered. This becomes apparent for instance for non-jump processes like a system of Brownian particles, where jump rates are not even defined. A popular alternative approach for extracting transport coefficients are Green-Kubo formulas (see e.g. [43, I.7.2, II.2.2]). These use equilibrium correlations between particle currents at different points in time. However, this ansatz confines them to systems in equilibrium, which can be too restrictive, if such a setup is difficult to provide experimentally. Also in a numerical context the ability to measure out of equilibrium can be advantageous, as mentioned above, for example for extracting the mobilities for various values of ρ in one setup. Finally note that for the equilibrium methods typically long-term observations (for instance theoretically the current-current correlations integrated over all times until infinity for the classical Green-Kubo formulas [44, result 9.1]) are necessary, while the new method only considers infinitesimal observation times δt.

To conclude this paragraph we want to point out that the new method is directly aiming at the mobility, not the self diffusivity of the particle process. Also, it does not require the knowledge of the entropy $\mathcal{S}$ (or its changes $\mathcal{DS}$) itself to find this mobility but can be extracted independently; only for finding the diffusivity $\tilde{D}$ is the entropy required - see remark 15.

3 Extending the method to a more general setup

In the previous section 2 we considered processes that follow a weighted Wasserstein gradient flow along the steepest descent of the entropy functional, see eq. (2.4). Such processes cover a wide range of transport phenomena, but with a closer inspection of our settings and result in subsection 2.1 and thm. 16, we can even hope to extend the method to a wider class of irreversible processes. Note that many of these considerations become only formal at this level of generality, but we state the example

of the weighted Wasserstein case in parallel to highlight the analogy.

The metric $\mathcal{K}$ In fact, if we deviate from the setting of subsection 2.1 by replacing eq. (2.4) with the more general gradient flow from eq. (1) and replacing eq. (2.6) with the following equation:

$$dY_\gamma(t) = \langle \gamma, D(\rho)\, y(t,.)\, dt \rangle_{L^2(\Omega)} + \left\langle \gamma, \sqrt{2}\mathcal{A}(\rho)\, dW \right\rangle_{L^2(\Omega)}, \tag{3.1}$$

for a linear operator $\mathcal{A}(\rho)$ (which is only formal at this level of generality), but otherwise similar notation, we have achieved a generalisation of the original setup: For $\mathcal{A}(\rho)(.) = \mathrm{div}(\sqrt{m}(.))$ we recover the weighted Wasserstein case $\mathcal{K}(\rho)(.) = -\mathrm{div}(m(\rho)\nabla(.))$. Note that in general, like in the Wasserstein scenario, the dependence of $\mathcal{A}$ on ρ can be functional, but we assume it is local in time (so $\mathcal{A}(\rho(t,.))$). Moreover, notice that the line of arguments of thm. 16 formally carry over, when doing the same substitution: $\mathrm{div}(\sqrt{m}(.)) \to \mathcal{A}(\rho)(.)$, $-\sqrt{m(\rho)}\nabla(.) \to \mathcal{A}^\dagger(\rho)(.)$ (the adjoint operator of $\mathcal{A}$ in the L^2-sense), giving:

$$\left\langle \gamma, \mathcal{A}(\rho(t_0,.))\, \mathcal{A}^\dagger(\rho(t_0,.))\, \gamma \right\rangle_{L^2(\Omega)} = \lim_{\delta t \searrow 0} \mathbb{E}\left[\frac{(Y_\gamma(t_0+\delta t) - Y_\gamma(t_0))^2}{2\cdot \delta t} \right], \tag{3.2}$$

instead of eq. (2.19). This characterises the diagonal elements of the symmetric operator $\mathcal{A}\mathcal{A}^\dagger$ at time t_0. To get the off-diagonal elements, we can consider formula (3.2) for a set of test functions γ_l, γ_r, $\gamma_l + \gamma_r$ and make use of the symmetry of $\mathcal{A}\mathcal{A}^\dagger$ in combination with the binomial formula to get:

$$\left\langle \gamma_l, \mathcal{A}\mathcal{A}^\dagger \gamma_r \right\rangle_{L^2(\Omega)} = \frac{1}{2}\left(\left\langle \gamma_l+\gamma_r, \mathcal{A}\mathcal{A}^\dagger(\gamma_l+\gamma_r) \right\rangle_{L^2(\Omega)} - \left\langle \gamma_l, \mathcal{A}\mathcal{A}^\dagger \gamma_l \right\rangle_{L^2(\Omega)} - \left\langle \gamma_r, \mathcal{A}\mathcal{A}^\dagger \gamma_r \right\rangle_{L^2(\Omega)} \right), \tag{3.3}$$

where the right hand side only contains diagonal terms. Simplifying eq. (3.2) this way gives the (seemingly) more general version:

$$\lim_{\delta t \searrow 0} \mathbb{E}\left[\frac{(Y_{\gamma_l}(t_0+\delta t) - Y_{\gamma_l}(t_0)) \cdot (Y_{\gamma_r}(t_0+\delta t) - Y_{\gamma_r}(t_0))}{2\cdot \delta t} \right] = \left\langle \gamma_l, \mathcal{A}(\rho(t_0,.))\, \mathcal{A}^\dagger(\rho(t_0,.))\, \gamma_r \right\rangle_{L^2(\Omega)}. \tag{3.4}$$

Note, this only contains projections on $\gamma_{l,r}$, not $\gamma_l + \gamma_r$. Thus, although not fully giving $\mathcal{A}$, we can characterise its square $\mathcal{A}\mathcal{A}^\dagger$ (and hence $\mathcal{A}$ up to a unitary "phase").

The potential $\mathcal{S}$ We now additionally assume $\mathcal{A}\mathcal{A}^\dagger$ to be surjective on the cotangent space of the macroscopic state space of the dynamical system, i.e. along all macroscopic, physical trajectories there is a suitable $\mathcal{D}\mathcal{S}$ for the equation $\partial_t \rho = -\mathcal{A}\mathcal{A}^\dagger \mathcal{D}\mathcal{S}$ to hold, where we already identify $\mathcal{K} := \mathcal{A}\mathcal{A}^\dagger$. Physically speaking, this assumption amounts to the dynamics being (possibly) induced by the noise

term in the mesoscopic evolution equation similar to eq. (2.7):

$$d\rho^{\epsilon}(t,x) = -\mathcal{A}(\rho^{\epsilon})\mathcal{A}^{\dagger}(\rho^{\epsilon})\mathcal{D}\mathcal{S}(\rho^{\epsilon})\,dt + \sqrt{2\epsilon}\cdot\mathcal{A}(\rho^{\epsilon})\,dW \tag{3.5}$$

(which is a formal motivation only). If $\mathcal{D}\mathcal{S}$ on the right hand side of the gradient flow equation is not determined uniquely, yet, i.e. $\mathcal{A}\mathcal{A}^{\dagger}$ is not invertible (like in the Wasserstein case), we choose $\mathcal{D}\mathcal{S}$ such that $\left\|\mathcal{A}^{\dagger}\mathcal{D}\mathcal{S}\right\|^2_{L^2(\Omega)}$ is minimised. If we can observe a macroscopic path $t \mapsto \rho(t)$, thus knowing its derivative $\partial_t\rho$, this functional reads: $\left\|\mathcal{A}^{\dagger}\mathcal{D}\mathcal{S}\right\|^2_{L^2(\Omega)} = \left\langle \mathcal{D}\mathcal{S}, \mathcal{A}\mathcal{A}^{\dagger}\mathcal{D}\mathcal{S}\right\rangle_{L^2(\Omega)} = \left\langle \mathcal{D}\mathcal{S}, \partial_t\rho\right\rangle_{L^2(\Omega)}$. This is the time derivative of $\mathcal{S}$ along the macroscopic path and, upon time integration and up to an initial offset $\mathcal{S}(t_0)$, allows to identify $\mathcal{S}(t)$ along this observed path.

Remark 22. (Wasserstein as a special case)
Note the analogy of this approach to the Wasserstein case for which $\mathcal{A}(\rho)(.) = \operatorname{div}(\sqrt{m}(.)) = \operatorname{div}\left(\sqrt{\rho}(.)\right)$: There the variational derivative of the entropy, $\mathcal{D}\mathcal{S}$, is just the Kantorovich potential $\frac{1}{2}\varphi_{t_0\to t_0+1}$, that characterises the optimal transport from the initial state $\rho(t_0)$ to the final state $\rho_0(t_0+1)$ on the unit time interval $[0,1]$ (see eq. (1.49) and thereafter). From the Benamou-Brenier formula (thm. 5 in connection with eq. (1.41)) we know that the Wasserstein cost for this is just the minimisation of

$$\left\|\frac{1}{2}\nabla\varphi_{t\to t+1}\right\|^2_{L^2(\rho dx;\Omega)} = \left\|-\sqrt{\rho(t,.)}\nabla\frac{1}{2}\varphi_{t\to t+1}\right\|^2_{L^2(\Omega)} = \left\|\mathcal{A}^{\dagger}\mathcal{D}\mathcal{S}\right\|^2_{L^2(\Omega)} \tag{3.6}$$

under the condition $\partial_t\rho = \operatorname{div}\left(\rho\nabla\left(\frac{1}{2}\varphi_{t\to t+1}\right)\right) = -\mathcal{A}\mathcal{A}^{\dagger}\mathcal{D}\mathcal{S}$. From remark 13 we know, $\mathcal{S}$ is linked to the probabilistic cost for time reversal.

Remark 23. (The GENERIC framework)
While the above setting is a much more general one than the Wasserstein case studied before, it is itself embedded in the so-called GENERIC formalism. This is short for "General Equation for Non-Equilibrium Reversible-Irreversible Coupling" and stands for a theoretical framework around the PDE (see [45, eq. (1.1)]):

$$\partial_t\rho(t,x) = \mathcal{K}_{as}(\rho(t,.))\,\mathcal{D}\mathcal{E}(\rho(t,.)) + \mathcal{K}_s(\rho(t,.))\,\mathcal{D}\mathcal{S}(\rho(t,.)), \tag{3.7}$$

where $\mathcal{K}_{as}$ is a anti-symmetric operator, $\mathcal{K}_{as} = -\mathcal{K}_{as}^{\dagger}$, whereas $\mathcal{K}_s$ is a symmetric operator, $\mathcal{K}_s = \mathcal{K}_s^{\dagger}$, which is even positive semi-definite, i.e. $\forall\xi$: $\langle\xi, \mathcal{K}_s\xi\rangle \geq 0$ and $\mathcal{E}$ and $\mathcal{S}$ are functionals, usually referred to as energy or entropy, respectively. Additionally, a non-interaction requirement is imposed, namely $\forall\rho$:

$$\mathcal{K}_s(\rho)\,\mathcal{D}\mathcal{E}(\rho) = 0 = \mathcal{K}_{as}(\rho)\,\mathcal{D}\mathcal{S}(\rho), \tag{3.8}$$

with which we could rewrite eq. (3.7) in the gradient flow shape: $\partial_t\rho = (\mathcal{K}_{as} + \mathcal{K}_s)(\rho)\,\mathcal{D}(\mathcal{E}+\mathcal{S})(\rho)$ (in

the usual GENERIC notation the minus sign is absorbed in the other quantities). Using eqns. (3.7), (3.8) and the (anti-) symmetry properties of the operators $\mathcal{K}_{(a)s}$, it is easy to see:

$$\begin{aligned}\partial_t \mathcal{E}(\rho(t,.)) &= \langle \mathcal{D}\mathcal{E}(\rho), \partial_t \rho\rangle = \langle \mathcal{D}\mathcal{E}(\rho), \mathcal{K}_{as}(\rho)\mathcal{D}\mathcal{E}(\rho)\rangle + \langle \mathcal{D}\mathcal{E}(\rho), \mathcal{K}_s(\rho)\mathcal{D}\mathcal{S}(\rho)\rangle = \\ &= -\langle \mathcal{K}_{as}(\rho)\mathcal{D}\mathcal{E}(\rho), \mathcal{D}\mathcal{E}(\rho)\rangle + \langle \mathcal{K}_s(\rho)\mathcal{D}\mathcal{E}(\rho), \mathcal{D}\mathcal{S}(\rho)\rangle = 0 + 0 = 0 \end{aligned} \tag{3.9}$$

and

$$\begin{aligned}\partial_t \mathcal{S}(\rho(t,.)) &= \langle \mathcal{D}\mathcal{S}(\rho), \partial_t \rho\rangle = \langle \mathcal{D}\mathcal{S}(\rho), \mathcal{K}_{as}(\rho)\mathcal{D}\mathcal{E}(\rho)\rangle + \langle \mathcal{D}\mathcal{S}(\rho), \mathcal{K}_s(\rho)\mathcal{D}\mathcal{S}(\rho)\rangle = \\ &= 0 + \langle \mathcal{D}\mathcal{S}(\rho), \mathcal{K}_s(\rho)\mathcal{D}\mathcal{S}(\rho)\rangle \geq 0. \end{aligned} \tag{3.10}$$

Hence, the energy $\mathcal{E}$ is conserved, whereas the entropy $\mathcal{S}$ increases in time (as mentioned above, here the "physical" notion of entropy is used, that contains an extra minus sign). Consequently, the first term on the right hand side of eq. (3.7) corresponds to reversible dynamics and the second one to irreversible dynamics. Obviously our setup above fits into this framework for $\mathcal{E} \equiv 0 \equiv \mathcal{K}_{as}$ and $\mathcal{K}_s = \mathcal{K} = \mathcal{A}\mathcal{A}^\dagger$.

For further reading on the GENERIC formalism see for instance [13, sec. 1.2], [45].

We now test this approach by trying to forecast the macroscopic evolution of the processes studied earlier (see subsection 2.3.2) based on short snapshot measurements on-the-fly of the full metric $\mathcal{K}$ via formula (3.4). Afterwards we apply the method in more speculative setups, a reaction-diffusion system and a nearest-neighbour Ising model with Glauber dynamics, for which rigorous results on the metric are not known.

3.1 On-the-fly simulations

One particular property of the method outlined in subsection 2.2 is that we are not confined to equilibrium systems, but only require local equilibrium. Another important advantage is that only measurements on short time intervals δt are needed, on which the fluctuations are dominant, but the deterministic motion is not noticeable yet. We can benefit from this, as well as the fact that the method is "non-invasive" (i.e. does not require actively perturbing the system for the measurement), when trying to forecast its future behaviour: We make short term analyses of the current evolution by means of eq. (3.4) to then evolve the system according to the gradient flow model in eq. (2.4). This typically allows for much longer extrapolation times, than the time needed for estimating the operator $\mathcal{K}$ from particle observations, thus being more efficient than running the particle process in parallel throughout. Besides, there is no a-priori knowledge required about the type of the thermodynamic metric (apart from it being consistent with our purely dissipative setup specified in subsection 2.1, which implies positive semi-definiteness and symmetry).

3.1.1 Semi-implicit scheme for gradient flow equation

To implement this numerically, we directly use the more general approach from section 3 and discretise eq. (3.4) in time in a partly implicit and partly explicit scheme: The thermodynamic metric $\mathcal{K}$ is implemented explicitly, as it requires a lot of computational effort to determine. The variational derivative of the entropy, which we assume to be known by different means (see for instance [46] for an overview of experimental methods), is implemented implicitly and then estimated by a Newton approximation procedure. For brevity, we write $\rho^n = \rho(t,.)$ and $\rho^{n+1} = \rho(t+\delta t^{ev},.)$, where $\delta t^{ev} > 0$ is a timestep typically much larger than the measurement time δt from eq. (3.4):

$$\left\langle \gamma, \frac{\rho^{n+1}-\rho^n}{\delta t^{ev}} \right\rangle_{L^2} = \left\langle \gamma, \operatorname{div}\left(m(\rho^n)\nabla \mathcal{DS}\left(\rho^{n+1}\right)\right)\right\rangle_{L^2}. \tag{3.11}$$

As the left hand side of this equation is linear in ρ^{n+1}, as well as the metric $\operatorname{div}(m(\rho^n)\nabla(.))$ is linear in its argument, the Newton approximation at step j is simply:

$$\begin{aligned} 0 \;=\; & -\left\langle \gamma, \frac{\rho^{n+1}_{(j)}-\rho^n}{\delta t^{ev}} \right\rangle_{L^2} + \left\langle \gamma, \operatorname{div}\left(m(\rho^n)\nabla \mathcal{DS}\left(\rho^{n+1}_{(j)}\right)\right)\right\rangle_{L^2} - \\ & -\left\langle \gamma, \frac{\rho^{n+1}_{(j+1)}-\rho^{n+1}_{(j)}}{\delta t^{ev}} \right\rangle_{L^2} + \left\langle \gamma, \operatorname{div}\left(m(\rho^n)\nabla\left(\mathcal{DDS}\left(\rho^{n+1}_{(j)}\right)\left(\rho^{n+1}_{(j+1)}-\rho^{n+1}_{(j)}\right)\right)\right)\right\rangle_{L^2} \end{aligned} \tag{3.12}$$

hence, for $\rho^{n+1}_{(0)} = \rho^n$ and $\rho^{n+1}_{(1)} = \rho^{n+1}$ (i.e. we confine ourselves to only one Newton step, i.e. approximations up to the first order):

$$\left\langle \gamma, \frac{\rho^{n+1}-\rho^n}{\delta t^{ev}} \right\rangle_{L^2} = \left\langle -\nabla\gamma, m(\rho^n)\nabla\left(\mathcal{DS}(\rho^n) + \mathcal{DDS}(\rho^n)\left(\rho^{n+1}-\rho^n\right)\right)\right\rangle_{L^2}. \tag{3.13}$$

The overall idea behind this semi-implicit approach is, to benefit from the better stability, that is usually associated with implicit methods, to get relatively long extrapolation timesteps δt^{ev} (this is generally typically only known for linear equations, like the evolution of the RW or SEP; see for instance [47, Ch. 2,3]), while keeping the computational cost small for the observations of the fluctuations of the particle processes (thus implementing the metric in an explicit way). The hope is, this will give short observation periods δt and allow for long extrapolations δt^{ev}.

We express all quantities in eq. (3.18) in terms of the finite element basis from eq. (2.31) with $a_2 = 1$, i.e. piecewise linear shape in each coordinate direction. Making use of Einstein's summation

rule, we define: $\rho_l^n := \langle \gamma_l, \rho^n \rangle_{L^2}$ and Z_{lr}, $\mathcal{K}_{lr}^n$, $\mathcal{DS}_l^n$, $\mathcal{DDS}_{lr}^n$ such that:

$$
\begin{aligned}
Z_{lr} &:= \langle \gamma_l, \gamma_r \rangle_{L^2} && (3.14)\\
\mathcal{K}_{lr}^n &:= \langle \gamma_l, \mathcal{K}(\rho^n)\gamma_r \rangle_{L^2} && (3.15)\\
\mathcal{DS}_{\tilde{l}}^n Z_{\tilde{l}r} &:= \langle \mathcal{DS}(\rho^n), \gamma_r \rangle_{L^2} && (3.16)\\
Z_{l\tilde{r}}\mathcal{DDS}_{\tilde{l}\tilde{r}}^n Z_{\tilde{l}r} &:= \langle \gamma_l, \mathcal{DDS}(\rho^n)\gamma_r \rangle_{L^2} && (3.17)
\end{aligned}
$$

(for consistency, we could have also added the Z_{lr} term to the ρ_l^n definition, but it ends up making the equations (and numerics) more cumbersome). With this notation we can rewrite eq. (3.13) and solve for ρ_l^n:

$$
\rho_l^{n+1} - \rho_l^n = A_{l\tilde{r}}^{-1}\left(-\delta t^{ev}\mathcal{K}_{\tilde{r}r}^n \mathcal{DS}_r^n\right) \tag{3.18}
$$

for $A_{lr} := \delta_{l,r} + \delta t^{ev}\mathcal{K}_{l\tilde{r}}^n \mathcal{DDS}_{\tilde{r}r}^n$ an invertible operator for small enough δt^{ev} (for a twice as good spatial resolution, i.e. $a_1 \to 2\cdot a_1$, the time increment δt^{ev} must be one quarter the original size, $\delta t^{ev} \to {}^{\delta t^{ev}}/_4$; the steepest slope, that is still reproducible in the basis of eq. (2.31) is a_1).

3.1.2 "Classical" implicit scheme

To compare the validity of our results, we will consider the same particle systems as examples as in subsection 2.3.2 (the independent nearest neighbour random walkers, RW, a zero-range process with quadratic jump rate per site, ZRP, and a symmetric simple-exclusion process, SEP) and also implement their analytically known limit equations in an implicit scheme with one Newton step. All our systems are known analytically to have macroscopic evolution equations of the shape:

$$
\partial_t \rho(t,x) = \Delta\Phi\left(\rho(t,x)\right), \tag{3.19}
$$

where

$$
\Phi(\rho) = \begin{cases} \frac{1}{2}\rho & \text{for the RW} \\ m_{ZRP}(\rho) & \text{for the ZRP} \\ \frac{1}{2}\rho & \text{for the SEP} \end{cases} \tag{3.20}
$$

and m_{ZRP} is the mobility of the zero-range process with quadratic jump rate, as specified implicitly in eq. (2.42). This can be seen for instance by direct algebraic simplification via the gradient flow data given below. A purely implicit, backward-Euler numerical scheme for this evolution would read:

$$
\left\langle \gamma, \frac{\rho^{n+1} - \rho^n}{\delta t^{ev}} \right\rangle_{L^2} = \left\langle \gamma, \Delta\Phi\left(\rho^{n+1}\right) \right\rangle_{L^2}, \tag{3.21}
$$

which is directly implementable for the RW and the SEP, as their Φ are linear functions (and the evolution becomes just the heat equation). For the ZRP the approach is to linearise Φ via one Newton step, just like for $\mathcal{DS}$ in eq. (3.13):

$$\left\langle \gamma, \frac{\rho^{n+1}-\rho^n}{\delta t^{ev}} \right\rangle_{L^2} = \left\langle \gamma, \Delta\left(\Phi\left(\rho^n\right) + \Phi'\left(\rho^n\right)\left(\rho^{n+1}-\rho^n\right)\right)\right\rangle_{L^2}, \tag{3.22}$$

which becomes in the finite element representation analogous to eq. (3.18):

$$\rho_l^{n+1} - \rho_l^n = \tilde{A}_{l\tilde{r}}^{-1}\left(\delta t^{ev} \Delta_{\tilde{r}r} \Phi_r^n\right) \tag{3.23}$$

for $\tilde{A}_{lr} = \delta_{l,r} - \delta t^{ev} \Delta_{l\tilde{r}} \Phi'_{\tilde{r}r}$ with $\Delta_{lr} = \langle \gamma_l, \Delta\gamma_r \rangle_{L^2}$, $\Phi_{\tilde{l}}^n Z_{\tilde{l}r} := \langle \Phi\left(\rho^n\right), \gamma_r \rangle_{L^2}$, $Z_{l\tilde{r}} \Phi'_{\tilde{l}\tilde{r}} Z_{\tilde{l}r} = \langle \gamma_l, \Phi'\left(\rho^n\right)\gamma_r \rangle_{L^2}$, i.e. similar to eqns. (3.14)-(3.17) with Δ, Φ, Φ' playing the role of $(-\mathcal{K})$, $\mathcal{DS}$, $\mathcal{DDS}$, respectively (note, that in the algorithmic implementation, this is implemented with an additional factor Z in front of ρ_l^n, which is mathematically equivalent and was done for convenience of the graphical output).

3.1.3 Comparison between on-the-fly results with "classical" finite element approach

Note, the gradient flow implementation described above deviates from the "classical" scheme, because our approach is only semi-implicit. Making use of the identities:

$$\Phi'\left(\rho^n\right)\nabla\rho^n = \nabla\Phi\left(\rho^n\right) = m\left(\rho^n\right)\nabla\mathcal{DS}\left(\rho^n\right) = m\left(\rho^n\right)\mathcal{DDS}\left(\rho^n\right)\nabla\rho^n \tag{3.24}$$

we can quantify the difference between the two approaches, denoting by ρ^{n+1} the state one timestep δt^{ev} after ρ^n, when computed based on the semi-implicit gradient flow scheme, i.e. via eq. (3.13):

$$\begin{aligned}
&\left\langle \gamma, \frac{\rho^{n+1}-\rho^n}{\delta t^{ev}} \right\rangle_{L^2} = \\
&= \left\langle -\nabla\gamma, m\left(\rho^n\right)\nabla\left(\mathcal{DS}\left(\rho^n\right) + \mathcal{DDS}\left(\rho^n\right)\left(\rho^{n+1}-\rho^n\right)\right)\right\rangle_{L^2} = \\
&= \left\langle -\nabla\gamma, \nabla\left(\Phi\left(\rho^n\right) + \Phi'\left(\rho^n\right)\left(\rho^{n+1}-\rho^n\right)\right)\right\rangle_{L^2} + \\
&\quad + \left\langle -\nabla\gamma, -\nabla\left(m\left(\rho^n\right)\mathcal{DDS}\left(\rho^n\right)\left(\rho^{n+1}-\rho^n\right)\right) + m\left(\rho^n\right)\nabla\left(\mathcal{DDS}\left(\rho^n\right)\left(\rho^{n+1}-\rho^n\right)\right)\right\rangle_{L^2} = \\
&= \left\langle \gamma, \Delta\left(\Phi\left(\rho^n\right) + \Phi'\left(\rho^n\right)\left(\rho^{n+1}-\rho^n\right)\right)\right\rangle_{L^2} + \left\langle \nabla\gamma, m'\left(\rho^n\right)\left(\rho^{n+1}-\rho^n\right)\nabla\mathcal{DS}\left(\rho^n\right)\right\rangle_{L^2} = \\
&= \left\langle \gamma, \Delta\left(\Phi\left(\rho^n\right) + \Phi'\left(\rho^n\right)\left(\rho^{n+1}-\rho^n\right)\right)\right\rangle_{L^2} + \left\langle \gamma, \delta\mathcal{K}^{n,n+1}\mathcal{DS}\left(\rho^n\right)\right\rangle_{L^2},
\end{aligned} \tag{3.25}$$

where we set

$$\delta\mathcal{K}^{n,n+1} := -\mathrm{div}\left(m'\left(\rho^n\right)\left(\rho^{n+1}-\rho^n\right)\nabla(.)\right). \tag{3.26}$$

Note that, while the error term $\left\langle \gamma, \delta\mathcal{K}^{n,n+1}\mathcal{DS}\left(\rho^n\right)\right\rangle_{L^2}$ is given here in the evolution equation only (and not solved for ρ^{n+1}), this is still the highest-order error term for the state ρ^{n+1} in a single timestep,

due to the linear shape of the equation. Specifically for sufficiently small δt^{ev} (note that all operators are bounded for our finite element representation, if ρ^n is bounded away from 0 (and 1 for the SEP)):

$$\begin{aligned}\frac{\rho^{n+1}-\rho^n}{\delta t^{ev}} &= \left(\mathbb{I}-\delta t^{ev}\Delta\left(\Phi'\left(\rho^n\right)(.)\right)+\delta t^{ev}\mathrm{div}\left(m'\left(\rho^n\right)(.)\nabla\mathcal{DS}\left(\rho^n\right)\right)\right)^{-1}\left(\Delta\Phi\left(\rho^n\right)\right)= \\ &= \sum_{j=0}^{\infty}\left[\left(\delta t^{ev}\cdot\left(\Delta\left(\Phi'\left(\rho^n\right)(.)\right)-\mathrm{div}\left(m'\left(\rho^n\right)(.)\nabla\mathcal{DS}\left(\rho^n\right)\right)\right)\right)^j\right]\left(\Delta\Phi\left(\rho^n\right)\right)= \\ &= \Delta\Phi\left(\rho^n\right)+\left(\delta t^{ev}\cdot\left(\Delta\left(\Phi'\left(\rho^n\right)(.)\right)-\mathrm{div}\left(m'\left(\rho^n\right)(.)\nabla\mathcal{DS}\left(\rho^n\right)\right)\right)\right)\Delta\Phi\left(\rho^n\right)+\mathcal{O}\left(\left(\delta t^{ev}\right)^2\right),\end{aligned} \tag{3.27}$$

where we omitted the index notation from eqns. (3.18), (3.23) and used the geometric series expansion of $\left(\mathbb{I}-A\right)^{-1}=\sum_{j=0}^{\infty}\left[A^j\right]$ (if the maximal modulus of the eigenvalues of a matrix A is strictly below 1, i.e. δt^{ev} is small enough in our case). Comparing this with a similar expansion for the reference scheme from eq. (3.23) gives the first-order error of: $-\delta t^{ev}\mathrm{div}\left(m'\left(\rho^n\right)\left(\Delta\Phi\left(\rho^n\right)\right)\nabla\mathcal{DS}\left(\rho^n\right)\right)=\delta\mathcal{K}^{n,n+1}\mathcal{DS}\left(\rho^n\right)+\mathcal{O}\left(\left(\delta t^{ev}\right)^2\right)$. Note, however, that this effect seems to be negligible compared to statistical deviations when determining the thermodynamic metric $\mathcal{K}$ from the particle fluctuations, see item on the RW below and fig. 3.1.

Conservation-of-mass property Although such statistical deviations in $\mathcal{K}$ can occur in many ways, the conservation-of-mass property still carries over from the microscopic process, if $a_2=1$ for the basis functions from eq. (2.31): Due to $\sum_l\left[\gamma_l(x)\right]\equiv a_1$ in combination with the left hand side of eq. (3.18) conservation of mass amounts to the column-sums of $\mathcal{K}$ being zero, which can be seen from eq. (3.2) via:

$$\begin{aligned}&\sum_l\left[\left\langle\gamma_l,\mathcal{K}\left(\rho^n\right)\gamma_r\right\rangle_{L^2}\right]\approx \\ &\approx\sum_l\left[\left(Y_{\gamma_l}^{\epsilon}\left(t_0+\delta t\right)-Y_{\gamma_l}^{\epsilon}\left(t_0\right)\right)\right]\cdot\frac{Y_{\gamma_r}^{\epsilon}\left(t_0+\delta t\right)-Y_{\gamma_r}^{\epsilon}\left(t_0\right)}{2\cdot\delta t}= \\ &=\left(\frac{\left\langle 1,\rho^{\epsilon}\left(t_0+\delta t,.\right)-\rho\left(t_0+\delta t,.\right)\right\rangle_{L^2}}{\sqrt{\epsilon}}-\frac{\left\langle 1,\rho^{\epsilon}\left(t_0,.\right)-\rho\left(t_0,.\right)\right\rangle_{L^2}}{\sqrt{\epsilon}}\right)\cdot\frac{Y_{\gamma_r}^{\epsilon}\left(t_0+\delta t\right)-Y_{\gamma_r}^{\epsilon}\left(t_0\right)}{2\cdot\delta t}= \\ &=\left(\frac{\left\langle 1,\rho^{\epsilon}\left(t_0+\delta t,.\right)-\rho^{\epsilon}\left(t_0,.\right)\right\rangle_{L^2}}{\sqrt{\epsilon}}-\frac{\left\langle 1,\rho\left(t_0+\delta t,.\right)-\rho\left(t_0,.\right)\right\rangle_{L^2}}{\sqrt{\epsilon}}\right)\cdot\frac{Y_{\gamma_r}^{\epsilon}\left(t_0+\delta t\right)-Y_{\gamma_r}^{\epsilon}\left(t_0\right)}{2\cdot\delta t}= \\ &=0,\end{aligned} \tag{3.28}$$

where the last line comes from the fact that $\left\langle 1,\partial_t\rho\left(t,.\right)\right\rangle_{L^2}=0=\left\langle 1,\partial_t\rho^{\epsilon}\left(t,.\right)\right\rangle_{L^2}$ for all times $t\geq 0$. The notation "$\approx$" in the first line refers to omitting the limits $\delta t\searrow 0$, $\epsilon\searrow 0$ and not taking the expectation $\mathbb{E}$, as these operations are only approximated in the numerical scheme (analogue to subsection 2.3.1). As can be seen from the last line, this still holds, if the "continuous" method is

applied.

Entropy-reduction property Also note that the symmetric and positive semi-definite structure of $\mathcal{K}$ is preserved for any estimate made on basis of eq. (3.2). This implies the entropy to be non-increasing in each timestep, up to first order, as the following calculation shows (using the notation $\delta\mathcal{S}^{n,n+1} := \mathcal{DS}(\rho^n) + (\rho^{n+1} - \rho^n)\,\mathcal{DDS}(\rho^n)$):

$$\begin{aligned}
&\left\langle \mathcal{DS}(\rho^n), \frac{\rho^{n+1} - \rho^n}{\delta t^{ev}} \right\rangle_{L^2} + \frac{1}{2}\left\langle (\rho^{n+1} - \rho^n)\,\mathcal{DDS}(\rho^n), \frac{\rho^{n+1} - \rho^n}{\delta t^{ev}} \right\rangle_{L^2} = \\
&= \left\langle \mathcal{DS}(\rho^n), -\mathcal{K}(\rho^n)\,\delta\mathcal{S}^{n,n+1} \right\rangle_{L^2} + \frac{1}{2}\left\langle (\rho^{n+1} - \rho^n)\,\mathcal{DDS}(\rho^n), -\mathcal{K}(\rho^n)\,\delta\mathcal{S}^{n,n+1} \right\rangle_{L^2} = \\
&= \left\langle \mathcal{DS}(\rho^n) + (\rho^{n+1} - \rho^n)\,\mathcal{DDS}(\rho^n), -\mathcal{K}(\rho^n)\left(\mathcal{DS}(\rho^n) + \mathcal{DDS}(\rho^n)(\rho^{n+1} - \rho^n)\right) \right\rangle_{L^2} - \\
&\quad - \frac{1}{2}\left\langle (\rho^{n+1} - \rho^n)\,\mathcal{DDS}, -\mathcal{K}(\rho^n)\,\mathcal{DS}(\rho^n) \right\rangle_{L^2} - \\
&\quad - \frac{1}{2}\left\langle (\rho^{n+1} - \rho^n)\,\mathcal{DDS}, -\mathcal{K}(\rho^n)\left(\mathcal{DDS}(\rho^n)(\rho^{n+1} - \rho^n)\right) \right\rangle_{L^2} = \\
&= \left\langle \delta\mathcal{S}^{n,n+1}, -\mathcal{K}(\rho^n)\,\delta\mathcal{S}^{n,n+1} \right\rangle_{L^2} - \frac{1}{2}\left\langle (\rho^{n+1} - \rho^n)\,\mathcal{DDS}(\rho^n), \frac{\rho^{n+1} - \rho^n}{\delta t^{ev}} \right\rangle_{L^2} \leq 0,
\end{aligned} \tag{3.29}$$

where, for the final inequality, we used the positive semi-definiteness of $\mathcal{K}$ and the convexity of $\mathcal{S}$ (i.e. $\mathcal{DDS} \geq 0$), that holds for all our examples. Note that, while conservation of mass holds all the same for the "classical" method (the column-sums of the discrete Laplace operator Δ_{lr} are zero), the first order approximation of the entropy changes per timestep gets an additional additive term via eq. (3.25) and eq. (3.27):

$$-\left\langle \mathcal{DS}(\rho^n), \delta\mathcal{K}^{n,n+1}\mathcal{DS}(\rho^n) \right\rangle_{L^2} = -\left\langle \nabla\mathcal{DS}(\rho^n), m'(\rho^n)(\rho^{n+1} - \rho^n)\,\nabla\mathcal{DS}(\rho^n) \right\rangle_{L^2}, \tag{3.30}$$

where the states ρ^{n+1}, ρ^n could be viewed as either derived via the "classic" or the semi-implicit method, as their differences are higher order. Since $\delta\mathcal{K}^{n,n+1}$ is (typically) not positive semi-definite (depending on $m'(\rho^n)$ and $\rho^{n+1} - \rho^n$), this term may be positive as well, which would lead to a slower entropy reduction.

Default settings and numerical implementation As far as applicable, the same parameters were chosen for the semi-implicit gradient flow implementation (eq. (3.18)) as well as the implicit reference scheme (eq. (3.23)): Namely, the macroscopic timesteps $\delta t^{ev} = 5 \cdot 10^{-5}$ for the evolution, while the time increment for determining the fluctuations is $\delta t = 1 \cdot 10^{-11}$ and the waiting times are $t_{fw} = 1 \cdot 10^{-9}$, $t_{sw} = 0$ (see the paragraph on local equilibrium in subsection 2.3.2 for the definition of these times). In each timestep a total of $R = R_{fw} \cdot R_{sw} = 1 \cdot 1000$ samples were used. We consider systems, that macroscopically live on the one-dimensional unit-interval $\Omega = [0, 1]$ with

periodic boundary conditions and initial density profile $x \mapsto \frac{1}{2} \cdot \left(1 + \frac{1}{2} \sin\left(2\pi\left(x - \frac{1}{2}\right)\right)\right)$ for the SEP and $x \mapsto 5 \cdot \left(1 + \frac{1}{2} \sin\left(2\pi\left(x - \frac{1}{2}\right)\right)\right)$ for the RW and ZRP. The numerical space-discretisation, for estimating integrals via a Riemann sum and derivatives via a symmetric Euler scheme, equals the number of microscopical sites in the particle simulations, $L = 10000$. Derivatives with respect to the states are based on Euler schemes with increments of 0.001. The finite element basis $\{\gamma_l\}_l$ consists of 40 functions of the type specified in eq. (2.31) with the settings $a_0 = 1$, $a_1 = 40$, $a_2 = 1$ and $x_0 \in \{0.0125, 0.0375, \ldots, 0.9875\}$. The variational derivatives $\mathcal{DS}$ of the entropy and the Φ- and Φ'-values are given analytically (see below and eq. (3.20), respectively), where for the ZRP the implicit characterisation of m_{ZRP} in eq. (2.42) is solved via Maple and saved as a list for the ρ-values:

$$\{0, 0.001, 0.005, 0.01, 0.05, 0.1, \ldots, 1.2, 1.3, \ldots, 3.2, 3.5, 4, \ldots, 10, 11, \ldots, 30\}. \tag{3.31}$$

The required values are then looked up from this list via a piecewise linear interpolation of $\frac{m_{ZRP}(\rho)}{\rho}$ (which is almost linear; see fig. 2.2). If values beyond $\rho = 30$ are needed, they are approximated by $\rho \mapsto \frac{1}{2} \cdot \rho \cdot \left(\rho + \frac{1}{2}\right)$. Matrix inversions, as they occur in eqns. (3.18), (3.23), are implemented as fixed point iterations as described in [48]. The iteration is aborted and thus the current candidate A_c^{-1} accepted as estimate for the inverse of a matrix A, if the Frobenius norm of the matrix $AA_c^{-1} - \mathbb{I}$ (i.e. $\sqrt{\sum_l \sum_r \left[\left(\left(AA_c^{-1} - \mathbb{I}\right)_{lr}\right)^2\right]}$) is below the threshold of $1 \cdot 10^{-8}$.

The extraction of the thermodynamic metric $\mathcal{K}$ from the particle processes is done in an analogous way to subsection 2.3.1, except that - unlike the data for the mobility in subsection 2.4 - observed particle configurations are not saved externally but the procedure from around eq. (2.37) is applied with Kahan summation.

Numerical results How the deviations in eq. (3.25) look like, depends on the specific process the procedure is applied to:

- For the RW the mobility is $m_{RW}(\rho) = \frac{1}{2}\rho$ and the entropy is $\mathcal{S}_{RW}(\rho) = \int \rho \cdot (\ln(\rho) - 1)\, dx$, thus giving $\mathcal{DS}_{RW}(\rho) = \ln(\rho)$ and $\mathcal{DDS}_{RW}(\rho) = \frac{1}{\rho}$. Plugging this into eq. (3.25) we get:

$$\left\langle \gamma, \frac{\rho^{n+1} - \rho^n}{\delta t^{ev}} \right\rangle_{L^2} = \frac{1}{2} \left\langle -\nabla\gamma, \nabla\rho^{n+1} \right\rangle_{L^2} + \left\langle \nabla\gamma, \frac{1}{2}\left(\rho^{n+1} - \rho^n\right) \cdot \frac{\nabla\rho^n}{\rho^n} \right\rangle_{L^2}. \tag{3.32}$$

  In practice, though, this error has been dominated by the statistical error, with which the operator $\mathcal{K}_{RW}$ was determined from the fluctuations. For results, see fig. 3.1. The data is based on the default settings. As can be seen, the deviations can barely be noticed with the naked eye and do not blow up over long periods of time. In fact, the particle-informed gradient flow method is even closer to the analytically computed result than the "classic" finite element approach. Note that the total observation time $R \cdot \delta t$ is only about 0.02% of the time step for extrapolating the

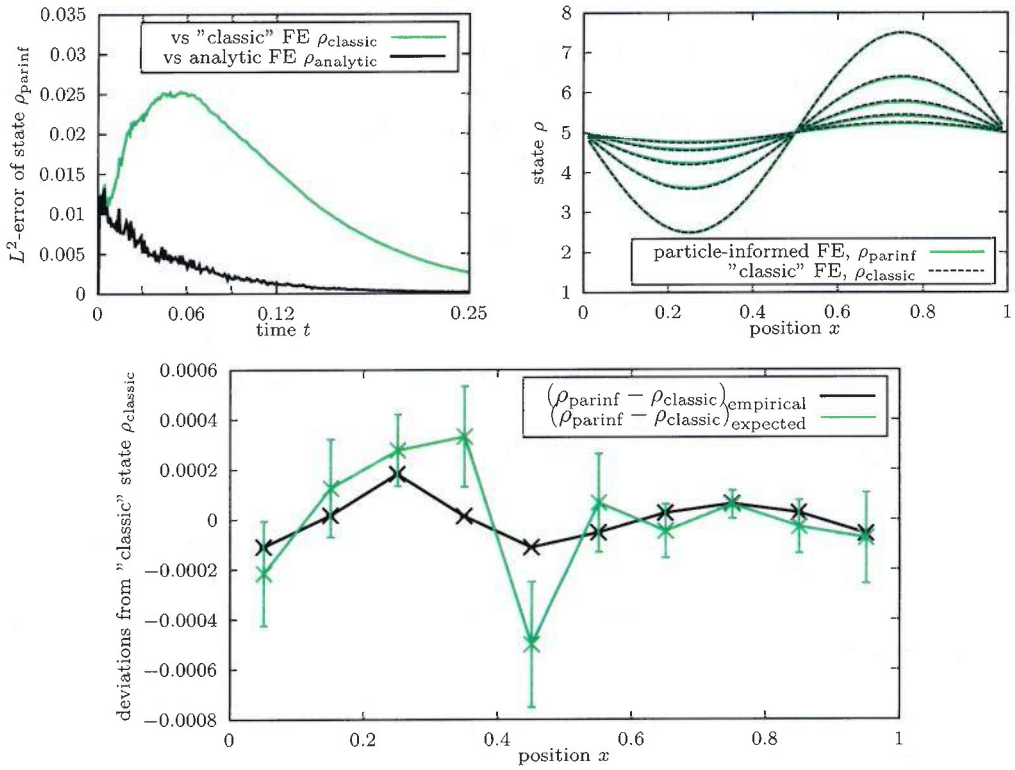

Figure 3.1: Evolution results for the one-dimensional system of independent random walkers. On the top row the left image shows the L^2-error of the gradient flow scheme from eq. (3.18), when compared to the "classical" finite element approximation ρ_{classic} (see eq. (3.23)). The picture on the right shows snapshots of the evolution of an initial sin-profile via each of the two approaches at the times $t \in \{0, 0.03, 0.06, 0.09, 0.12\}$. The bottom image shows the error $\rho^1_{\text{parinf}} - \rho^1_{\text{classic}}$ after a single evolution timestep of $\delta t^{ev} = 10^{-3}$ for a basis of ten test functions $x_0 \in \{0.05, 0.15, \ldots, 0.95\}$, $a_1 = 10$ and $L = 1000$ sites, $\delta t = 10^{-8}$ measurement time and a total of 256000000 samples. Note that despite having measured more than $1 \cdot 10^5$ times as many samples as in the other examples shown here, the analytic differences can only be adumbrated.

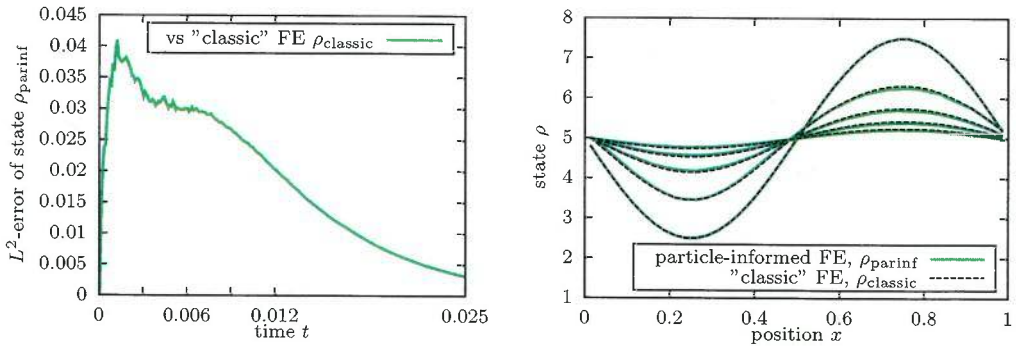

Figure 3.2: Evolution results for the one-dimensional zero-range process with jump rate of $g(k) = k^2$ per site with occupation number k. The left image shows the L^2-error of the gradient flow scheme from eq. (3.18), when compared to the "classical" finite element approximation ρ_{classic} (see eq. (3.23)). The picture on the right shows snapshots of the evolution of an initial sin-profile via each of the two approaches at the times $t \in \{0, 0.003, 0.006, 0.009, 0.012\}$.

evolution, δt^{ev}, meaning we can extrapolate a future period about 5000 times longer, than the one we just observed.

- For the ZRP the mobility $m_{ZRP}(\rho)$ is implicitly given by eq. (2.42) and the entropy is $\mathcal{S}_{ZRP}(\rho) = \int (\rho \ln(2 \cdot m_{ZRP}(\rho)) - \ln(Z(2 \cdot m_{ZRP}(\rho)))) dx$, thus giving $\mathcal{DS}_{ZRP}(\rho) = \ln(2 \cdot m_{ZRP}(\rho))$ and $\mathcal{DDS}_{ZRP}(\rho) = \frac{m'_{ZRP}(\rho)}{m_{ZRP}(\rho)}$. By means of eq. (3.25) we get:

$$\begin{aligned} \left\langle \gamma, \frac{\rho^{n+1} - \rho^n}{\delta t^{ev}} \right\rangle_{L^2} &= \left\langle -\nabla\gamma, \nabla\left(m_{ZRP}(\rho^n) + m'_{ZRP}(\rho^n)\left(\rho^{n+1} - \rho^n\right)\right)\right\rangle_{L^2} + \\ &\quad + \left\langle \nabla\gamma, \frac{\left(m'_{ZRP}(\rho^n)\right)^2}{m_{ZRP}(\rho^n)} (\nabla\rho^n)\left(\rho^{n+1} - \rho^n\right)\right\rangle_{L^2}. \end{aligned} \tag{3.33}$$

For results see fig. 3.2. The data is based on the default settings, except $\delta t^{ev} = 1 \cdot 10^{-5}$ to account for the faster dynamics. As can be seen, the deviations can barely be noticed with the naked eye and do not blow up over long periods of time. In fact, the particle-informed gradient flow method is even closer to the analytically computed result than the "classic" finite element approach. Note that the total observation time $R \cdot \delta t$ is only about 0.1% of the time step for extrapolating the evolution, δt^{ev}.

- For the SEP the mobility is $m_{SEP}(\rho) = \frac{1}{2} \cdot \rho \cdot (1 - \rho)$ and the entropy $\mathcal{S}_{SEP}(\rho) = \int (\rho \ln(\rho) + (1 - \rho) \ln(1 - \rho)) dx$, thus giving $\mathcal{DS}_{SEP}(\rho) = \ln\left(\frac{\rho}{1-\rho}\right)$ and $\mathcal{DDS}_{SEP}(\rho) = \frac{1}{\rho(1-\rho)}$. Via

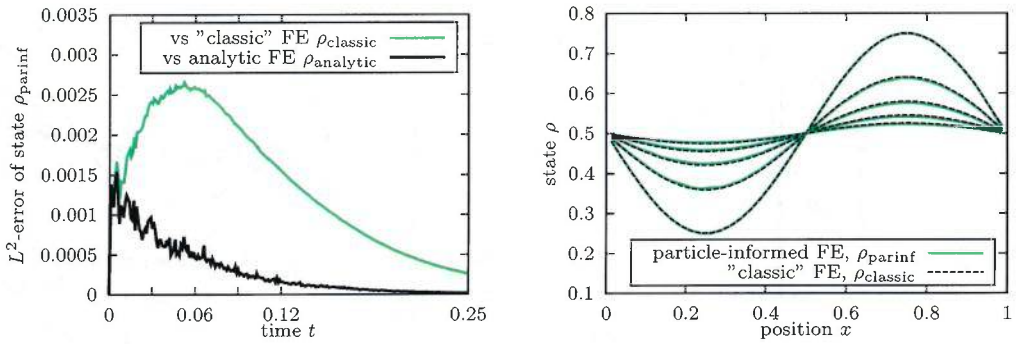

Figure 3.3: Evolution results for the one-dimensional symmetric simple-exclusion process. The left image shows the L^2-error of the gradient flow scheme from eq. (3.18), when compared to the "classical" finite element approximation ρ_{classic} (see eq. (3.23)). The picture on the right shows snapshots of the evolution of an initial sin-profile via each of the two approaches at the times $t \in \{0, 0.03, 0.06, 0.09, 0.12\}$.

eq. (3.13) we get:

$$\left\langle \gamma, \frac{\rho^{n+1} - \rho^n}{\delta t^{ev}} \right\rangle_{L^2} = \frac{1}{2} \left\langle -\nabla\gamma, \nabla\rho^{n+1} \right\rangle_{L^2} + \\ + \left\langle \nabla\gamma, \frac{1 - 2\rho^n}{2} \left(\rho^{n+1} - \rho^n\right) \cdot \frac{\nabla\rho^n}{\rho^n \left(1 - \rho^n\right)} \right\rangle_{L^2}. \tag{3.34}$$

For results see fig. 3.3. The data is based on the default settings. As can be seen, the deviations can barely be noticed with the naked eye and do not blow up over long periods of time. In fact, the particle-informed gradient flow method is even closer to the analytically computed result than the "classic" finite element approach. Note that the total observation time $R \cdot \delta t$ is only about 0.02% of the time step for extrapolating the evolution, δt^{ev}.

About getting the entropy via observations of the deterministic paths In principle, it would be desirable to get the entropy $\mathcal{S}$ (or at least $\mathcal{DS}$) from this method as well. Given that the particle dynamics is (macroscopically) purely diffusive and the metric $\mathcal{K}(\rho)(.) = -\text{div}(m(\rho)\nabla(.))$ is invertible (up to a constant, which does not contribute to the dynamics), we could observe a trajectory $t \mapsto \rho(t)$ of the evolution and then extract:

$$\mathcal{DS}(\rho) = -\mathcal{K}^{-1}(\rho)(\partial_t \rho). \tag{3.35}$$

However, it turns out that to get the deterministic $\partial_t \rho$ correct, we need to observe the system much longer, than just for the (short term) fluctuations, that were used for finding the mobility m. See

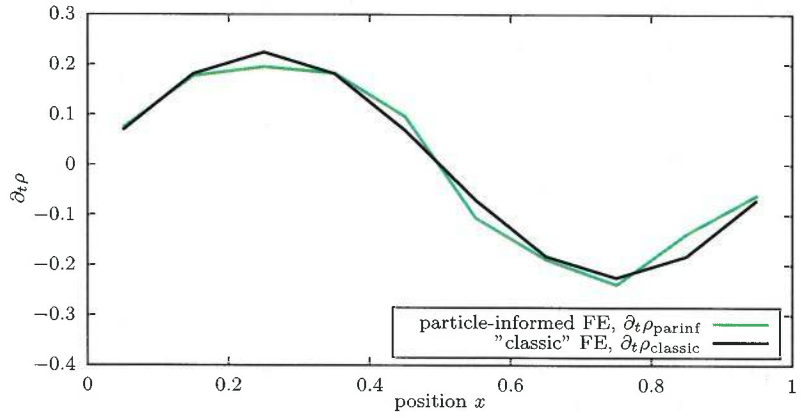

Figure 3.4: $\partial_t\rho$ analytically and numerically for the system of independent, one-dimensional random walkers and a sin-profile. The data is based on a timestep $\delta t = 0.1$, 10000 samples and a system of 1000 sites and ca. $N = 500$ particles.

fig. 3.4.

3.2 Reaction-diffusion example

We test the above-mentioned ideas for a two-dimensional nearest neighbour reaction-diffusion model on a periodic lattice of $L \times L$ sites. The notation will be borrowed from subsections 2.3.1, 2.3.2. A two-species process is considered, where, on top of the random walk of each species independently, there is a fixed frequency with which existing particles of one species transform into particles of the other species (while staying at the same location) and vice versa (again by a Poisson process):

$$0 \cdot (\text{spec. } 1) + 1 \cdot (\text{spec. } 2) \rightleftharpoons 1 \cdot (\text{spec. } 1) + 0 \cdot (\text{spec. } 2)\,. \tag{3.36}$$

The jump- and transformation-rates, $\tilde{\beta}$ and $\tilde{\alpha}$, are distinct from one another, but identical for all particles across both species. The generator of such a process can be written as:

$$\begin{aligned}
&\int_0^1 |\dot{\mu}_t|\, dt = \\
&= \tilde{\alpha} \cdot \sum_X \left[k_1(X) \cdot \left(f\left(k_1^{X;-}, k_2^{X;+}\right) - f(k_1,k_2) \right) + k_2(X) \cdot \left(f\left(k_1^{X;+}, k_2^{X;-}\right) - f(k_1,k_2) \right) \right] + \\
&\quad + \tilde{\beta} \cdot \sum_{X,\tilde{X}} \left[k_1(X) \cdot \left(f\left(k_1^{X,\tilde{X}}, k_2\right) - f(k_1,k_2) \right) + k_2(X) \cdot \left(f\left(k_1, k_2^{X,\tilde{X}}\right) - f(k_1,k_2) \right) \right],
\end{aligned} \tag{3.37}$$

where the sums are over all X in the domain and their nearest neighbours $\tilde{X}$. Furthermore, k_1 and k_2 are the particle configurations of the respective species (i.e. $k_{1,2}(X)$ the corresponding occupation numbers at location X), $k_{1,2}^{X;\pm}$ are the configurations, when one particle is added (or subtracted respectively) at position X and $k_{1,2}^{X,\tilde{X}}$ are the configurations, when one particle is subtracted at X and one added at $\tilde{X}$. For a process like this, we expect the thermodynamic metric to be positive definite, symmetric and specifically of Onsager type:

$$\mathcal{K}(\rho)(.) = \alpha \cdot \rho \cdot (.) - \operatorname{div}(\beta \cdot \rho \cdot \nabla(.)), \tag{3.38}$$

for $\alpha, \beta > 0$ depending on the frequencies, i.e. the Wasserstein metric with an additional noise α, accounting for the reaction between the two species. This is a type of reaction-diffusion system, that was recently cast in gradient flow shape: For an overview see [49] and references therein, particularly [50]. Note that, while these references are concerned with establishing the metric and the corresponding transport process on the state space, the connection with microscopic reaction-diffusion systems is still only heuristic and thus the application to our particular particle system speculative. The evolution equation then reads: $\partial_t \rho = -\alpha \rho \mathcal{D}\mathcal{S}(\rho) + \operatorname{div}(\beta \cdot \rho \cdot \nabla(\mathcal{D}\mathcal{S}))$ for a convenient entropy $\mathcal{S}$ (see e.g. the last equation of introduction of [50]) - note that it is a particularly beneficial property of the new method to find the thermodynamic metric $\mathcal{K}$ that it can be extracted without explicit knowledge of the entropy.

Default settings and numerical implementation Microscopically, we consider a square space of $L \times L$ sites with $L = 500$ and periodic boundary condition, which is populated by a total of 250000 particles ($N = 125000$ for each species). In the diffusive rescaling with $\epsilon = \frac{1}{L^d} = \frac{1}{L^2}$ (as in subsection 2.3) this domain becomes $\Omega = [0,1]^2$. The measurements are carried out in the "continuous" method (see remark 20) with overall one initial wait of $t_{fw} = 4 \cdot 10^{-5}$ and snapshots taken every $\delta t = 4 \cdot 10^{-8}$. As only the first derivatives are expected to act on them, we stick to the same finite element basis as defined in eq. (2.31) with $a_0 = 1$. The concentration points are located at a square grid with spacing a_1, i.e. $x_0 \in \frac{1}{a_1} \cdot \left(\left(\frac{1}{2}, \frac{1}{2}\right) + \mathbb{Z}^2/(L\mathbb{Z})^2\right)$. This way only test functions at nearest neighbouring and next to nearest neighbouring sites will have overlapping support.

When evaluating the Onsager operator for comparison with our results, the parameters α, β are modelled after the microscopic rates: While, as it holds for the pure classical random walk, β is assumed to be directly given by the microscopic jump rate, the microscopic transformation rate needs to be adjusted according to the rescaling of time, i.e. multiplied by L^2.

There are two approaches, to identify the metric $\mathcal{K}$ in eq. (3.38) from numerical experiments:

By considering the off-diagonal elements This is the most nearby approach, that directly implements eq. (3.4). By direct computation of $\langle \gamma_l, \mathcal{K}\gamma_r \rangle_{L^2(\Omega)}$ with $\gamma_r = \gamma_{(r_x, r_y)}$ being centred at

$x_r = \left(x_{r_x}, x_{r_y}\right) = \frac{1}{a_1} \cdot (r_x, r_y)$ by means of eq. (3.38) and for the test function parameters $a_0 = 1 = a_2$ we get:

$$\left(\left\langle \gamma_l, \mathcal{K}\gamma_{(r_x,r_y)}\right\rangle_{L^2(\Omega)}\right)_{r_x,r_y} =$$

$$= \begin{pmatrix} \ddots & & \vdots & & \iddots \\ & 0 & 0 & 0 & 0 & 0 & \\ & 0 & \frac{\rho}{36}\frac{\alpha}{a_1^2} + \frac{\partial_x\rho - \partial_y\rho}{12}\frac{\beta}{a_1} - \frac{\rho}{3}\beta & \frac{\rho}{9}\frac{\alpha}{a_1^2} - \frac{\partial_y\rho}{3}\frac{\beta}{a_1} - \frac{\rho}{3}\beta & \frac{\rho}{36}\frac{\alpha}{a_1^2} - \frac{\partial_x\rho + \partial_y\rho}{12}\frac{\beta}{a_1} - \frac{\rho}{3}\beta & 0 & \\ \cdots & 0 & \frac{\rho}{9}\frac{\alpha}{a_1^2} + \frac{\partial_x\rho}{3}\frac{\beta}{a_1} - \frac{\rho}{3}\beta & \frac{4\rho}{9}\frac{\alpha}{a_1^2} + \frac{8\rho}{3}\beta & \frac{\rho}{9}\frac{\alpha}{a_1^2} - \frac{\partial_x\rho}{3}\frac{\beta}{a_1} - \frac{\rho}{3}\beta & 0 & \cdots \\ & 0 & \frac{\rho}{36}\frac{\alpha}{a_1^2} + \frac{\partial_x\rho + \partial_y\rho}{12}\frac{\beta}{a_1} - \frac{\rho}{3}\beta & \frac{\rho}{9}\frac{\alpha}{a_1^2} + \frac{\partial_y\rho}{3}\frac{\beta}{a_1} - \frac{\rho}{3}\beta & \frac{\rho}{36}\frac{\alpha}{a_1^2} - \frac{\partial_x\rho - \partial_y\rho}{12}\frac{\beta}{a_1} - \frac{\rho}{3}\beta & 0 & \\ & 0 & 0 & 0 & 0 & 0 & \\ \iddots & & \vdots & & \ddots & & \end{pmatrix}_{r_x,r_y}, \tag{3.39}$$

where the middle entry is the diagonal entry (i.e. $l = r = (r_x, r_y) = (0.5, 0.5)$) and all others are off-diagonal with the concentration points being translated in the two-dimensional domain Ω in the respective direction (i.e. one $\frac{1}{a_1}$-increment North for the element shown above the diagonal one in the formula etc.). As the metric $\mathcal{K}$ is expected to only act locally in space, all off-diagonal elements farther than next to nearest neighbours should be zero.

We consider an out-of-equilibrium situation in the default settings, where the particles are, for both species independently, initially distributed at random positions with distribution proportional to the profile $\frac{1}{2}\left(1 + \frac{1}{2}\sin\left(2\pi\left(\frac{x}{L} - \frac{1}{2}\right)\right)\right)$. Their fluctuations are evaluated for a total time of $8 \cdot 10^{-4}$, i.e. $R = 2000$ many samples. If applicable (i.e. for those cases with a diffusion or reaction part, respectively), the jump rate is chosen as 1, while the microscopic transformation rate is chosen to be 0.1. For the test function we have chosen $a_2 = 1$ here, i.e. the less smooth version of the test functions, as these are a partition of one. The other parameters are $a_0 = 1$, $a_1 = 20$. Fig. 3.5 shows the results in comparison with the regular independent random walkers, i.e. the same setup with $\alpha = 0$, as well as the pure reaction process, i.e. for $\beta = 0$. Note that we here focus only on the centre of the domain, i.e. γ_l has concentration point $(0.5, 0.5)$ for convenience of the depiction, but could of course evaluate the entire domain analogously. Likewise, we confine ourselves to only evaluate the data of one species, due to the symmetry of the setup. This shows that the results for each entry in the matrix representation of the metric $\mathcal{K}$ is consistent with two hypotheses: The fact that the reaction-diffusion metric is just the sum of the respective metrics of the pure reaction and the pure diffusion process. And second - more specifically - the reaction-diffusion metric appears to be of the shape of the Onsager operator (see eqns. (3.38), (3.39)), where α is the combined transformation rate over both species and β is the jump rate of the respective species in question. Note also that the pure processes concur with the analytical expectation, although omitted in the picture.

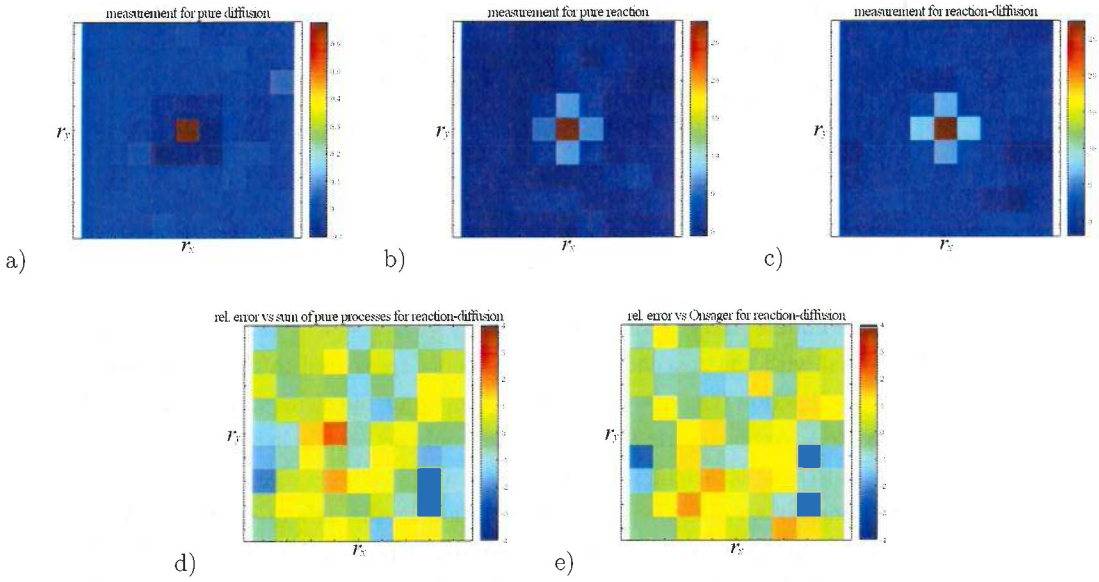

Figure 3.5: Numerical results for metric $\mathcal{K}$ for the reaction-diffusion dynamics, where the depiction follows the same logic as described around eq. (3.39) and the colour specifies the actual value of the entry in the matrix representation of $\mathcal{K}$. Note that only a small part at the centre of the domain of the altogether $a_1^{2 \cdot d} = 160000$ entries are depicted. The top row shows the measurements made for the three cases considered here, from left to right: The pure 2D system of independent, nearest neighbour random walkers in a). The pure reaction process in b). And the combined reaction-diffusion process in c). Based on this data the bottom row of pictures show, from left to right: The deviations of the metric of the reaction-diffusion process minus the sum of the metrics of the two pure processes, divided by the standard error of this sum d). And the error of the metric of the reaction-diffusion process minus the expectations based on eq. (3.39) (for $\alpha = 50000$, $\beta = 1$), normalised by the statistical standard error in e).

By considering the dependence on the test function γ As eq. (3.39) shows, different orders of derivatives scale differently with the parameter a_1, that scales the slope of the test functions. The more localised the test function is (i.e. smaller $\frac{1}{a_1}$), the more dominant the higher derivatives become. This is beneficial in two ways: First, because this allows to anticipate higher order terms and adjust the basis of test functions appropriately. Our choice of test functions in eq. (2.31) is not able to represent curvature correctly, but only is a piecewise linear approximation (in the Cartesian directions). It thus only allows for approximations in the Sobolev space $W^{1,2}(\Omega)$. For more complex metrics, however, we would need approximations in the tangent space, with respect to $\left\|\mathcal{A}^\dagger(\rho)(.)\right\|_{L^2(\Omega)}$. Second, because it allows to expand the metric $\mathcal{K}$ in powers of derivatives. For our simple case, for instance, it suffices to only consider the dependence of the diagonal element on a_1 and fit a respective power law to it.

To be able to study this for an as wide range of a_1 parameters (which is inverse to the support of the test functions), we consider a system in equilibrium, i.e. the particles of both species are initially distributed independently from one another again, proportional to $\frac{1}{2}$ uniformly in the domain. The total observation time is $8 \cdot 10^{-5}$, i.e. comprises $R = 200$ samples. The jump-rate is chosen as 1 and the microscopic transformation rate is 0.0002 (for each species) to better showcase the different scalings in a_1 for the reaction and diffusion part (larger values for the transformation rate are of course possible, too, but make the reaction part more dominant and push the "transition"-area between the two regimes further towards larger a_1, which collides with the relatively small systems size of $L = 500$ here; likewise a larger jump rate would collide with the finite domain size). For the smoothing parameter of the test function we here choose $a_2 = 2$, as we are only going to evaluate the metric on the diagonal and this allows for a better results towards smaller supports of γ. In this case the diagonal entry of the Onsager operator has the same shape as in eq. (3.39), but with different coefficients (here given numerically up to three digits):

$$\langle \gamma, \mathcal{K}\gamma \rangle_{L^2(\Omega)} \approx 0.660 \cdot \frac{\alpha}{a_1^2}\rho + 3.96 \cdot \beta\rho. \tag{3.40}$$

Results are shown in fig. 3.6 giving the expected picture over a large range of a_1-values. In this particular example the transformation rate is slightly over- and the jump-rate slightly underestimated, but within the error bounds (note that all data points arise from only one measurement, just post-processed with different a_1-values; repeated measurement of the same setting shows, this is not systematical).

Note that both approaches rely on post-processing techniques only and do not need manipulations of the system or impose further constraints on the experimental setup. Furthermore, this allows to combine both of them, to get the best results.

Finally note, while the consistency of these results with the Onsager operator from eq. (3.38) is encouraging, the applicability of the method for this scenario is speculative, as neither of the assumptions is tested or known rigorously. On the other hand, the Gaussian property of the fluctuations could be tested a posteriori by comparing them to a normal distribution with the covariance matrix given by the finite element representation of $\mathcal{K}$. And a suggestion for the entropy $\mathcal{S}$ could be obtained once

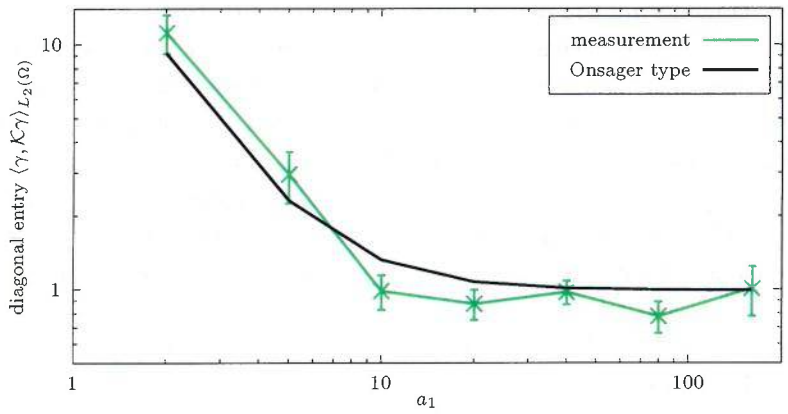

Figure 3.6: Dependence of the diagonal entry $\langle \gamma, \mathcal{K}\gamma \rangle_{L^2(\Omega)}$ on the parameter a_1, which is proportional to the slope of the test function γ in eq. (2.31). All data points are derived from one measurement only, so note that the points are correlated. The green line shows the empirical result, while the black line is computed based on the finite element representation of the Onsager operator in eq. (3.40).

the metric is measured, via the procedure outlined at the end of subsection 3.1. Furthermore, note we only considered a very specific example here: Evaluating the metric in other settings (other initial profiles, less symmetric setups between the species) and more complete post-processing (beyond the centre of the domain, with different test functions γ) might reveal further insights into the metric.

3.3 Mobility in the nearest neighbour Ising model

Here a two-dimensional, ferromagnetic, nearest neighbour Ising model with Glauber dynamics is studied at sub-critical temperatures, to find the mobilities of interfaces between different phases of the system.

3.3.1 Setup and motivation

The domain is a square lattice again: $\Lambda_L \subset \mathbb{Z}^2$. The overall setup looks like this: There is a spin s at each lattice site, that can attain two states, plus or minus one. If a spin flips it changes the sign of its spin, i.e. changes to the other possible state. The spins are flipped dependent on the energy functional:

$$E = -\sum_{X_i, X_j \in \Lambda_L} \left[s\left(X_i\right) \cdot J\left(X_i, X_j\right) \cdot s\left(X_j\right) \right], \tag{3.41}$$

where $J\left(X_i, X_j\right) = \frac{1}{4}\delta_{|X_i - X_j|=1}$ is the interaction term for our nearest neighbour case. The flips occur based on a Poisson process (see subsection 2.3.2 for a more detailed description) with a flip rate for

Glauber dynamics given by:

$$G(X) = \frac{e^{-\beta\delta E(X)}}{e^{-\beta\delta E(X)} + e^{+\beta\delta E(X)}}, \tag{3.42}$$

with $\beta = \frac{1}{T} > 0$ representing an inverse temperature T. Here

$$\delta E(X) = \left(- \sum_{X_j \in \Lambda_L} \left[-s(X) \cdot J(X, X_j) \cdot s(X_j) \right] \right) - \left(- \sum_{X_j \in \Lambda_L} \left[s(X) \cdot J(X, X_j) \cdot s(X_j) \right] \right) \tag{3.43}$$

is the difference (after minus before) of the overall energy, if the spin at X flips. Note that due to the local nature of the interaction term, this energy difference only needs to take into account the nearest neighbours of the flipped spin. In the ferromagnetic case considered here, alignment of spins in the same direction as their environment leads to a decrease in energy and thus to a lower jump rate, which leads to a tendency of aligned spins to agglomerate. The temperature T scales energy differences, thus lower temperatures lead to a more distinct flip rate difference for the same change in energy. Many aspects of these models are analytically well known, see for instance [52, 54]. In particular, it is known that such systems exhibit a phase transition with two equilibrium states (mostly plus or mostly minus spins, respectively) for low temperatures, but for temperatures beyond a critical value of $T_c = \frac{1}{2 \cdot \ln\left(1+\sqrt{2}\right)} \approx 0.567$ only one equilibrium measure exists for which there is a homogeneous mixture of both spins (see [54, Ch. 7]).

Our domain will be a slanted rectangle with L_x sites in horizontal direction and L_y sites in the vertical direction. For the vertical direction, we will consider constant minus and plus spins at the top or bottom, respectively. In the horizontal direction, there will be periodic boundary conditions with a potential offset, that enforces a tilt to the system: For a given angle $\theta \in [0, 2\pi[$ and for site $X = \left(X_{(x)}, X_{(y)}\right) = \left(L_x, X_{(y)}\right)$ on the right edge of the domain, $\left(1, L_x \cdot \tan(\theta) + X_{(y)}\right)$ will be the neighbour to the right and vice versa. Note that angles can not be represented properly unless $L_x \cdot \tan(\theta) \in \mathbb{Z}$ (otherwise we round to the nearest integer). If we stay below the critical temperature T_c, we expect an interface between the mostly negative top part of the domain and the mostly positive bottom, due to the imposed vertical boundaries. The tilt θ should lead to a respectively tilted interface. A snapshot of this setup is depicted in fig. 3.7.

For a long-range type of interaction J in the energy functional from eq. (3.41) (so-called Kac-potentials), such interfaces have been shown to move by mean curvature flow (see [55], [56]; for more recent results on large deviations see [57], [58]) in the hydrodynamic limit and in a diffusive space-time scaling. This means that the evolution of the interface follows (in local equilibrium) locally in the direction of the normal of the interface and scales with the mean curvature:

$$\partial_t I(t,x) = \vartheta_x\left(I(t,.)\right) \cdot \kappa_x\left(I(t,.)\right) \cdot n_x^{\perp}\left(I(t,.)\right), \tag{3.44}$$

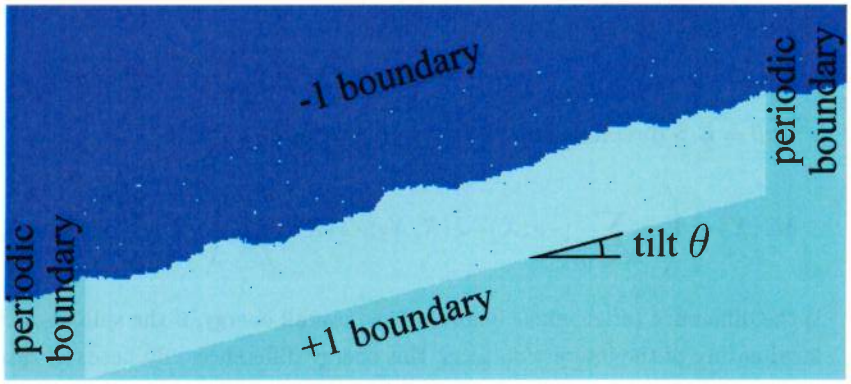

Figure 3.7: Snapshot of a state of the Ising system as described in subsection 3.3.1. The vertical boundary conditions enforce the formation of an interface, while the horizontal boundary conditions enforce a tilt θ of this interface (at subcritical temperatures, here $T = 0.3 < T_c$).

where we assume the interface to be a graph in the horizontal space component x for simplicity of notation, but the concept of mean curvature is not confined to this. The parameters on the right hand side are only locally dependent on the current interface: κ_x is the mean curvature of the interface at position x (see e.g. [59, sec. VII.5]) and $n_x^{\perp}$ the corresponding outward-oriented normal. The prefactor ϑ_x scales the speed of the motion and is dependent on the mobility and surface tension of the interface (thus being dependent on the inverse temperature β and the orientation θ). As is shown in [12], mean curvature flows can be expressed in a minimising movement scheme, where the Wasserstein metric from eq. (1.48) is replaced by an Almgren-Taylor-Wang type of distance (i.e. $\int_{A_{t+\delta t} \triangle A_t} \operatorname{dist}(., A_t)\, d\mathscr{L}^d$ for $A_{t+\delta t} \triangle A_t = (A_{t+\delta t} \cup A_t) \setminus (A_{t+\delta t} \cap A_t)$ being the symmetric difference of the set $A_t \subset \Omega$ with $\partial A_t = \{(x, I(t,x)) | \, x \in \Omega\}$ at two points in time; see [51]) and the energy term is given by the length of the interface $\int_{A_t} d\mathcal{H}^{d-1}$. In our anisotropic case, the distance in the integral of the Almgren-Taylor-Wang term is anisotropic as well and is characterised by what we will call mobility in this setting (see below). The anisotropic energy term is weighted with the surface tension, i.e. $\int_{A_t} s(.)\, d\mathcal{H}^{d-1}$ for surface tension s (see [52, ch. 7] for a characterisation in terms of partition functions as well as the connection to the free energy). Note that in case the interface is graph-like, $x \mapsto I(t,x)$, and if we only consider short enough time increments δt, the Almgren-Taylor-Wang term can be approximated by a simple L^2-distance and the non-linearities can be absorbed in one overall potential (see [53]).

We want to investigate, if there is numerical evidence for such a behaviour for the nearest neighbour interaction as well. The first step is, to find the mobility of the interfaces: If we denote the mean of the vertical component over all interface points by I and observe its evolution in time $t \mapsto I(t)$, we hope the interface motion $\delta I = I(t_0 + \delta t) - I(t_0)$ to be normally distributed to fit into our framework. Note that, thanks to our translation invariant setup (in the horizontal direction), we can just use the ODE

version of the approach from the beginning of subsection 2.1 (here the drift μ is expected to be zero). This will be the first subject of investigation. If this is true, we can characterise this distribution by its standard deviation σ by using mean square displacement: $\frac{(\delta I)^2}{\delta t}$ (I is a one-dimensional quantity). This we will refer to as mobility m (slightly abusing notation, compared to before). The mobility will be studied in its dependence on temperature T and tilt θ.

3.3.2 Numerical approach

The Ising process The actual Ising dynamics is implemented with a Kinetic Monte-Carlo approach, see top part of alg. 2. The initial condition will be a flat profile and no waiting t_{fw} will be performed, as the normality will be checked explicitly. If there is a tilt $\theta > 0$ applied, not all spins in the entire rectangle will be simulated, but rather a parallelogram-shaped stripe, that is tilted along the expected shape of the interface (i.e. with θ; see fig. 3.7). This is done by mapping this parallelogram to a rectangle by imposing a "tilted" nearest neighbour definition (for the horizontal direction only; the nearest neighbours in North and South direction are not affected): For $\left(X_{(x)}, X_{(y)}\right)$ being the horizontal and vertical component of the location of a spin, then $\left(X_{(x)}+1, X_{(y)}+\left[\!\left[X_{(y)} \cdot \tan(\theta)\right]\!\right]\right)$ is its neighbour to the right, where $[\![.]\!]$ denotes rounding to the next integer.

As the overall observation time can get very long (see paragraph below about computing the mobility), the overall motion $I(t_{\text{final}}) - I(t_0)$ can get large as well. To not have to always simulate such a large domain in the vertical direction, we co-move the domain with the interface, i.e. each time the interface is measured (i.e. at each $t_0 + r \cdot \delta t$) we re-adjust the domain, such that the interface mean is not more than half a site away from the middle $\frac{L_y}{2}$. Note that this deletes some spins at the far end from the interface and creates new spins at the closer end (these are chosen as uniformly positive or negative aligned with the boundary condition next to it). As L_y is still considered large compared to the vertical span of the interface, this is still far away from the interface itself, thus considered not significantly interacting with its motion.

Interface tracking Numerically, the interface is a vector of pairs of spins with opposite sign: One just "above" the interface and one just "below" (of course geometrically this depends on the orientation of the interface). The spins in this pair are nearest neighbour to each other. Practically speaking this vector contains the elements directly adjacent to the interface in the order, when walking along the interface (which is not necessarily unique). We generate such a vector of pairs of spin locations from a starting point, by walking along the interface: This is a local approach as such and there might be bifurcations, where several options can be considered a viable continuation of the interface.

In this case a depth-first search is applied, i.e. one option is chosen by some heuristic argument (see below), but the location of the bifurcation is memorised in case the first choice ends in a dead end (i.e. the path followed leads back to a point of the interface we already visited earlier). If this is not the case and we get to an actual, complete interface, connecting back to the start point, the search

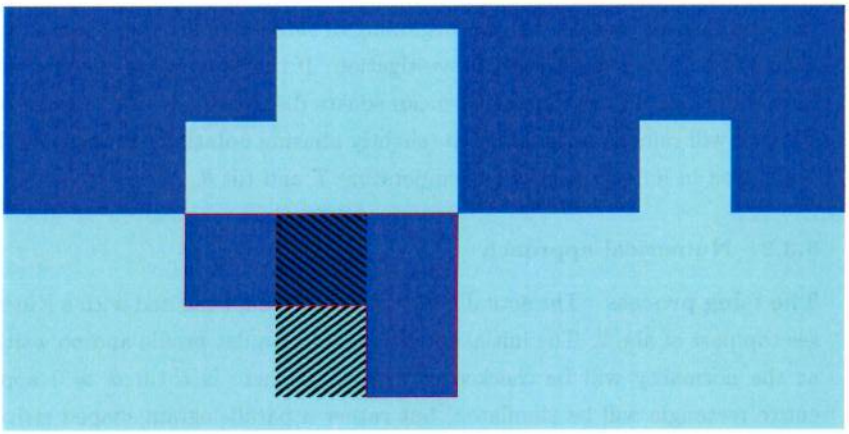

Figure 3.8: Pathological case for interface tracking, due to an island, that connects to the actual interface on both sides of the starting point. Here the starting point pair is indicated by the hatching, while a possible connecting path is highlighted by the red outline. Such a path would only turn out to be unsuccessful, once it is completed and recognized as not spanning the entire domain in the horizontal direction.

process is aborted and other options are not explored further. While this saves time, it ignores possible other interfaces. We expect, however, that for large L_x and temperature T not too close to the critical one, there is only one interface spanning the entire horizontal length (i.e. ignoring "islands") up to only small ambiguities, where (small) islands are corner-to-corner adjacent to interface points (similar to the way the connections in the particularly case in fig. 3.7 occur). In the latter case, the interface is not unique. If, on the other hand, the first choice does lead to a dead end, the intermediate path is deleted and the search restarts at the last bifurcation, but forbidding the dead-end-path for the future. Note, it is numerically beneficial that dead ends only occur, if we hit a bifurcation, for which we did not check all paths yet, i.e. the path connects two bifurcations. Hence, for checking dead-ends, we only have to compare the path with the options at bifurcation points, not with the entire interface so far. This procedure will explore all paths, if necessary, but stop earlier, if successful.

One problem occurs, however, if the additional condition comes into play that we do not only want to find the interface the start point belongs to, but also require it to span the entire horizontal direction (i.e. for each $X_{(x)} \in \{1, \ldots, L_x\}$, there is an interface point (on each side of the interface) with this x-component): If there is an island (that does not span the entire horizontal domain), that connects to the actual interface on both sides of the starting point (see fig. 3.8), we might walk along this island first, to then delete parts of the correct path, due to the bad experience with the island. Nonetheless, these parts can be vital for the correct path. In this case, we have to restart the search process and remove all paths, but then alternate the order with which we walk along the path options at the bifurcation points. As islands typically are small, this rarely happens.

The heuristic, mentioned above, only serves as a guideline, which options to try first and can thus help to reduce the computation time, if "more likely successful" options are preferred. For our measurements, we prefer those options, that avoid the interface to get "twisted", i.e. we keep track how often the pair of points in our interface vector turn clockwise (adding minus one to the the twist) or anti-clockwise (adding plus one to the twist) and try to locally minimise the absolute value of the twist.

An alternative approach to find the interface would be breadth-first search, for which all possible paths are followed simultaneously. Here, the process is stopped, as soon as the first viable solution is found (i.e. an interface, that connects the start point with itself, while spanning the horizontal domain entirely). This always leads to the shortest path (if all path options are followed with the same speed). The depth-first search is preferred here, as we expect many but small islands, leading to many paths to explore simultaneously via breadth-first search, while unsuccessful long detours, that would make depth-first search less efficient, are rare.

Computing the mobility The interface motion is studied by the "continuous" version of mean square displacement, i.e.: One long evolution is simulated (for a time span of $R \cdot \delta t$) and snapshots of the interface position I are taken every δt, then the mean square displacement is computed for each pair of subsequent measurements, giving a total of R measurements, labelled by $r \in \{1, \ldots, R\}$ again. Based on the symmetry of the setup, it is assumed that the expectation for δI_r is zero for each measurement r, thus giving the approximated mobility:

$$m(\theta) = \frac{1}{R} \cdot \sum_{r=1}^{R} \left[\frac{(\delta I_r)^2}{\delta t} \right]. \tag{3.45}$$

This corresponds to the mobility, as it also shows up in large deviations rate functionals for Kac-interactions in one space dimension, if no nucleations occur (see [57]).

3.3.3 Numerical results

The following aspects were studied, using the approach described above:

Normality of the displacements δI_r Results are depicted in fig. 3.9. The settings for the simulations were $L_x = 500$, $L_y = 137$, $\theta = 15°$, $T = 0.3$. All data points are derived from one measurement, but processed with different measurement times δt. One can see that for too short measurement times δt not enough spins flip and the distribution is not normal. For long enough measurement times, this issue can be overcome. For the results below, the normality was tested via an Anderson-Darling test (for a brief description and comparison with alternatives see [60]) to ensure validity of the assumption.

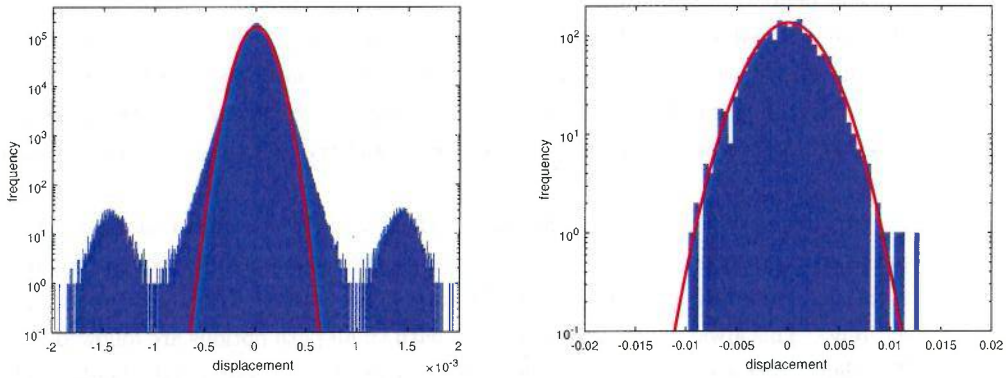

Figure 3.9: Comparison of the normal distribution (red line; with mean zero and same standard deviation as the data; note the logarithmic scaling of the vertical axis) with the histograms obtained from measuring the interface displacement δl_r for $L_x = 500$, $\delta t = 1 \cdot 10^{-6}$ and $R = 20000000$ samples on the left and $L_x = 500$, $\delta t = 1 \cdot 10^{-2}$, $R = 2000$ on the right. Both histograms are obtained for the same data set, but just a different measurement times δt in the post-processing.

Dependence of the mobility on measurement time and system size Results are depicted in fig. 3.10. Here $L_y = \lceil 6 \cdot \sqrt{L_x} \rceil$, $\theta = 15°$, $T = 0.3$ was chosen for the simulations. One can see that for large enough δt and L_x the mobilities give consistent results.

Dependence on the temperature Results are depicted in fig. 3.11. Here $L_x = 500$, $L_y = 137$, $\theta = 15°$ were chosen for the simulations and $\delta t = 0.01$ for the measurement time in the post-processing of the $R = 50$ samples. One can observe a power-law dependence of the mobility on the temperature below the critical value T_c: $m(T) \propto (T_c - T)^{\alpha}$ with $\alpha = -1.021$.

Dependence on the orientation of the interface (tilt θ) Results are depicted in fig. 3.12. Here $L_x = 500$, $L_y = 137$, $T = 0.3$ was chosen for the simulations and $\delta t = 0.01$ for the measurement time in the post-processing of the $R = 2000$ samples. The cushion shape can be understood heuristically, because adding another particle to a flat, horizontal (or vertical) interface creates two new (three minus one) neighbours of the opposite spin sign, making it less likely compared to say a staircase-shaped interface of a 45° tilt, where no new neighbours of opposite spin sign are created, if a particle is added. While this gives an intuition, of course the microscopic interface is typically not entirely flat or staircase-shaped.

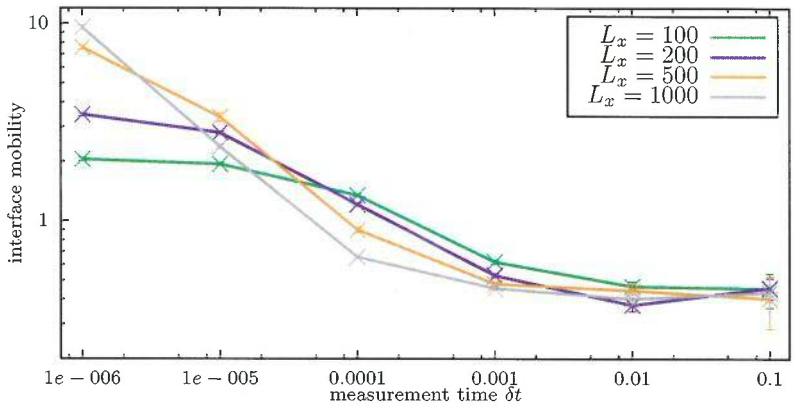

Figure 3.10: Mobilities of the Ising model for different systems sizes L_x and measurement times δt. Like in fig. 3.9 only one measurement was made for each L_x-setting and different δt were used in the post-processing only. As this also means that the total observation time $R \cdot \delta t$ of the system is identical for all data points, the number of samples R scales inversely with the measurement time δt, starting off at $R = 5 \cdot 10^6$ at $\delta t = 10^{-6}$ and ending up at $R = 50$ at $\delta t = 0.1$.

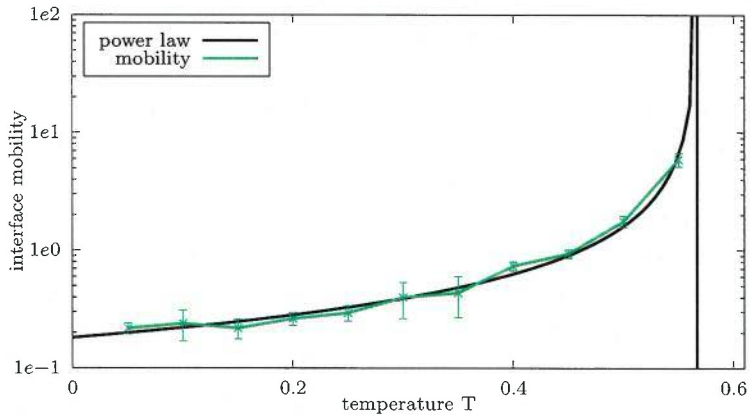

Figure 3.11: Dependence of the mobility of the Ising model on the temperature T.

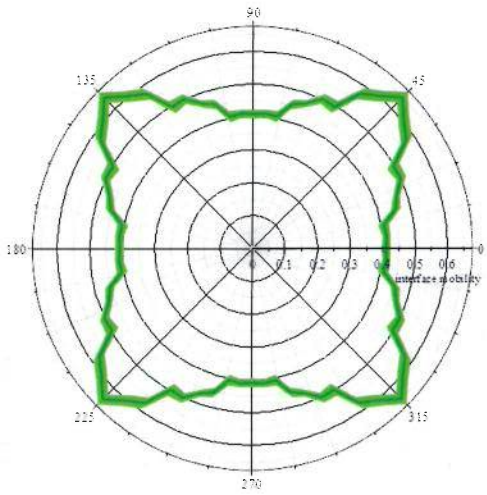

Figure 3.12: Dependence of the interface mobility of the Ising model on the tilt angle θ. The dark green line is the mean of the measurements, while the area represents the errorbars. Only the first 45° were measured in 5°-increments, while the remainder of the full circle is extrapolated via symmetry.

III

Closing remarks

Summary This text studied how diffusive particle processes can be characterised as gradient flows.

First, in section 1, we focused on transport processes, that can be linked to the Wasserstein metric on the space of probability measures. This lead to a theoretical framework including notions like the gradient flow description of constant-speed geodesics and the Benamou-Brenier formula, that we could recognise later in the context of the stochastic processes. In subsection 2.1 a setup was presented, for which these analogies were drawn and that fixes the assumptions on local equilibrium and stochasticity of the dynamic system of interest, that allowed to formulate thm. 16 in the next section. This theorem establishes a method to find the mobility in a system evolving along a weighted Wasserstein gradient flow. In such a case, the mobility uniquely defines the thermodynamic metric, that corresponds to the thermodynamic entropy as Lyapunov functional in the gradient flow description, thus linking the deterministic, macroscopic evolution to these probabilistic quantities of the microscopic system. A numerical implementation of this new approach was described in subsection 2.3. This algorithm was tested on numerical processes, for which the validity of this theoretical framework had been rigorously proven in the past: Indeed, subsection 2.4 shows overall agreement of the numerical outcomes using the new method, both, with the theoretical predictions and with results obtained via the existing

mean square displacement approach. Moreover, prop. 21 connects the new method to mean square displacement under certain circumstances, thus also outlining criteria, when the new method provides meaningful results, while the latter might not, as has been shown for the simple-exclusion process.

Section 3 formally extended this the method beyond weighted Wasserstein metrics, thus providing a much broader framework for irreversible processes. To better test as well as further expand the applicability of this procedure, the method was used to forecast parameters in on-the-fly simulations of stochastic systems: Thanks to the new method being based on measurements on very short time-scales only, the method is predestinated for synchronisation of the estimated parameters (with the observed evolution) in parallel to the experiments. This was showcased in subsection 3.1 by an explicit-implicit finite element ansatz. Then the approach was applied to study the metric of a simple example of a reaction-diffusion system, showing promising results (see subsection 3.2). Subsection 3.3 applies a simplified approach to the two-dimensional nearest neighbour Ising model with Glauber dynamics. Also in this example, consistent results could be obtained, although proving benefit for describing the macroscopic evolution remains for future research.

Outlook If we want to make on-the-fly simulations, it would greatly enhance the performance, if we could remember old measurements and extrapolate from them, rather than only forecasting from the very recent set of measurements (in the time interval δt). Note, though, that the dependence of the metric on the state space is in general functional. Thus, for using memory, it would be vital to get a better understanding on this functional dependence to be able to interpolate between existing measurements. Using the suitably chosen test functions, as mentioned in subsection 3.2 could be a promising starting point. A similar problem occurs for measuring the entropies, as their dependence is functional on the states as well and even more so, because their identification via the approach in section 3 requires larger time scales, than just the metric. In this context, it would also be very helpful to have valid error estimates for the results obtained for $\mathcal{DS}$ but also $\mathcal{K}$, which are currently not known.

Even in the more general setup of section 3, only purely dissipative processes can be treated in the way described in this text (i.e with symmetric, positive semi-definite thermodynamic metric). As outlined in remark 23, this is just one part of a more universal framework. The applicability of the gradient flow ansatz could be greatly enhanced, if a generalised approach could be found, in which the method described in this text is embedded and extended to processes with reversible components as well.

References

[1] Murray, J.D.: Mathematical Biology: I. An Introduction, 3rd edition, Springer-Verlag Berlin Heidelberg, 2002, ISBN: 0-387-95223-3

[2] Hull, J.C.: Options, Futures and other Derivatives, 8th edition, Pearson Education, Inc., publishing as Prentice Hall, 2012, ISBN: 0-13-216494-9

[3] Jordan, R., Kinderlehrer, D., Otto, F.: The Variational Formulation of the Fokker–Planck Equation, SIAM J. Math. Anal., vol. 29, no. 1, pp. 1-17, 1998, DOI: 10.1137/S0036141096303359

[4] Otto, F.: The Geometry of Dissipative Evolution Equations: The Porous Medium Equation, Comm. Partial Differential Equations, vol. 26, is. 1&2, pp. 101-174, 2000, DOI: 10.1081/PDE-100002243

[5] Dolbeault, J., Nazaret, B., Savaré, G.: A new class of transport distances between measures, Calc. Var. Partial Differential Equations, vol. 34, is. 2, pp. 193-231, 2009, DOI: 10.1007/s00526-008-0182-5

[6] Matthes, D., McCann, R.J., Savaré, G.: A Family of Nonlinear Fourth Order Equations of Gradient Flow Type, Comm. Partial Differential Equations, vol. 34, is. 11, pp. 1352-1397, 2009, DOI: 10.1080/03605300903296256

[7] Arnrich, S., Mielke, A., Peletier, M.A., Savaré, G., Veneroni, M.: Passing to the limit in a Wasserstein gradient flow: from diffusion to reaction, Calc. Var., vol. 44, is. 3-4, pp. 419–454, 2012, DOI: 10.1007/s00526-011-0440-9

[8] Maas, J. Gradient flows of the entropy for finite Markov chains, Journal of Functional Analysis, vol. 261, is. 8, pp. 2250-2292, 2011, DOI: 10.1016/j.jfa.2011.06.009

[9] Ambrosio, L., Gigli, N., Savaré, G.: Gradient Flows in Metric Spaces and in the Space of Probability Measures, Birkhäuser Verlag Basel-Boston-Berlin, 2005, ISBN: 3-7643-2428-7

[10] Adams, S., Dirr, N., Peletier, M.A., Zimmer, J.: From a Large-Deviations Principle to the Wasserstein Gradient Flow: A New Micro-Macro Passage, Commun. Math. Phys., vol. 307, pp. 791–815, 2011, DOI: 10.1007/s00220-011-1328-4

[11] Duong, M.H., Laschos, V., Renger, M.: Wasserstein gradient flows from large deviations of many-particle limits. ESAIM: Control, Optimisation Calc. Var., vol. 19, no. 4, pp. 1166–1188, 2013, DOI: 10.1051/cocv/2013049

[12] Luckhaus, S., Sturzenhecker, T.: Implicit time discretization for the mean curvature flow equation, Calc. Var., vol. 3, is. 2, pp. 253–271, 1995, DOI: 10.1007/BF01205007

[13] Öttinger, H.C.: Beyond equilibrium thermodynamics, John Wiley & Sons, 2005, ISBN: 0-471-66658-0

[14] Ambrosio, L., Gigli, N.: A User's Guide to Optimal Transport, published in: Modelling and Optimisation of Flows on Networks, edited by Piccoli, B., Rascle, M., Springer-Verlag Berlin Heidelberg, pp. 1-155, 2013, ISBN: 978-3-642-32159-7

[15] Villani, C.: Topics in Optimal Transportation, Graduate Studies in Mathematics, vol. 58, American Mathematical Society, Rhode Island, 2003, ISBN: 0-8218-3312-X

[16] Gangbo, W., McCann, R.J.: The geometry of optimal transportation, Acta Math., vol. 177, no.2, pp. 113-161, 1996, DOI: 10.1007/BF02392620

[17] Benamou, J.-D., Brenier, Y.: A computational fluid mechanics solution to the Monge-Kantorovich mass transfer problem, Numer. Math. 84, pp. 375-393, 2000, DOI: 10.1007/s002119900117

[18] Rockafellar, R.T.: Convex Analysis, Princeton Math. Series, vol. 28, Princeton University Press, 1970

[19] Embacher, P., Dirr, N., Zimmer, J., Reina, C.: Computing diffusivities from particle models out of equilibrium, Proc. Roy. Soc. London Ser. A 474, 2018, DOI: 10.1098/rspa.2017.0694

[20] Dirr, N., Stamatakis, N., Zimmer, J.: Entropic and gradient flow formulations for nonlinear diffusion, Journal of Mathematical Physics 57, 081505, 2016, DOI: 10.1063/1.4960748

[21] Touchette, H.: The large deviation approach to statistical mechanics, Physics Reports, vol. 478, is. 1-3, pp. 1-69, 2009, DOI: 10.1016/j.physrep.2009.05.002

[22] Dupuis, P., Ellis, R.S.: A Weak Convergence Approach to the Theory of Large Deviations, John Wiley & Sons, 1997, ISBN: 978-0-471-07672-8

[23] Kipnis, C., Olla, S.: Large Deviations from the hydrodynamical limit for a system of independent Brownian particles, Stochastics and Stochastics Reports, vol. 33, pp. 17-25, 1990, DOI: 10.1080/17442509008833661

[24] Koukkous, A., Guiol, H.: Large deviations for a zero mean asymmetric zero range process in random media, Technical report, Relatorio de Pesquisa RP 16/00 IMECC-UNICAMP, 2000, preprint arXiv:math/0009110v1

[25] Adams, S., Dirr, N., Peletier, M., Zimmer, J.: Large deviations and gradient flows, Phil Trans R Soc A, vol. 371, 2013, DOI: 10.1098/rsta.2012.0341

[26] Crooks, G.E.: Entropy production fluctuation theorem and the nonequilibrium work relation for free energy differences, Phys. Rev. E, vol. 60, is. 3, pp. 2721-2726, 1999, DOI: 10.1103/PhysRevE.60.2721

[27] Jarzynski, C: Equilibrium free-energy differences from nonequilibrium measurements: A master-equation approach, Phys. Rev. E, vol. 56, no. 5, pp. 5018-5035, 1997, DOI: 10.1103/PhysRevE.56.5018

[28] Bertini, L., De Sole, A., Gabrielli, D., Jona Lasinio, G., Landim, C.: Macroscopic fluctuation theory, Rev. Mod. Phys., vol. 87, is. 2, pp. 593-636, DOI: 10.1103/RevModPhys.87.593

[29] Gielis, G., Koukkous, A., Landim, C.: Equilibrium fluctuations for zero range processes in random environment, Stochastic Processes and their Applications, vol. 77, is. 2, pp. 187-205, 1998, DOI: 10.1016/S0304-4149(98)00044-1

[30] Landim, C., Milanés, A., and Olla, S.: Stationary and nonequilibrium fluctuations in boundary driven exclusion processes, Markov Process. Related Fields, 14(2), pp. 165-184, 2008

[31] Øksendal, B.: Stochastic Differential Equations - An Introduction with Applications, Springer-Verlag Heidelberg New York, 5th edition, 2003, ISBN 978-3-642-14394-6

[32] Guckenheimer J, Holmes P.J.: Nonlinear Oscillations, Dynamical Systems, and Bifurcations of Vector Fields, Applied Mathematical Sciences. vol. 42, Springer-Verlag New York, revised and corrected reprint of the 1983 original, 1990, ISBN: 3540908196

[33] Einsiedler, M., Ward, T.: Functional Analysis, Spectral Theory, and Applications, Graduate Texts in Mathematics 276, Spinger, 2017, ISBN: 978-3-319-58540-6

[34] Dixit, U.J.: Examples in parametric inference with R, Springer, Singapore, 2016, ISBN: 978-981-10-0888-7

[35] Kahan, W: Further remarks on reducing truncation errors, Communications of the ACM, vol. 8, is. 1, 1965, DOI: 10.1145/363707.363723

[36] Kipnis, C., Landim, C.: Scaling limits of interacting particle systems, Grundlehren der Mathematischen Wissenschaften [Fundamental Principles of Mathematical Sciences], vol. 320, Springer-Verlag Berlin, 1999, ISBN: 978-3-540-64913-7

[37] Großkinsky, S., Schütz, G.M., Spohn, H.: Condensation in the Zero Range Process: Stationary and Dynamical Properties, Journal of Statistical Physics, vol. 113, nos. 3/4, November 2003, DOI: 10.1023/A:1026008532442

[38] Norris, J.R.: Markov Chains, Cambridge Series on Statistical and Probabilistic Mathematics, Cambridge University Press, 1997, ISBN: 978-0-521-48181-6

[39] Voter, A.F.: Introduction to the Kinetic Monte Carlo Method, Radiation Effects in Solids, in: Sickafus, K.E., Kotomin, E.A., Uberuaga, B.P. (eds): Radiation Effects in Solids, NATO Science Series, vol 235, Springer, Dordrecht, pp. 1-23, 2007, ISBN: 978-1-4020-5295-8

[40] Battaile, C.C.: The Kinetic Monte Carlo method: Foundation, implementation, and application, Comput. Methods Appl. Mech. Engrg., vol. 197, is. 41-42, pp. 3386–3398, 2008, DOI: 10.1016/j.cma.2008.03.010

[41] Arratia, R.: The motion of a tagged particle in the simple symmetric exclusion system in $\mathbb{Z}$, Ann. Prob., vol. 11, no. 2, pp. 362-373, 1983, DOI: 10.1214/aop/1176993602

[42] Mörters, P., Peres, Y.: Brownian Motion, Cambridge University Press, 2010, ISBN: 978-0-521-76018-8

[43] Spohn, H.: Large Scale Dynamics of Interacting Particles, Springer-Verlag Berlin Heidelberg, 1991, ISBN: 978-3-642-84373-0

[44] Pavliotis, G.A.: Stochastic Processes and Applications - Diffusion Processes, the Fokker-Planck and Langevin Equations, Texts in Applied Mathematics vol. 60, Springer Science+Business Media, 2014, ISBN: 978-1-4939-1323-7

[45] Mielke, A.: Formulation of thermoelastic dissipative material behavior using GENERIC, Contin. Mech. Thermodyn., vol. 23, is. 3, pp. 233-256, 2011, DOI: 10.1007/s00161-010-0179-0

[46] Gunsteren, W.F.v., Daura, X., Mark, A.E.: Computation of Free Energy, Helv. Chimica Acta, vol. 85, 2002, pp. 3113-3129, DOI: 10.1002/1522-2675(200210)85:10

[47] Morton, K.W., Mayers, D.: Numerical Solution of Partial Differential Equations - An Introduction, Cambridge University Press, 2nd edition, 2005, ISBN: 978-0-521-60793-3

[48] Decell, H.P., Kahng, S.W.: An iterative method for computing the generalized inverse of a matrix, NASA technical note, 1966

[49] Santambrogio, F.: {Euclidean, metric, and Wasserstein} gradient flows: an overview, Bulletin of Mathematical Sciences, no. 7, pp. 87–154, 2017, DOI: 10.1007/s13373-017-0101-1

[50] Liero, M., Mielke, A., Savaré, G.: Optimal Transport in Competition with Reaction: The Hellinger-Kantorovich Distance and Geodesic Curves, SIAM J. Math. Anal., vol. 48, no. 4, pp. 2869–2911, 2016, DOI: 10.1137/15M1041420

[51] Almgren, F., Taylor, J.E., Wang, L.: Curvature-Driven Flows: A Variational Approach, SIAM J. Control and Optimization, vol. 31, no. 2, pp. 387-437, 1993, DOI: 10.1137/0331020

[52] Presutti, E.: Scaling Limits in Statistical Mechanics and Microstructures in Continuum Mechanics, Springer Berlin Heidelberg, 2009, ISBN: 978-3-540- 73304-1

[53] Oberman, A., Osher, S., Takei, R., Tsai, R.: Numerical methods for anisotropic mean curvature flow based on a discrete time variational formulation, Communications in Mathematical Sciences, vol. 9, no. 3, pp. 637-662, 2011, DOI: 10.4310/CMS.2011.v9.n3.a1

[54] Baxter, R.J.: Exactly Solved Models in Statistical Mechanics, Academic Press, London, 1982, ISBN: 0-12-083180-5

[55] De Masi, A., Orlandi, E., Presutti, E., Triolo, L.: Glauber evolution with Kac potentials. I. Mesoscopic and macroscopic limits, interface dynamics, Nonlinearity, vol. 7, no. 3, pp. 633-696, 1994

[56] Katsoulakis, M.A., Souganidis, P.E.: Generalized Motion by Mean Curvature as a Macroscopic Limit of Stochastic Ising Models with Long Range Interactions and Glauber Dynamics, Commun. Math. Phys. 169, pp. 61-97, 1995

[57] Birmpa, P., Dirr, N., Tsagkarogiannis, D.: Large deviations for the macroscopic motion of an interface. Journal of Statistical Physics 166(5), pp. 1163-1192, 2017, DOI: 10.1007/s10955-017-1720-3

[58] Bertini, L., Buttà, P., Pisante, A.: On large deviations of interface motions for statistical mechanics models, preprint, 2018, arxiv: 1802.04194v1

[59] Kobayashi, S., Nomizu, K.: Foundation of Differential Geometry vol. 2, Interscience Publishers, John Wiley & Sons, 1969

[60] Yap, B.W., Sim, C.H.: Comparisons of various types of normality tests, Journal of Statistical Computation and Simulation, vol. 81, no. 12, pp. 2141-2155, 2011, DOI: 10.1080/00949655.2010.520163